REPUBLIC OF TURKEY YILDIZ TECHNICAL UNIVERSITY GRADUATE SCHOOL OF SCIENCE AND ENGINEERING

SEMICONDUCTING JUNCTIONS FOR SOLAR ENERGY PRODUCTION

HUDA M. MUNEER ABD ALQADER

DOCTOR OF PHILOSOPHY THESIS

Department of Physics

Physics Program

Supervisor

Assoc. Prof. Dr. Serço Serkis YEŞİLKAYA

REPUBLIC OF TURKEY

YILDIZ TECHNICAL UNIVERSITY

GRADUATE SCHOOL OF SCIENCE AND ENGINEERING

SEMICONDUCTING JUNCTIONS FOR SOLAR ENERGY PRODUCTION

A thesis submitted by Huda M. Muneer ABD ALQADER in partial fulfillment of the requirements for the degree of DOCTOR OF PHILOSOPHY is approved by the committee on 11.08.2021 in Department of Physics, Physics Program.

Assoc. Prof. Dr. S. Serkis YEŞİLKAYA Yıldız Technical University Supervisor

Approved By the Examining Committee

Assoc. Prof. Dr. Serço Serkis YEŞİLKAYA, Supervisor	
Yıldız Technical University	
Assoc. Prof. Dr. Murat ÇALIŞKAN, Member	
Yıldız Technical University	
Asst. Prof. Dr. Ercüment AKAT, Member	
Yeditepe University	
Prof. Dr. Orhan ÖZDEMİR, Member Yıldız Technical University	
·	
Assoc. Prof. Dr. Timur CANEL, Member	
Kocaeli University	

I hereby declare that I have obtained the required legal permissions during data collection and exploitation procedures, that I have made the in-text citations and cited the references properly, that I haven't falsified and/or fabricated research data and results of the study and that I have abided by the principles of the scientific research and ethics during my Thesis Study under the title of Semiconducting Junctions for Solar Energy Production supervised by my supervisor, Assoc. Prof. Dr. Serço Serkis YEŞİLKAYA. In the case of a discovery of false statement, I am to acknowledge any legal consequence.

Huda M. Muneer ABD ALQADER

Signature



Dedicated to my family and my best friends

ACKNOWLEDGEMENTS

All praises to Allah Almighty who created the universe and knows whatever in it, for giving me the ability, faith and power that were essential to complete this thesis. I would like to extend my deep sincere thanks to my supervisor, Assoc. Prof. Dr. SERÇO SERKİS YEŞİLKAYA, who give me a wealth of knowledge in physics for his support, thoughtful guidance, encouragement, inspiration and valuable information that he given to me that have had the greatest impact during of my studies and the work in my thesis.

My thanks and gratitude goes to Prof. Dr. Ahmet ALTINDAL, Prof. Dr. Erol KAM, Prof. Dr. Orhan ÖZDEMİR, Assoc. Prof. Dr. Mustafa OKUTAN, Assoc. Prof. Dr. Murat ÇALIŞKAN and Asst. Prof. Dr. Ercüment AKAT for all valuable knowledges, and support that they provided throughout the graduate lectures. Many thanks and appreciate goes to the staff of Marmara University, Physics department specially Prof. Dr. Zikri ALTUN, Prof. Dr. Uğur YAHŞİ, Dr. Ayşe YUMAK YAHŞİ and others.

I am grateful to all academic and management staff in YILDIZ TECHNICAL UNIVERSITY who introduced their knowledge and help during my studies to obtain a DOCTORA's Degree. Record my appreciation to my colleagues Yalçin URFA, Ayşe Nur ŞAHIN, Kubra ALBAYRAK and others, thank you all.

My appreciation also goes to Iraqi governments/ Mosul University for the financial of my scholarship.

I want to express my deep thanks to my parents, my husband, my daughter and my son for the immense love and moral support they have given to me which is truly immeasurable. A spacial thank goes out to my brother and sisters who wish me the best thank you all. Finally, I would like to thank everyone who helps me to reach this goal.

Huda M. Muneer ABD ALQADER

TABLE OF CONTENTS

LIST	OF SYMBOLS	x
LIST	OF ABBREVIATIONS	xii
LIST	OF FIGURES	xiii
LIST	OF TABLES	xvi
ABST	TRACT	xvii
ÖZET	r	xix
1 IN	TRODUCTION	1
1.1	Literature Review	1
1.2	Objective of the Thesis	8
1.3	Hypothesis	8
2 MA	ATERIALS AND FABRICATION TECHNIQUES	10
2.1	Semiconductor Materials	10
2.2	Direct and Indirect Semiconductors	13
2.3	Doping Semiconductors	14
	2.3.1 P-type and n-type Semiconductors	15
	2.3.2 P-n Junction	16
	2.3.3 Bult in Electric Field	17
2.4	Zinc Sulfide and Zinc Oxide	17
	2.4.1 Properties of Zinc Sulfide	17
	2.4.2 Properties of Zinc Oxide	19
2.5	Structural Characterization Techniques	20
	2.5.1 X-Ray Diffraction (XRD)	20
	2.5.2 Scanning Electron Microscope (SEM)	21
	2.5.3 UV Spectroscopy	22
2.6	Growth Techniques	23
	2.6.1 Chemical Bath Deopsition Technique	23
	2.6.2 Sol-gel (Spin Coating) Technique	24
	2.6.3 Spray Pyrolysis Technique	25
3 BA	SICS OF PHOTOVOLTAICS	26
3.1	Solar Irradiance	26
	2.1.1 Dhotona	27

		3.1.2 The Solar Spetrum and Atmospheric Impacts	27
	3.2	Physics of Solar Cells	28
		3.2.1 Photovoltaic Effect	29
		3.2.2 Theory of Heterojunction Solar Cell	29
		3.2.3 Light Absorption and Electron-Hole Generation	31
		3.2.4 Separation of Photogenerated Carriers	32
		3.2.5 Collection of Gharge Carriers at the Terminals of the Junction	32
	3.3	Equivelent Circuit of Solar Cell	33
	3.4	Basics Parameters and Device Characterization	35
		3.4.1 The Current Density-Voltage Characteristics	35
		3.4.2 Short Circuit Current Density	36
		3.4.3 Open Circuit Voltage	36
		3.4.4 Fill Factor	37
		3.4.5 Maximum Power Point	38
		3.4.6 Power Conversion Efficiency	38
		3.4.7 Series and Shunt Resistance Effects	38
4	EXI	PERIMENT DETAILS	40
	4.1	Deposition of Doped and Undoped ZnS Thin Films Using CBD Technique	40
		4.1.1 Reaction Mechanism	40
		4.1.2 Preparation of Bath Solution and Cleaning Process	41
	4.2	The Deposition of ZnS Thin Films Using Spin Coating Technique	42
		4.2.1 Film Preparation and Processing	43
	4.3	Deposition of Doped and Undoped ZnS and ZnO Thin Films Using Spra Pyrolysis Technique	
		4.3.1 Spray Pyrolysis Structure	45
		4.3.2 Fabrication of ZnO via Spray Pyrolysis	46
		4.3.3 Fabrication of ZnS via Spray Pyrolysis	46
		4.3.4 Growth ZnS and ZnO in Specific Temperature	47
	4.4	Measuring Instruments and Characterizations	47
		4.4.1 Structural Properties	47
		4.4.2 Morphological Properties	48
		4.4.3 Optical Characterisation	48
		· · · 1	

5 RES	SULTS AND DISCUSSION	50
5.1	Experiments Done by CBD Technique	50
	5.1.1 Investigation the Impact of Thermal Treatment Time on the Optical Properties of Na Doped ZnS Deposited on Glass Substrate	
	5.1.2 Thermal Treatment Effectiveness on the Optical Properties of Undoped ZnS with Double Molarity Deposited on Glass Substrate	52
	5.1.3 Optical Properties of Undoped ZnS with 4-Times Molarity Deposite on Glass Substrate	
	5.1.4 Influence of Thermal Treatment on The Optical Properties of Na Doped ZnS Deposited on FTO Substrate	54
	5.1.5 Effect of Annealing on the Optical Properties of Undoped ZnS with Double and 4-Times Molarity Deposited on FTO Substrate	
5.2	Experiment Done by Spin Coating Technique	57
	5.2.1 Optical Properties	57
5.3	Experiments Done by Spray Pyrolysis Technique	58
	5.3.1 Impact of Film Thickness on The Optical and Electrical Properties ZnO Thin Films	
	5.3.2 The Effect of Thermal Treatment Time on Optical Properties of Undoped and Na Doped ZnS Thin Films	59
	5.3.3 Influence Amount of Precursor Solution on the Optical Properties ZnO Thin Films	
	5.3.4 Optical Properties of ZnO Prepared by Different Precursor Solution	66
	5.3.5 Properties of ZnO Thin Films and ZnO/Si Heterojunction Cells \dots	67
	5.3.6 The Properties of Undoped and Na Doped ZnS Thin Films and ZnS/Si Heterojunction Cells	71
5.4	Conclusion	77
REFE	RENCES	79
DITRI	ICATIONS FROM THE THESIS	25

LIST OF SYMBOLS

 N_A^- Acceptor concentration

k Boltzmann constant

B Boron

 V_{bi} Built in potential

p Crystal momentum

 J_D Dark current density

 N_D^+ Donor concentration

q Electron charge

A Energy independent constant

 E_F Fermi energy level

t Film thickness

 E_{ν} Highest level of VB

*I*_o Incident intensity

 P_{in} Input power

d Lattice spacing

L light intensity

 R_L Load resistance

 E_c Lowest level of CB

 J_{mp} Maximum current density

 P_{max} Maximum power

 V_{mp} Maximum voltage

 V_{oc} Open circuit voltage

 E_g Optical band gap

n Order of diffraction

 J_L Photogenerated current density

h Planck's constant

*J*_o Saturated current density

Se Selenium

 $R_{\rm S}$ Series resistance

 J_{sc} Short circuit current density

 J_{SH} Shunt current density

 R_{SH} Shunt resistance

Si Silicon

Na Sodium

c Speed of light

T Temperature

I Transmitted intensity

V Voltage

 V_D Voltage across shunt resistance and diode

LIST OF ABBREVIATIONS

ALD Atomic layer deposition

AM Air mass

CB Conduction band

CBD Chemical bath deposition

CVD Chemical vapour deposition

FF Fill factor

FTO Fluorine tin oxide

IR Infrared

ITO Indium tin oxide

MBE Molecular beam epitaxy

MOCVD Metalorganic chemical vapour deposition

PCE Power conversion efficiency

PV Photovoltaic

RS Rock salt

SEM Scanning electron microscopy

STC Standard testing conditions

UV Ultraviolet

VB Valance band

VIS Visible renge

WZ Wurtzite

XRD X-ray diffraction

ZB Zincblende

LIST OF FIGURES

Figure 1.1 Installed power generation capacity by the Stated Policies Scenario, 2000-2040
Figure 1.2 Register efficiency chart published by the National Renewable Energy Laboratory (NREL, status 2019) as an overview of all the different photovoltaic technologies
Figure 2.1 The schematic band diagrams of electrical conductor, semiconductor and insulator
Figure 2.2 Diagram of the band structure of conductors, semiconductors and insulators where E_g represents the band gap
Figure 2.3 Impurity energy levels in semiconductors, (a) donor impurity, (b) acceptor impurity
Figure 2.4 The basic bonds of semiconductors, (a) intrinsic Si, (b) n-type Si with donor (phosphorus), (c) p-type Si with acceptor (boron)16
Figure 2.5 Illustrate the p-n junction in thermal equilibrium
Figure 2.6 Crystal structure of ZnO and ZnS showing the tetrahedral coordination of the Zn with both O and S: (a) cubic rocksalt, (b) cubic zinc blend, and (c) hexagonal wurtzite
Figure 2.7 Diagram of (a) diffraction of x-rays by a crystal, (b) the x-ray spectroscopy
Figure 2.8 Diagram of the core components of an SEM microscope22
Figure 2.9 Classification of thin film deposition techniques
Figure 3.1 Solar irradiance spectrums with respect to the wavelength28
Figure 3.2 (a) Energy band diagram of n-ZnS/p-Si heterojunction in equilibrium [87], (b) schematic diagram of n-ZnO/p-Si heterojunction in equilibrium
Figure 3.3 Photon transitions in semiconductor at (a) $hv = E_g$, (b) $hv > E_g$,
(c) $h\nu < E_g$ 32
Figure 3.4 Equivalent circuit diagram of solar cell
Figure 3.5 The J-V characteristics of a solar cell in dark and under illumination
Figure 3.6 The J - V characteristic of a solar cell under illumination. The short circuit current J_{sc} and the open circuit voltage V_{oc} are shown. The maximum power point is also illustrated
Figure 4.1 Chemical bath deposition (CBD) system41
Figure 4.2 The process of spin coating deposition technique44

Figure -	4.3 Flow chart diagram of the synthesis of ZnS thin film
Figure -	4.4 Schematic of spray pyrolysis deposition technique45
Figure -	4.5 Schematic diagram of n-ZnS/p-Si or n-ZnO/p-Si heterojunctions48
Figure	5.1 (a) Transmittance spectra and (b) plots of $(\alpha h \nu)^2$ as a function of photon energy of unannealed and annealed Na doped ZnS thin films
Figure	5.2 (a) Transmittance spectra and (b) plots of $(\alpha h v)^2$ as a function of photon energy of unannealed and annealed Na doped ZnS thin films with double molarity
Figure	5.3 (a) Transmittance spectra and (b) plots of $(\alpha h \nu)^2$ as a function of photon energy of Na doped ZnS thin films with 4-times molarity52
Figure	5.4 (a) Transmittance spectra and (b) plots of $(\alpha h \nu)^2$ as a function of photon energy of Na doped ZnS thin films deposited on FTO substrate
Figure	5.5 (a) Transmittance spectra and (b) plots of $(\alpha h \nu)^2$ of the unannealed and annealed Na ZnS thin filmswith double molarity deposited on FTO substrate
Figure	5.6 (a) Transmittance spectra and (b) plots of $(\alpha h \nu)^2$ of the unannealed and annealed Na doped ZnS thin films with 4-times molarity deposited on FTO substrate
Figure	5.7 (a) Transmittance spectra (b) absorption coefficient of ZnS thin film prepared by spin coating56
Figure	5.8 Plots of $(\alpha h \nu)^2$ as a function of $h \nu$ for ZnO films at different thicknesses
Figure	5.9 (a) Transmittance spectra (b) absorpance of undoped ZnS thin films before and after annealing at 450 °C59
Figure	5.10 (a) Transmittance spectra (b) absorpance of 1% Na doped (0.05 M ZnCl ₂ +0.05 M of SC(NH ₂) ₂) of ZnS thin films before and after annealing at 450 °C
Figure	5.11 (a) Transmittance spectra (b) absorpance of ZnS (1% Na doped 0.025 M of ZnCl ₂ +0.025 M of SC(NH ₂) ₂), before and after annealing at 450 °C
Figure	5.12 (a) Transmittance spectra (b) absorpance of ZnS (5% Na doped 0.025 M of ZnCl ₂ +0.025 M of SC(NH ₂) ₂), before and after annealing at 450 °C Schematic of spray pyrolysis deposition technique62
Figure	5.13 (a) Transmittance spectra (b) absorpance of ZnS (10% Na doped 0.025 M of ZnCl ₂ +0.025 M of SC(NH ₂) ₂), before and after annealing at 450 °C e
Figure	5.14 (a) Transmittance spectra and (b) absorpance of ZnO thin film (0.05) M of zinc acetate dihydrate at different amount of precursor solution

Figure	5.15 (a) Transmittance spectra and (b) absorption of ZnO thin film prepared by zinc acetate and zinc chloride
Figure	5.16 XRD pattern of spray pyrolised ZnO thin film
Figure	5.17 J-V characteristics of (a) non-annealed ZnO/Si heterojunction cell (b) annealed ZnO/Si heterojunction cell (1: in dark, 2: under illumination)
Figure	5.18 J-V characteristics of non-annealed and annealed ZnO/Si Heterojunction cell under illumination chematic69
Figure	5.19 XRD patterns of undoped and doped ZnS thin films prepared by spray pyrolysis sprayed at 350°C70
Figure	5.20 SEM images of (a) undoped, (b) 15% Na doped ZnS films were grown on glass substrate at 350°C71
Figure	5.21 (a) Transmittance versus wavelength plots (b) absorption spectra, of undoped, 1%, 5%, 10% and 15% Na doped
Figure	5.22 Current-voltage characteristics of ZnS/Si heterostructures with doped and undoped ZnS layers under illumination

LIST OF TABLES

Table 2.1 Essential properties	of different classes of solid state materials	12
Table 4.1 Percentage of solver	nt materials	41
<u> </u>	en non-annealed and annealed ZnO/Si ls	69
	films and ZnS/Si cells with undoped and Na do	-

Semiconducting Junctions for Solar Energy Production

Huda M. Muneer ABD ALQADER

Department of Physics

Doctor of Philosophy Thesis

Supervisor: Assoc. Prof. Dr. Serço Serkis YEŞİLKAYA

Solar energy has regarded as the latest comparatively sustainable energy source due to its low cost, eco-friendly and large scale the productibility. Silicon-based solar cells having a significant interest for many years. However, production and fabrication techniques are demanded which make the solar cells more cheaper. Therefore, thin film solar cells have emerged to be an alternative. Thin film technology is considered as inexpensive given that devices have a small amount of material and are established on varied pattern of light absorbing semiconductors. Furthermore, appropriate materials should be prepared, inexpensive, and show a stable behavior over long periods of operation. Zinc sulfide and zinc oxide are considered as the most favorable materials for heterojunction solar cells.

This thesis aims to produce high efficiency and cost-effective solar cells by useing the energy that comes from the sun as an alternative and clean energy source. ZnS and ZnO thin films including silicon based solar cells were grown by using easy and economic techniques which are chemical bath deposition, spin coating, and spray pyrolysis techniques. Properties of undoped and Na doped ZnS thin films

were grown on glass and Si substrates by spray pyrolysis were investigated. Effect of annealing time and precursor solution amount of ZnO films on the optical properties were investigated. Structural, morphological, optical and electrical properties were examined by using XRD, SEM, UV-Visible spectrometry, and resistivity measurement.

It had been found that the band gap energy of ZnS film was decreased to 3.42 eV from 3.66 eV and the resistivity of the film was decreased to 2.00 x10 5 Ω from 5.17 x10 5 Ω with increasing Na doping concentration. Performance of ZnS/Si heterojunction cell was improved to increase from 2.20% to 5.06% by Na doping. Moreover, the conversion efficiency of undoped and Na doped ZnS/Si is higher than undoped ZnO/Si fabricated under the same condition.

Keywords: ZnS, ZnO, semiconductors, heterojunction, solar cells.

YILDIZ TECHNICAL UNIVERSITY

Güneş Enerjisi Üretimi İçin Yarı İletken Eklemler

Huda M. Muneer ABD ALQADER

Fizik Anabilim Dalı

Doktora Tezi

Danışman: Doç.Dr. Serço Serkis YEŞİLKAYA

Güneş enerjisi, düşük maliyeti, çevre dostu ve büyük ölçekli üretilebilirliği nedeniyle en son sürdürülebilir enerji kaynaklarından kabul edilmiştir. Silisyum esaslı güneş pilleri uzun yıllardır büyük ilgi görmektedir. Ancak güneş pillerini daha ucuz hale getiren üretim ve imalat teknikleri talep edilmektedir. Bu nedenle ince film güneş pilleri bir alternatif olarak ortaya çıkmıştır. İnce film teknolojisi, cihazların az miktarda malzemeye sahip olması ve çeşitli ışık soğurucu yarı iletkenleri modeline dayanması nedeniyle ucuz olarak kabul edilir. Ayrıca, uygun malzemeler hazırlanmalı, ucuz olmalı ve uzun çalışma süreleri boyunca kararlı bir davranış sergilemelidir. Çinko sülfür ve çinko oksit, heteroeklem güneş pilleri için en uygun malzemeler olarak kabul edilir.

Bu tez, güneşten gelen enerjiyi alternatif ve temiz bir enerji kaynağı olarak kullanarak yüksek verimli ve uygun maliyetli güneş pilleri üretmeyi amaçlamaktadır. Silisyum esaslı güneş pilleri içeren ZnS ve ZnO ince filmler kimyasal banyo biriktirme, döndürmeli kaplama ve kimyasal püskürtme teknikleri gibi kolay ve ekonomik teknikler kullanılarak büyütülecektir. Katkısız ve Na katkılı ZnS ince filmler cam ve Si alttaşlar üzerinde kimyasal püskürtme ile büyütülecektir. ZnO filmlerin tavlama sürelerinin ve öncü çözelti miktarının optik

özelliklere etkisi incelenmiştir. Yapısal, morfolojik, optik ve elektriksel özellikler XRD, SEM, UV-Görünür spektrometri ve özdirenç ölçümü kullanılarak incelenmiştir.

Artan Na katkılama konsantrasyonu ile ZnS filmin bant aralığı enerjisinin 3.66 eV'den 3.42 eV'a düştüğü ve filmin özdirencinin 5.17 x 10^5 Ω 'dan 2.00 x 10^5 Ω 'a düştüğü tespit edilmiştir. ZnS/Si heteroeklem pillerin verimi %2,20'den %5,06'ya artacak şekilde iyileştirilmiştir. Ayrıca, aynı koşulda katkısız ve Na katkılı ZnS/Si'nin dönüşüm verimliliği, katkısız ZnO/Si'den daha yüksektir.

Anahtar Kelimeler: ZnS, ZnO, yarı iletkenler, heteroeklem güneş pilleri.

YILDIZ TEKNİK ÜNİVERSİTESİ

1.1 Litrature Review

Energy is a principal item for civil development during the industrial revolution, and the required energy was provided by burning carbon-based fossil fuels in the form of oil, coal, and natural gas [1].

These energy sources have done their service; however, one-third of the world's population has no approach to this energy currently, as well as the massive use of carbon-based fossil fuels, which has also polluted the environment. Beside global population growing from 1 billion in the 1600s to 7.5 billion presently (2017), and a proposed increase to 9.7 billion by 2050 [2], this increase leads to not only an increase in global energy consumption but also the emission of the CO2 will rise to 150% of the present level by 2050 [3]. In addition, the rapid growth in energy demand coupled with the continuous depletion of easy-access fossil fuel, is constituting a significant deficit in the future energy industry [1]. In other words, we have to consider how life will continue when these sources of energy are gone and we must start to develop alternatives [4].

The major solution to this is the rapid submitting of renewable energy sources, such as biomass, hydro, solar, wind, etc., to generate our future energy, in order to fill this shortage and reducing the further environmental pollution [1]. Renewable energy has recognized an enormous interest during the last two decades. Solar energy comes at the topmost of the renewables list, since it is viewed as the cleanest source of energy and last polluting and inexhaustible of all energy sources.

Solar energy can be defined in simple as the energy collected directly from sunlight [5]. Each second, the sun converts more than four million tonnes of its own mass – mostly hydrogen and helium – into energy, producing neutrinos as well as solar radiation, radiated in all directions. A tiny fraction – half a trillionth

– of this energy falls on Earth after a journey of about 150 million kilometers, which takes a little more than eight minutes.

There is a great benefit to solar energy in terms of geographical location, owing to the fact that, solar energy displays a clean, climate-friendly, very abundant and inexhaustible energy resource to humankind, relatively well-spread over the globe and hence does not criminate against any country. However, this is not true for traditional sources, such as oil, which are located only in specific places.

All countries and economies are in a position to gain by understanding solar energy's potential to fill a very large part of total energy require economically, in a secure and sustainable way in the future. It can also help to curtail greenhouse gases (GHGs) that threaten irreversible climate change for the planet.

The entire life on earth is based on solar energy following the contrivance of photosynthesis by the algae. During the previous decades, the developments in solar energy applications have made it viable to use solar energy for most of our energy needs [5]. Electrical energy is one of the most advantageous forms of energy as it can be used for almost everything.

Consequently, producing electrical energy through photovoltaic energy conversion by solar cells is the human counterpart and it will be essential in the future because it is sustainable photovoltaic energy conversion.

The field of photovoltaics (PV) has been expanding since around 1995 owing to considerable cost reductions of solar cells, technological advances, panels, inverters, and by more advantageous regulatory frameworks. At present, photovoltaic (PV) systems have become an established part of the electrical energy mix in many countries all around the globe. Heretofore, no single other energy technology has displayed such a distributed set-up as PV systems, which can provide power in an expanded range, from tenths of watts up to hundreds of megawatts [6].

From Figure 1.1, we can see the total cumulative capacity of Solar PV and it will become the largest component of global installed capacity in the Stated Policies Scenario until 2040 [7].

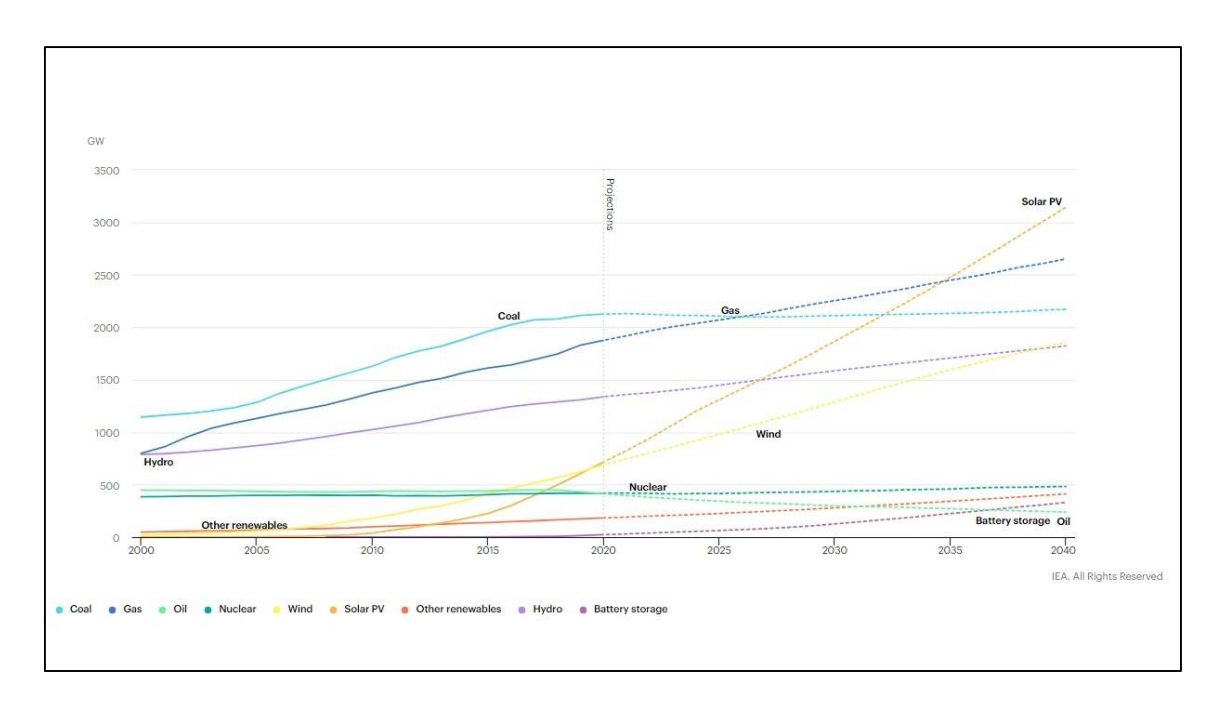


Figure 1.1 Installed power generation capacity by the Stated Policies Scenario, 2000-2040 [6]

Photovoltaic (PV) energy conversion technology is concerned with the direct conversion of solar energy (electromagnetic radiation from the sun, which consists of ultraviolet (UV), visible and infrared (IR)) into electricity by using solar cells without any "greenhouse" gas emission [8] [9]. Silicon (Si) solar cells currently dominate the photovoltaic (PV) market with over 80% of the market share, in view of the available and rich industrialization processes advanced for integrated circuit manufacturing [9].

Even so, the production of these thick silicon solar cells expensive as a consequence of the high cost of materials and high preparation process temperatures. Therefore, thin-film solar cells are 200 times thinner and thus carry the potential to reduce the cost of PV solar cells due to low material consumption, simple production methods as well as high productivity by depositing on huge areas [10].

Lowering the costs of PV modules is one of the most important scientific and technical topics, as a result of the current worldwide efforts to combat climate change. For this reason, two methodologies are generally pursued to achieve this goal, first is to utilize low-grade raw materials and the other is by rising the power conversion efficiency (*PCE*) [9]. Figure 1.2 illustrates the register efficiency chart

published by the National Renewable Energy Laboratory [11], which shows a wide spectrum of different solar cell technologies.

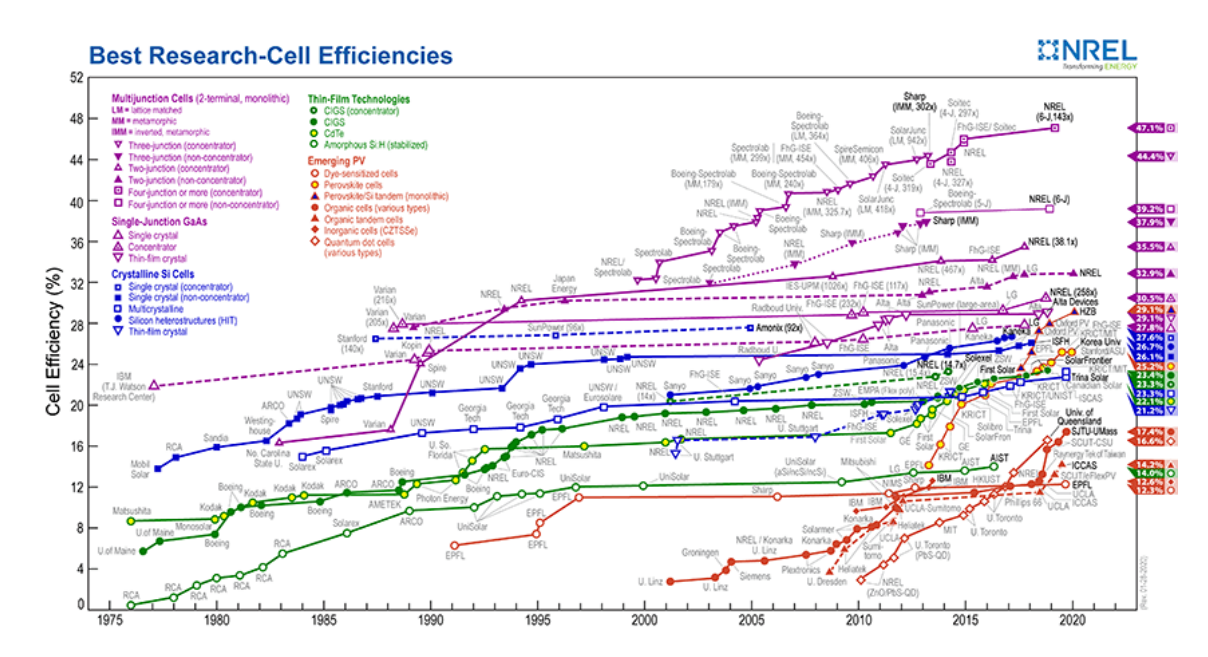


Figure 1.2 Register efficiency chart published by the National Renewable Energy Laboratory (NREL, status 2019) as an overview of all the different photovoltaic technologies [11]

The main differences between these techniques are related to the materials, production process as well as their recorded efficiencies. At present, technologies are based on crystalline silicon (c-Si), crystalline gallium arsenide (GaAs); thin-film technology [cadmium telluride (CdTe), copper indium gallium selenide (CIGS), and silicon (microcrystalline and amorphous)], and organic technology (organic-inorganic perovskite or organic dye-sensitized) [12]. Notwithstanding their differences, these technologies arrow a common ground with respect to the basic physics associated with the generation of power. The fabrication of PV cells is classified into three categories first-, second- and third-generation solar cells.

The first generation includes monocrystalline silicon (mono-Si) - and polycrystalline silicon (poly-Si) - based solar cells [13]. These solar cells are the most established of all the solar cell categories and they have known not only high material applications (as bulk materials) but also high fabrication costs.

The second-generation solar cells incorporate thin-film technology that utilizes inexpensive raw materials and cost-effective manufacturing techniques as

amorphous silicon (a-Si), copper indium gallium diselenide (CIGS) and cadmium telluride (CdTe) thin-film.

While, the third-generation solar cells are identified by thinner films, low fabrication temperatures, high efficiencies, and lower cost [8] [9]. Among various materials and structures, Si-based nanostructures, are particularly promising for enhancing the *PCE* [9].

The notable progress in nanostructured materials has received much consideration during the last decade owing to their novel properties, which contradict from those of bulk materials [14]. In addition, the performance of the material is extremely depending on the properties of the material surface. Recently, various hetero-structure photovoltaics have been widely studied, however, there are many limitations such as high ideality factor over one, high serious resistance, and low photocurrent [15]. So as, to overcome those limitations, transparent-conducting semiconductors/Si heterojunction have been investigated [16].

Among those semiconducting materials, Zinc sulfate (ZnS) and Zinc oxide (ZnO) have useful properties to act as a window layer in a heterojunction solar cell; moreover, they have been extensively utilized in optoelectronic device technology on account of their high chemical and thermal stability [17] as well as unique electrical and optical properties [16].

ZnS and ZnO are important II-VI semiconductor materials in wide band gap, E_g =3.68eV and 3.37eV, respectively. They have high transparency in visible and near infrared region, sizable exciton binding energy of 39meV and 60meV respectively [18], low resistivity, and high refractive index [17], ability to form textured coating via anisotropic growth that can be utilized in crystalline Si solar cell in addition to a good thermal and chemical stability [19]. These characteristics make ZnS and ZnO promising materials and might be able to satisfactorily the perform desired purpose efficiently and successfully [20]. They are used in a wide range of applications such as electroluminescent, flat panel display, piezoelectric devices [21], light emitting diode [16] [22], gas sensor [23] and solar cells [19] and so on.

The only considerable obstacle of ZnO that holds up its use in the fabrication of a homojunction device is due to cannot be p-doped deservedly. However, n-ZnO has been found to have applications in several optoelectronic devices [24]. Whereas ZnS may in principle support in both n-and p-doping. ZnS and ZnO exhibit polymorphism as two main crystalline forms can be observed, namely the most stable zincblende (ZB) and the high-temperature and synthetically achievable with wurtzite (WZ) symmetry. ZnS, ZnO can be transparent in an excessively wide energy range, with a very large transmittance from visible wavelengths [18].

The n-(ZnS, ZnO)/p-Si heterojunction have a great deal of interest, owing to the fact that silicone has a significant place in the microelectronic industry, with advantages such as high quality as well as a big area p-type substrate available at low cost. Nevertheless, the devices quality remains somewhat poor, attributed to the large energy band offset (or electron affinity) and the lattice mismatch between the deposited ZnO or ZnS films and Si substrate [25] [26].

Semiconducting materials supply the essential functions of a photovoltaic (PV) device, specifically the optical absorption and creation of rectifying junctions that convert light into electricity. Accordingly, the establishment of a convenient material growth technique is substantial in the PV development process [1].

ZnS and ZnO can be deposited by various semiconductor growth techniques such as molecular beam epitaxy (MBE), metalorganic chemical vapour deposition (MOCVD), and their modifications are well known as high-quality semiconductor growth techniques [1], pulsed laser deposition [16], chemical vapor deposition CVD [27], and atomic layer deposition ALD [24]. However, these techniques are not suitable for manufacturing large-area devices. Whereas semiconductor growth techniques such as sol-gel or spin coating [28], chemical bath deposition (CBD) [29] and spray pyrolysis [30] are popular on account to the fact that they are low costs, non-vacuum application and they have been developed to grow large-area thin films [1].

In CBD, which is well known as a prevalent low-temperature aqueous technique [31] that diverse nanostructures can be obtained simply by varying concentrations of the solution, precursor chemicals, not only growth temperature but also growth

time [32]. In the case of spin coating or sol-gel, is known as a cheap chemical technique that fabricates thin films through the process of phase transform from liquid (sol) to a solid phase (gel) [33]. While in spray pyrolysis, which is the most widely used one for the preparation of metal oxide thin films owing to its simplicity, affordable method with uniform coating, non-vacuum system of deposition and has large area coating with device quality [14].

Many issues related to ZnO and ZnS thin films and deposited on Si substrate have been studied in previous works. In [24] authors stated that the possibility of producing highest efficiency is established with n-ZnO/p-Si heterojunction solar cells by employing atomic layer deposition and hydrothermal methods and the efficiency of this solar cell is 10% and 14% for planar and textured structures respectively. Given that undoped ZnO thin films are not stable particularly at high temperature, doping the ZnO can decrease this disadvantages and minimize the resistivity which lead to increase in the conductivity . The ZnO doping is attained by replacing Zn^{2+} atoms with atoms of dopant elements, which behave as interstitials and vacancies in ZnO lattice.

Kahraman *et al* studied the influence of the Al, K, and Co dopant elements on the properties of ZnO thin films by CBD method. They established that the band gap values of the doped structures were greater than the intrinsic one. This increasing was attributed to a deterioration that happened in the lattice of the structure after doping [32].

In [16] zinc oxide (ZnO) thin films have been grown on p-Si substrate by means of using pulsed laser deposition, the fulfillment of the n-ZnO/p-Si heterojunction was enhanced by post-annealing at 200 C° which is presented power conversion efficiency (*PCE*) with and without Al-doped of 0.16% and 1.5% respectively from ultraviolet to infrared.

Qiu *et. al.* found in their study that ZnS thin films and ZnS/p-Si heterojunction solar cells, were fabricated by thermal evaporation technique, exhibited good smoothness and oriented in [111] direction. The band gap of 3.72eV was calculated from the optical transmittance. The power conversion efficiency of the

device was 8.83% as well as long term stability of the solar cell was also proved [34].

Jlassi *et. al.* [14] studied the structural, morphological, optical and electrical properties of undoped and Ni doped ZnO thin films prepared by spray pyrolysis technique. They found that X-ray diffraction spectra shows that the films (undoped and Ni doped) are of polycrystalline nature. From AFM images, they declared that the crystallite of the Ni doped ZnO films was decreased with increasing Ni concentration. The optical properties of the films obtained show that the layers are transparent in visible and absorb in the near UV. The electrical properties presented an improvement of the conductivity of the obtained layers by decreasing the electrical resistivity from 4.8×10^4 to $10^3 \Omega$.

1.2 Objective of the Thesis

Increasing population of the world and developing technology increase the need for energy day by day. Existing classical energy sources pollute the environment and will be depleted in the near future due to lack of reserves. This thesis aims to produce high efficiency and cost-effective solar cells in order to benefit from the sun as an alternative and clean energy source. ZnS and ZnO including Silicon based solar cells will be fabricated using non vacuum methods such as spray pyrolysis, chemical bath deposition and spin coating. Materials and methods had chosen considering the ease and economy of the production method, use of nontoxic and economic materials. We aim to improve the fabrication techniques and properties of ZnS and ZnO thin films as well as the characteristics of silicon based solar cells.

1.3 Hypothesis

Characteristics and efficiency of solar cells strongly depend on the properties of the materials and the fabrication techniques. We assume that properties of ZnS and ZnO films can be improved by modifying the fabrication techniques and applying some effects such as doping and thermal annealing and therefore we can achieve higher efficiency solar cells. This thesis is organized as follows: in chapter 2 the materials fundamental and concepts related to fabrication techniques are introduced. Chapter 3 presented the basics parameters of photovoltaics as well as the basic parameters and device characterization. Experimental techniques employed in this study are discussed in chapter 4. Results and discussion are explained in chapter 5. In chapter 6, conclusions for the results related to this work are displayed.

MATERIALS AND FABRICATION TECHNIQUES

This chapter discuss the background of semiconductor materials. Direct and indirect semiconductors are reviewed first; including details of doping semiconductor, p-type and n-type, then the p-n junction are reviewed. The importance of ZnS and ZnO as well as the structural characterization technique are presented. The chapter will conclude with the growth methods that used in this study.

2.1 Semiconductor Materials

Solid state materials can be categorized into three assembles; conductors, insulators, and semiconductors. The outstanding property peculiar to this classification is their band gap (E_g) as specified by the interatomic interaction resulting in both the energy valence band (E_v) and the energy conduction band (E_c) [8]. Insulators are materials that are not conduction electrical current under the normal condition as well as having a high resistivity. Moreover, electrons presents in valance band are extremely bonded to their atoms. On other words, the energy band of insulators have a full valance band (VB), empty conduction band (CB), and the energy band gap is very large. In case of conductors, the materials have a good conductivity and a large number of free electrons available in electrical conduction. Normally, most of metals are perfect conductors, such as gold (Au), silver (Ag), and copper (Cu) [1].

Semiconductor are the fundamental materials that are used in photovoltaic (PV) devices, having a conductivity σ that is used to differentiate between those of insulators and of conductors. The conductivity of a semiconductor is sensitive to each of temperature, magnetic field, illumination as well as impurity atoms which makes the semiconductor a fundamental materials for electronic applications [35][6]. Through the years, many semiconductors have been investigated and categorized in groups. Semiconductors could occur in distinct chemical

construction with a large assortment of crystal structures. They can be either elemental semiconductors, which consist of single species of atoms like silicon (Si) and selenium (Se) or compound semiconductors such as gallium arsenide (GaAs) which formed from elements from groups III and V of the periodic table, zinc sulfide (ZnS) and zinc oxide (ZnO) from groups II and VI [36].

Figure 2.1 illustrates the graphical band diagrams of an electrical conductor, a semiconductor and an insulator, respectively. The conduction band CB represents the electron-empty energy band and E_c represents the lowest level of energy in the CB, while the valence band VB is the allowed energy band that is saturated with electrons at 0 K and represents the highest level of energy in the VB is labeled E_{ν} [8].

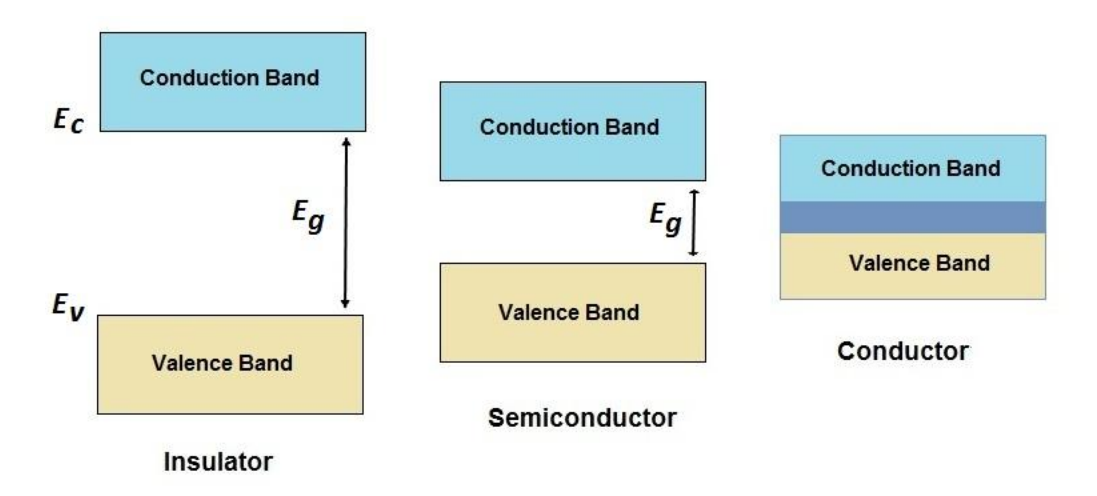


Figure 2.1 The schematic band diagrams of electrical conductor, semiconductor and insulator [35]

The generation of electric energy in photovoltaic devices depends on the direct conversion of sunlight into an electric potential through the photovoltaic effect, which is qualified to derive a current. For an electron to reach a conducting state, it needs to absorb a particular quantity of energy (equal or higher than E_g), which can be provided either thermally or by irradiation. In metal (conductor), the conduction band CB overlaps with the valence band VB, which is partly filled with electrons. Therefore, there is no energy required to excite an electron. Whereas in both insulators and semiconductors, their conduction bands are empty of electrons and valence band are totally filled with electrons and the main difference between

them is in the band gap E_g as it is very large in the insulator, while it is lower in semiconductors and it can be variated by changing many factors [8] [37].

The representative values for the band gap of semiconductors are on the range of 0.5-2 eV corresponding the energies correlating with the light of the spectral range from ultraviolet (UV, $\lambda \le 400$ nm), visible, to infrared (IR, $\ge \lambda$ 700-1050 nm) [37] Semiconductors are poor conductors at low temperatures due to the fact that at T= 0 K the entire electrons are in the valence band, and there are no electrons in the conduction band [33]. The excitation of electrons from the VB to the CB leaves behind an equal quantity of net positive charges in the VB are called holes; a hole is a quasi – particle representing the deficiency of electron. Further, the categorize of solid state materials with respect to the energy band gap E_g and conductivity are illustrated in Table 2.1[8].

Table 2.1 Essential properties of different classes of solid state materials [8]

Parameter	Electrical conductors	Semiconductors	Electrical insulator
Electrical conductivity σ (Ω cm) ⁻¹ \equiv S	~10 ⁶ -10 ⁰	~10°-10-8	~10 ⁻⁸ -10 ⁻²⁰
Band gap E_g (eV)	≤ 0.3	~0.3-4.0	> 4.0

Both of the valence band and conduction band depend on the value of k-vector, which is characterizes the crystal momentum (p) of semiconductor material. Furthermore, semiconductors materials can be also classified in regard to their band alignment to direct and indirect semiconductors [35]. In the following sections we will introduc the classification of semiconductor based on their band alignment and dopant incorporation.

2.2 Direct and Indirect Semiconductors

The electronic states of semiconductor materials may be further characterised by their crystal momentum p. Typically, optical transition (such as the excitation or relaxation of an electron between bands), must conserve electron momentum, thus, if the electron momentum changes between bands a third body (generally a lattice phonon) must be involved in the transition.

On condition that the maximum point of the valance band and the minimum point of the conduction band take place at (p=0), the transitions of the electrons momentum do not change, so, that referred to as direct transitions. If the maximum-energy state in a semiconductor's valence band has the same crystal momentum as the minimal-energy state in its conduction band, such direct transitions occurs regularly, and the materials are known as a direct-band gap semiconductors, such as Si, ZnS and ZnO [14]. In the event that, the valence band maximum and the conduction band minimum do not have the same crystal momentum, such direction transitions are forbidden, and the material is known as a indirect-band gap semiconductor, for instance GaAs and AlAs. Both cases including direct and indirect band gap semiconductors are illustrated in Figure 2.2

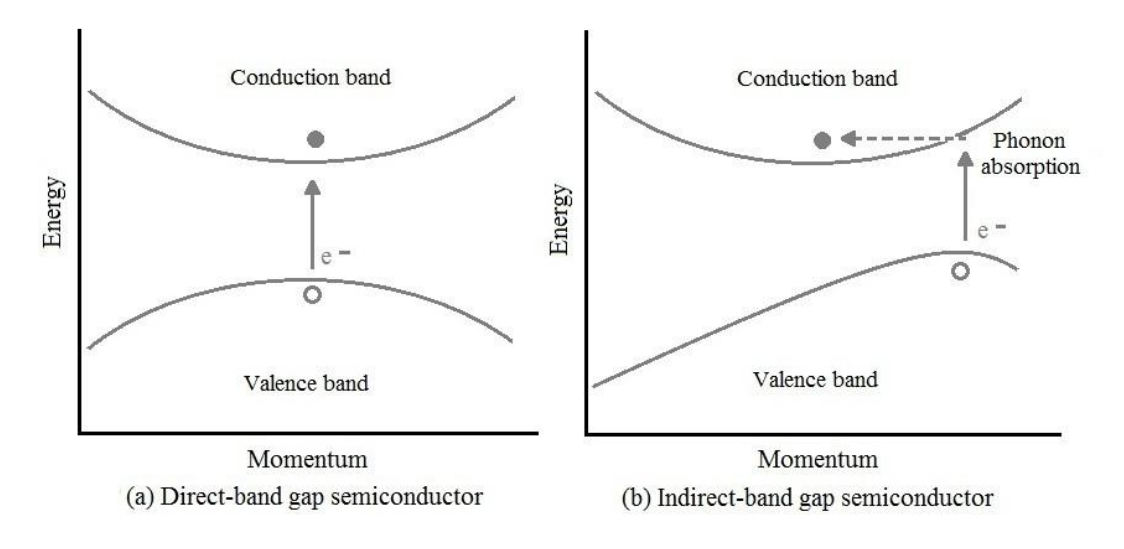


Figure 2.2 Diagram of the band structure of conductors, semiconductors and insulators where E_g represents the band gap [35]

Charge recombination in direct-band gap semiconductors generally proceeds by a process recognized as direct recombination, in which an electron relaxes from the conduction band to the valence band without any change in momentum. Such a

phenomenon is uncommon in indirect-band gap semiconductors, since electrons at the bottom of the conduction band and holes at the top of the valance band do not have the same momentum. In a situation like this, the electron may relax by simultaneous interaction with a lattice phonon, or it may relax through localized energy states caused by lattice defects. These indirect recombination processes occur much more scarcely than direct recombination. Correspondingly, electronhole pairs on indirect-band gap semiconductors exhibit much longer lifetimes τ than those on direct-band gap semiconductors [35].

2.3 Doping Semiconductors

One of the most significant properties of a semiconductor is that it can be doped via different types of concentrations of impurities in order to improve its properties [38]. The doping process leads to a change in the conductivity of semiconductors by either donating electrons to the conduction band or accepting electrons from the valance band through generating holes. They are, as consequently called donors and acceptors respectively. Semiconductors are assorted, according to add impurities, into intrinsic and extrinsic semiconductors.

For undoped semiconductors, without adding any external dopant species are called intrinsic also are referred to as i-type semiconductors. Whereas semiconductors in which impurities are added, known as extrinsic semiconductor materials, and impurity energy levels are introduced. The conductivity of extrinsic semiconductors is larger than intrinsic semiconductor. For this reason, extrinsic semiconductors are highly used to fabricate electronic devices such as diodes and solar cells. There are two types of doping (impurities), pentavalent and trivalent materials that are added to intrinsic semiconductors to form extrinsic semiconductors, which are happend within the band structure of the semiconductor and that will be illustrated in the following section [37].

Figure 2.3 illustrates the band diagram of the intrinsic and extrinsic semiconductor. The acceptor energy level is near the VB and the donor energy level is located under the CB.

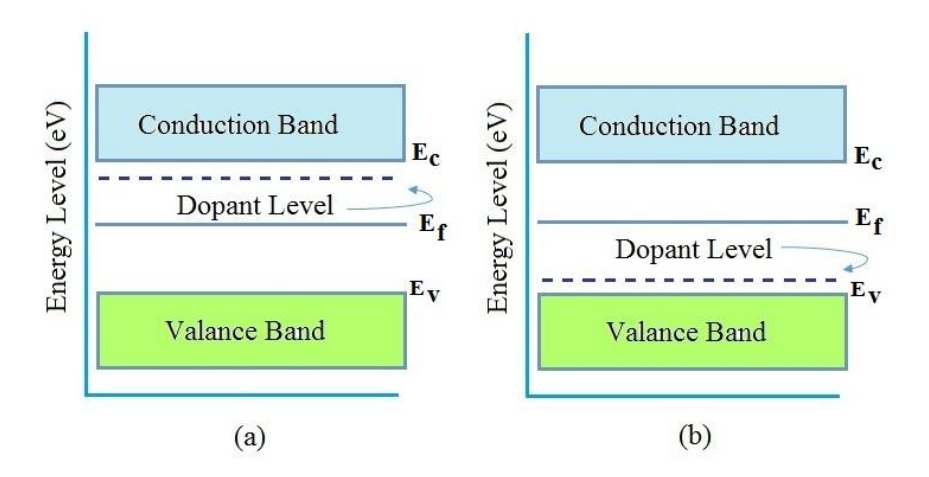


Figure 2.3 Impurity energy levels in semiconductors, (a) donor impurity, (b) acceptor impurity [37]

2.3.1 P-type and n-type Semiconductors

When trivalent impurities are added to the intrinsic semiconductor, the number of holes are increased and formed a p-type semiconductor, which is known as acceptor materials. For example, when a boron (B) atom with three valance electrons replaces a Si atom, a positively charged "hole" is created in the valance band and an additional electron is "accepted" to form four covalent bonds around the boron atom.

Similarly, by adding a pentavalent impurity in intrinsic semiconductor materials to increase the number of conducting electrons at conduction band and form n-type semiconductor. As in silicon atom Si which substituted by a phosphorous atom (P) with five valance electrons. The phosphorous atom constitutes covalent bonds with its four neighboring silicon atoms, and the fifth electrons can be ionized to become a "donated" conduction electron and the phosphorous atom is labeled as "donor" [35] [39]. Figure 2.4 presents that p-type and n-type semiconductors.

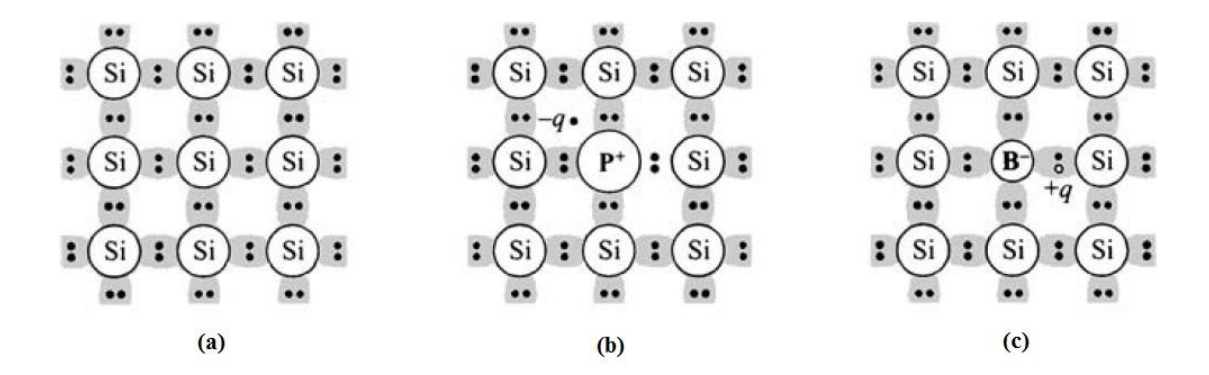


Figure 2.4 The basic bonds of semiconductors, (a) intrinsic Si, (b) n-type Si with donor (phosphorus), (c) p-type Si with acceptor (boron) [37]

In the case of p-type, the hole population in the VB is more than the free electron of the CB; therefore, the minority carriers in p-type semiconductor are free electrons while the majority carriers are holes. Likewise, in n-type the free electron population in the CB is more than holes of a VB, so the holes are the minority carriers whereas the free electrons are the majority carriers [37] [39].

2.3.2 P-n Junction

A p-n junction is the core of all semiconductor solar cells, which includes a p-type and n-type semiconductor combine together to form a junction. The basic theory of current-voltage characteristic of a p-n junction was confirmed by Shockley. Due to the fact that, the variation in the electrons and holes concentration on both sides, the large carrier concentration gradients across the junction. This means that holes diffused into the n-side from the p-side as well as electrons diffused into the p-side from the n-side. As holes continue to leave the p-side, some of the negative acceptor ions (N_A^-) near the junction are left uncompensated, fixed, and ionized charges. Similarly, electrons leave the n-type, they will leave some of the positive donor ions (N_D^+) near the junction uncompensated, fixed, and ionized charges. Consequently, accumulation of a negative charge on the p-side and a positive charge on the n-side will be created as illustration in Figure 2.5 [39].

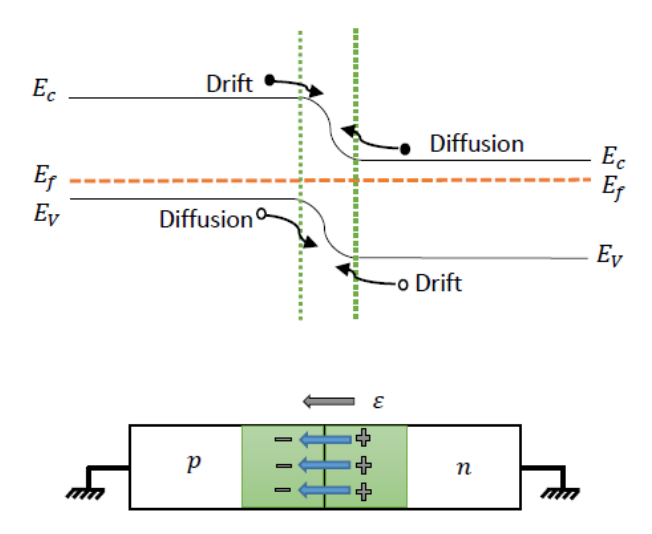


Figure 2.5 Illustrate the p-n junction in thermal equilibrium [39]

2.3.3 Built in Electric Field

When an n-type and p-type semiconductors are combine together, built-in electric field ε will establish whatever the semiconductors are the same or not. A charge region, which is called depletion region results in an electrostatic potential barrier created and hence an electric field ε will create in order to stop the further flow of the carriers. This electric field will help newly generated carriers to draft through the junction and after that to the external contacts of the solar cell [35].

2.4 Zinc Sulfide and Zinc Oxide

Zinc sulfide (ZnS) and zinc oxide (ZnO) are considered to be attractive II-VI binary compound semiconductors in the development of optoelectronic applications since they are wide band gap semiconductors [40] [41]. In the following sections, we will introduce the properties of both ZnS and ZnS in birefly.

2.4.1 Properties of Zinc Sulfide

ZnS is one of the first semiconductors discovered and has seriously attracted of many researchers. Studies on semiconductor devices showed that zinc sulfide ZnS is a good choice for many optoelectronic devices such as light emitting diodes, electroluminescent displays, sensors, photovoltaic cell etc [42] [43][44]. ZnS exists naturally in the common mineral sphalerite, although the ore form usually contains a big amount of iron, manganes or cadmium impurities [45] [46]. It

crystallize in the ambient temperature in three phases as hexagonal wurtzite (WZ), zinc blende (ZB) which has the most remarkable structure for optical materials, and rocksalt (RS) with band gaps of 3.77 eV, 3.6 eV, and 3.80 eV respectively as illustrated in Figure 2.6. Direct band gap, good optical and electrical properties make ZnS thin film preferable especially for photovoltaic devices [47].

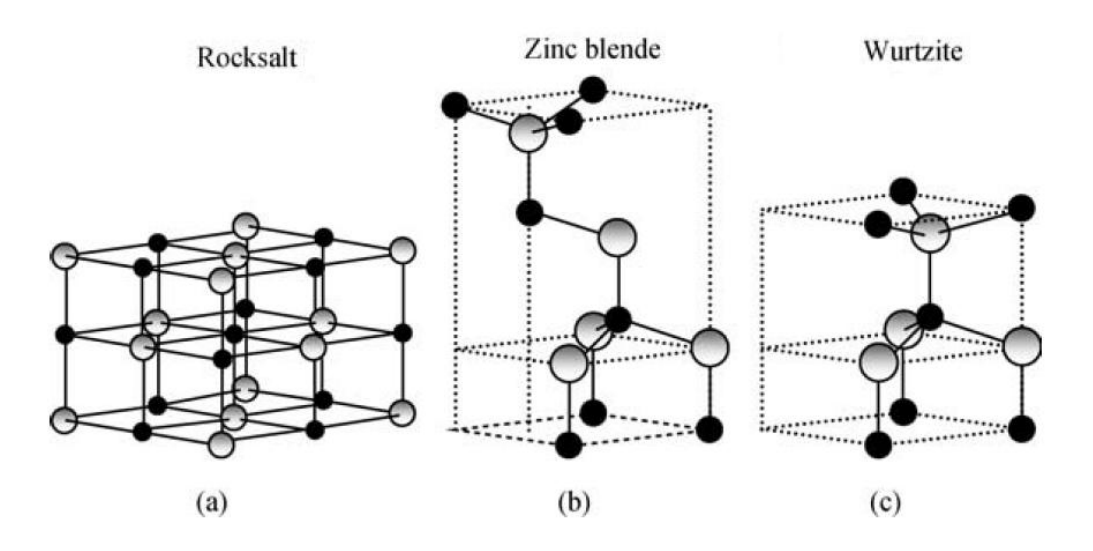


Figure 2.6 Crystal structure of ZnO and ZnS showing the tetrahedral coordination of the Zn with both O and S: (a) cubic rocksalt, (b) cubic zinc blend, and (c) hexagonal wurtzite [62]

Many theoretical and experimental studies using various methods have been reported to enhance the several properties of ZnS compound [48] and ZnS/Si heterojunction photovoltaic devices also considering the aboundancy, low cost and other advantages of Si [34] [49]. Materials used in a semiconducting device directly affect its performance, therefore, many studies have aimed to improve the properties of ZnS [50] [51] [52] [53].

Doping of ZnS film is a method used for improving its properties [54]. Numerous research done on doping ZnS film with Al [55], Cd [56], V [57], Mn [58] etc. but studies on Na doped ZnS thin films are limited [59]. So, in this study we aimed to investigate the effect of Na doping on the structural, optical and electrical properties of ZnS thin films. Moreover, we compared photovoltaic performance of ZnS/Si heterostructure cells with Na doped and undoped ZnS layers [60].

2.4.2 Properties of Zinc Oxide

Zinc oxide ZnO has been investigated already in 1912. With the beginning of the semiconductor age after the invention of transistor, systematic investigations of zinc oxide as a compound semiconductor were performed. Zinx oxide (ZnO) is a well-known semiconducting compound of the group II element zinc along with the group VI element oxygen. In addition, ZnO occurs naturally, as the rare mineral zincite even though most zinc oxide is produced synthetically [10]. ZnO plays significant roles in solar cell system, as silicon-based solar cells (first-generation), thin films (second-generation), and organic multi-junction, dyesensitized (third-generation) system either as a junction or as a transparent conductive oxide [61]. Due to the commercial demand for optoelectronic devices operating at blue and ultraviolet region, synthesis and characterizations of ZnO has been attracting attention for many years [62].

ZnO is naturally n-type owing to the fact that the high concentration of native shallow donor defects as: Zn interstitials or oxygen vacancies. To obtain the finite donor concentration, to optimize conductivity and diminishing un-controlled donor contents, the group III can be added as impurities (for example Al, Ga, or In) are used [17]. There is an extraordinary study to improve p-type electrical characteristics by implanting different dopants especially the group V such as N, P, As, and Sb. One of the most attractive materials to be a good choice for the production of p-n junction is Na dopant because of possible shallow acceptor production by replacing ZnO and Na [30].

ZnO crystalline structure varies between the zinc blende, hexagonal wurzite and the rocksalt as shown in Figure 2.6. It can be determined through the tetrahedrally coordinated bonding geometry. Each zinc ion has four oxygen neighbour ions in tetrahedral configuration and vice versa [63].

The thickness of the ZnO thin film layer has a remarkable effect on the change of the structural, electrical and optical properties. However, more application will play an important role to understand the thickness effect and surface properties of ZnO films for solar cell and other electronic application [64]. In this thesis, we study the effect of thickness on optical characteristics of ZnO thin film deposited on glass substrate

2.5 Structural Characterization Techniques

The crystallinity and morphology of the thin film play a significant role in the photovoltaics devices' performance [13]. In these sections, experimental techniques used in the present study for structural, morphological and optical properties of both ZnS and ZnO thin films will be briefly described.

2.5.1 X-Ray Diffraction (XRD)

X-ray diffraction is the method that used in the qualitative identification of crystalline materials based on Bragg's law.

$$2d_{hkl}\sin\theta = n\lambda\tag{2.1}$$

Where, d is the lattice spacing in nm, θ is the Bragg angle or the angle of the diffracted beam in degree, n is the order of diffraction and λ is the wavelength of the incident beam in nm. The XRD structure involves a beam source, a stage and a detector, as given in Figure 2.7. The wavelength of X-ray used is $K\alpha$ radiation from Cu sources, which emits X-ray at the wavelength 1.5418A°. For wurtzite structure, lattice parameters are determined using the spacing distance d of $\{hkl\}$ planes and Miller indices as.

$$\left(\frac{1}{d_{hkl}}\right)^2 = \frac{4}{3} \left(\frac{h^2 + k^2 + 2hk}{2a^2}\right) + \frac{l^2}{c^2}$$
 (2.2)

XRD has been carried out on numerous samples of as -deposited and heat-treated (ZnS and ZnO) to investigate any difference that might suggest mechanisms for visible scattering [65].

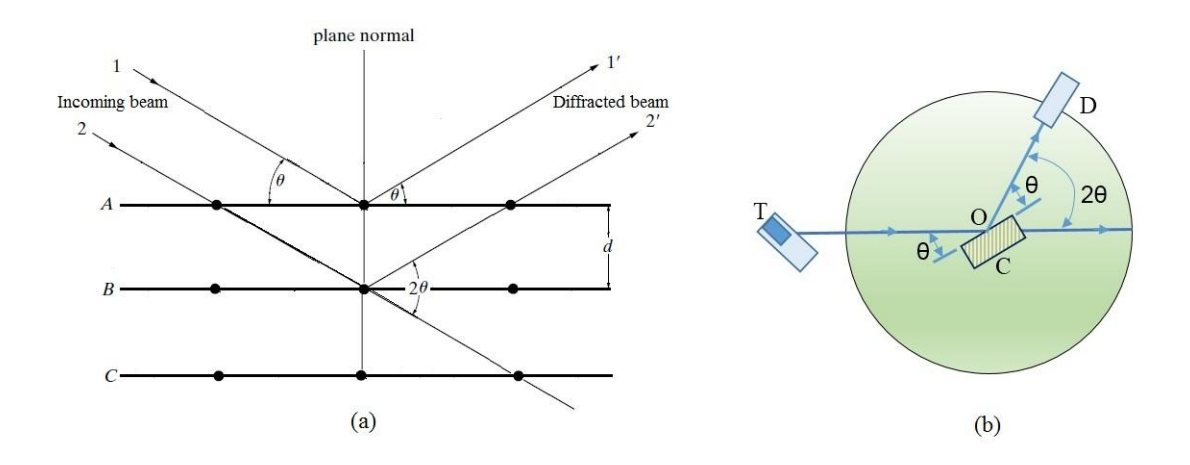


Figure 2.7 Diagram of (a) diffraction of x-rays by a crystal, (b) the x-ray spectroscopy [65]

2.5.2 Scanning Electron Microscope (SEM)

Scanning techniques have the mutual feature that a certain physical quantity is measured with not only spatial resolution but also recorded as a function of position on the surface. Generally, a screen is used to display the local distribution of this quantity obtained electrically. The greatest significance for the characterization of microstructures on a scale down to 10A° are Scanning electron microscopes (SEM). Along with simple imaging of surface topography (SEM), a local surface analysis in the matter of chemical composition can also be performed by the scanning electron microscopy [66]. The operation of a SEM is described in details in Figure 2.8.

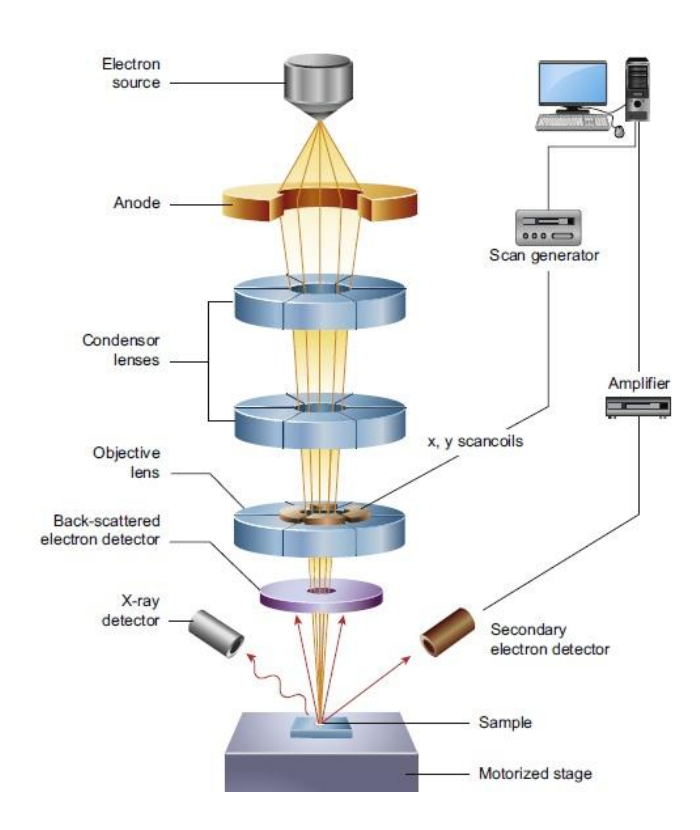


Figure 2.8 Diagram of the core components of an SEM microscope [65]

2.5.3 UV Spectroscopy

Spectroscopy is the branch of science that deals with intraction of electromagnetic radiation with materials. In other words, it is an analytical method for qualitative and quantitative analysis by use of light. Ultraviolet-Visible- Infrared (UV-VIS-IR) spectroscopy is one of the oldest method in molecular spectroscopy. It is a quantitative technique that used to take the measurement of how much chemical substrate absorbs light. This technique is done by measuring the intensity of light that passes throughout the sample as regards the intensity of light. The basic principle of spectroscopy is the Beer-lambert's law, which stated that absorbance is proportional to the concentration and thickness of the materials sample [67]. According to the Beer-lambert's law, the optical transmittance of the materials can be determined from the following relation.

$$I = I_0 \exp^{-\alpha t} \tag{2.3}$$

Where I and I_o are the transmitted and incident intensities, α is the absorption coefficient and t is the film thickness [68]. In this study, a Lambda 2 Perkin Elmer UV spectrometer in 320-1100 nm wavelength rang was used to register the

transmission and absorbance spectra of CBD, spin-coating and spray pyrolysis both ZnS and ZnO thin films.

2.6 Growth Techniques

Through the last decades, coating technologies have significant attention as a consequence of processing flexibility, cost consideration, and functional advantages over bulk materials [69]. Coating technologies may play an important role in the fabrication of next generation solar cells. Thin film deposition can be classified into three groups on the bases of its nature and deposition as shown in Figure 2.9 [70]. It was clearly confirmed that structural, electronic transport and optical properties of ZnS and ZnO are very sensitive to the preparation method and deposition technique [71]. This study will review the deposition of ZnS and ZnO thin films on glass, FTO and Si substrate using CBD, sol-gel and spray pyrolysis technique.

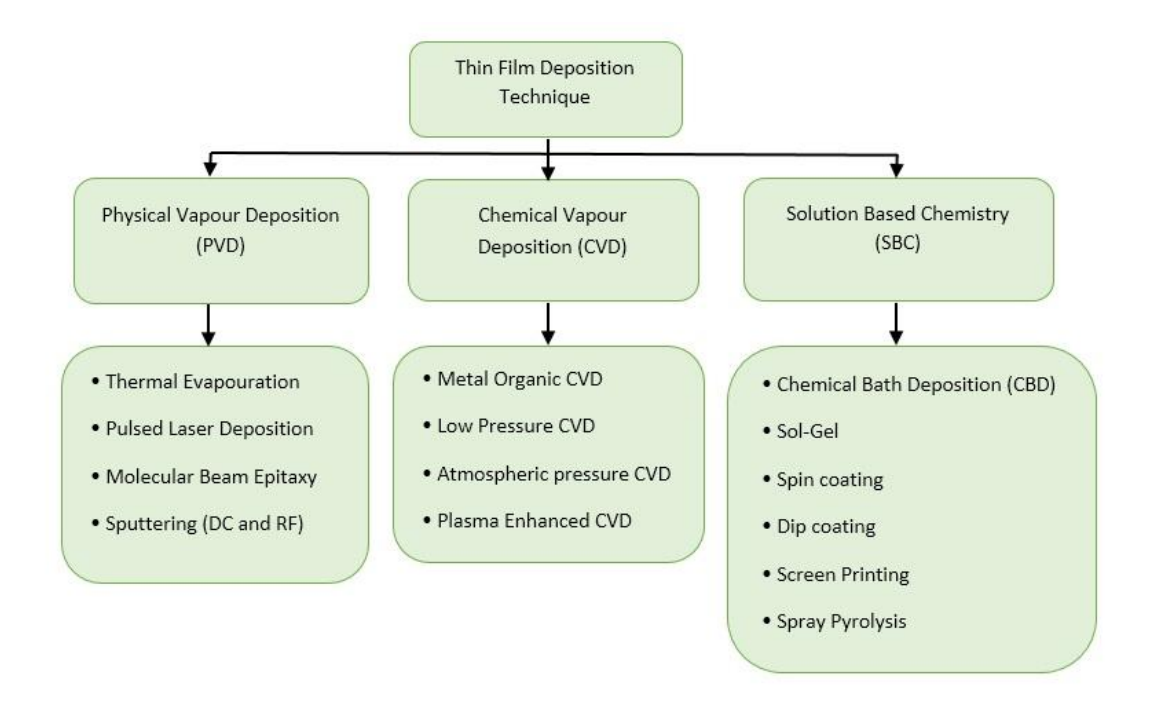


Figure 2.9 Classification of thin film deposition techniques [70]

2.6.1 Chemical Bath Deposition Technique

Chemical bath deposition (CBD) is an attractive method which is well known as a widespread low-temperature aqueous technique as it high deposition rate on a wide variety substrate thin film of semiconductor, has been confessed as easier

operation, low cost and most economical one [32][21]. CBD brings the possibility of controlling the ZnS and ZnO films thickness and crystallinity. For solar cell applications, the thickness of the window layer should be preserves close to 100 nm to prohibit more absorption of the incident light. For this reason, CBD is regarded one of the significant technique to deposit semiconductor thin films for solar cell applications [72] [73].

In this method, thin films are deposited on solid substrates immersed in a dilute solution, which is containing metallic cations, one or more complexing (chelating) agents as well as a source of anions [72]. A chelating agent is used to restrict some stability to the bath, which would otherwise undergo rapid hydrolysis and precipitation. [32]. Furthermore, the chemical reaction in the solution begin to compound formation, hence the principle of this method is controlled precipitations. Occasionally, prepared CBD thin films required a post-annealing treatment, so as to improve some physical properties [73].

2.6.2 Sol-gel (Spin Coating) Technique

Sol-gel technique is regarded as simple, low cost and large area deposition technique. It is used to produce silica modified ZnS or ZnO, which is a commonly reported route for nanoparticle synthesis. Ordinarily, precursors are mutated to a colloidal solution or sol; that gradually develops into a gel network (a matrix of solid nanoparticles dispersed in a liquid phase over time) also gelling agents may be used to accelerate the process. Through centrifugation, the nanoparticles can then be isolated to yield the product. As a low cost, facile synthesis method, which does not require any specialist equipment, sol-gel remains one of the most popular methods of nanoparticle synthesis. The apparent strength of the sol-gel method lies in its inherent adaptability and flexibility while maintaining the integrity and consistency of the materials produced [28] [74].

One of the primary advantages of this method is the ease of chemical composition control. This property makes sol-gel process is very important for doping especially for doping ZnO in order to achieve p-type conductivity [75].

2.6.3 Spray Pyrolysis Technique

Spray pyrolysis as a simple processing technique being considered in research to prepare thin and thick films. Spray pyrolysis is an aerosol process that atomizes a solution (liquid source) and heats the droplets formed by the atomizer, produces particles for thin film coating [76] [77].

The essential advantages for spray pyrolysis are simplicity and affordability, cost effectiveness, uniform and high quality coatings as well as no requirement of vacuum. The properties of spray deposited films rely on the substrate, substrate temperature; spray rate and droplet sizes [78]. The droplet size relys on the method of atomization, for example aerosol and ultrasonic spraying construct larger and smaller initial droplets respectively [69].

In spray pyrolysis technique, many sources for zinc can be applied and the most frequently used zinc sources are zinc chloride ($ZnCl_2$), zinc nitrate hexahydrate ($Zn(NO_3)_2$. $6H_2O$) and zinc acetate dihydrate ($Zn(C_2H_4O_2)_2$. $2H_2O$) [79].

In our work, the spray pyrolysis process is used for the deposition of both ZnS and ZnO layers on glass, FTO and Si for solar cell applications.

This chapter introduces the concepts of solar irradiance and the atmospheric effects as well as the fundamental characterizations based on photovoltaics. The theory of heterojunction solar cells of ZnS/Si-based photovoltaics will be introduced. The chapter will give an explanation in detail of the equivalent circuit of solar cells and discuss the fundamental electrical parameters including fill factor, maximum power, and conversion efficiency.

3.1 Solar Irradiance

Solar energy is the most essential source of renewable energy that is also the source of biomass, wind and waterpower. Irradiance might be defined as the amount of light energy that comes from an individual thing hitting a square meter of another in each second. Therefore, solar radiation can be interpreted as electromagnetic radiation emitted by the Sun in the spectrum ranging from X-rays to radio waves [80]. The greatest quantity of this radiation is in the visible and infrared part of the electromagnetic spectrum, less than 1% emitted in the radio, UV, and X-ray spectrum bands [5].

The radiative energy output from the sun acquires from a nuclear fusion reaction. In each second around $6x10^{11}$ kg of H_2 is converted to He, together with a net mass loss of about $4x10^3$ kg, which is converted by the Einstein relation (E=mc²) to $4x10^{20}$ J. This energy is emitted as electromagnetic radiation in the ranges (0.2 to 3 mm) which is principally transmitted to the Earth by electromagnetic waves, which can also be exemplified by particles (photons). Many factors are important such as Earth's atmosphere, surface, and diverse objects in the world that must be taken into account when modeling solar radiation because solar radiation reaches the surface of the Earth at a very long distance [80] [81].In the following sections, we will briefly talk about photons and solar spectrum.

3.1.1 Photons

At the beginning of the 19th century, German physicists Max Planck and Albert Einstein proposed that light or irradiance is composed of distinct particles. After that, the word "photon" become a synonym for the light quantum, which means in Greek word "photo" light, and the suffix "-on" at the end of the word indicates that the photon is an elementary particle associating with the same group as the proton, the electron, and the neutron.

Photons are particles of light, which have energies hv between 1.5 and 3 eV. They constantly move with the velocity of light, with a velocity in a vacuum $c_0 = 3 \times 10^8 m \ s^{-1}$ and in a medium with refractive index n with a velocity of $c = c_0/n$. The energy of such a photon is given by:

$$E = \frac{hc}{\lambda} \tag{3.1}$$

Where λ is the wavelength (in m), h is Planck's constant (6.626.10⁻³⁴ J.s) and c is the speed of light in vacuum (2.998.10⁸ m/s) [4] [6].

3.1.2 The Solar Spectrum and Atmospheric Impacts

The starting point of this discussion is the Sun itself. The sun is a big sphere of plasma composed of hydrogen (92%), helium (8%), and small amount of other atoms or elements with a diameter of 1.39×10^9 m, a mean Earth-Sun distance of 1.5×10^{11} m, and a blackbody surface temperature of 5777 K powered by a predominant hydrogen-helium fusion reaction. Sunlight consists of electromagnetic radiations in the regions of ultraviolet (UV), visible light, and infrared (IR) radiation.

The solar spectrum reaching the earth's surface undergoes various absorptions, mainly due to ozone absorption in the ultraviolet, water-vapor absorption in the infrared and scattering by aerosols and airborne dust [39]. The various regions of solar radiation illustrated in Figure 3.1 are characterized through wavelength range with the broad range of (0.20-4.0 μ m). This range consists of visible and near-visible (ultraviolet and near-infrared) radiation comes from the Sun and have

arranged as: Ultraviolet (0.20-0.39 μ m), Visible (0.39-0.78 μ m), Near-Infrared (0.78-4.0 μ m) and Infrared (4.00-100.00 μ m) [5] [83].

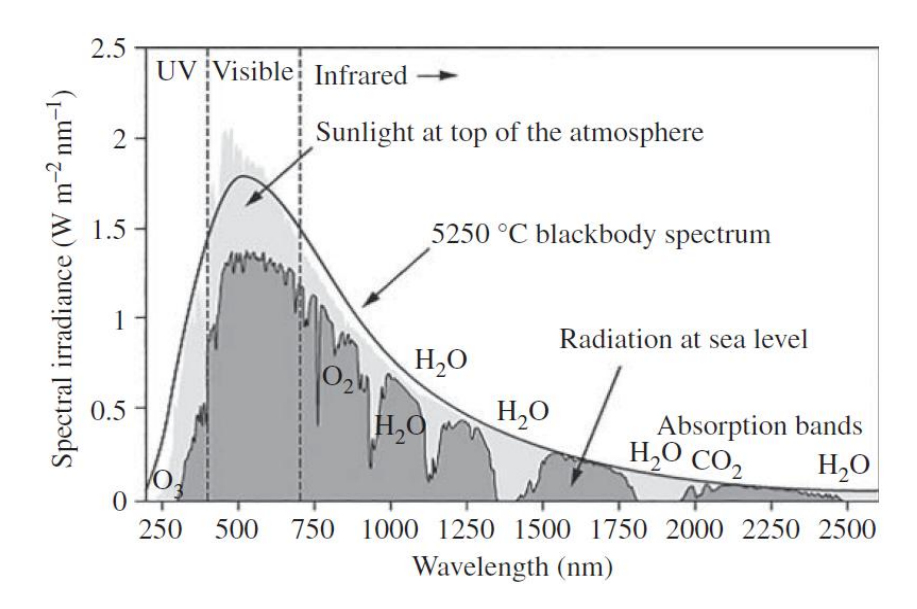


Figure 3.1 Solar irradiance spectrums with respect to the wavelength [83]

In order to characterize the effect of a clear atmosphere in sunlight using the concept "air mass", which is equal to the relative length of the direct beam path through the atmosphere. The average solar energy falling on the earth's surface is air-mass 1.5 (AM 1.5) irradiation, which is equal to approximately 100 mW/cm² [1] [81] [82].

The solar irradiance spectra for two air-mass (AM) conditions are shown in Figure 3.1. The upper curves is the AM0 solar irradiance spectrum that is measured above the earth's atmosphere and it is important for satellite applications of solar cells. The irradiant power of the sun under AM0 condition is 136.61 mW/cm², while the lower curve is the AM1 solar irradiance spectrum describes the sunlight on the earth's surface when the sun is at its zenith angle. [82] [84].

3.2 Physics of Solar Cells

These sections will provide an essential understanding of solar cells and energy conversion in the solar cell by absorption of the solar irradiance process in semiconductors. Besides, the conversion of solar radiation into electrical energy will be discussed.

3.2.1 Photovoltaic Effect

Photovoltaic, the conversion of sunlight into beneficial electrical energy, is one of the most significant parts of any strategies to decline a dependence on fossil fuels. The term "photovoltaic" consists up of the Grek words "photo" meaning light and "voltaic" meaning electricity that associated with the Italian physicist name Alessandra Volta. Electricity can be produced from the "photovoltaic effect", so the convenient definition of the photovoltaic effect is the generation of voltage when a device is exposed to light, and the result is the direct conversion of electromagnetic radiation into electrical energy. The device used for the conversion of sunlight into usable electrical energy is known as a solar cell. Four fundamental steps must be brought together simultaneously in order to make a solar cell that can be useful for different applictions,

- (a) Absorption of photons using a proper material
- (b) Creation of charge carriers (electron-hole pairs) by breaking bonds between atoms
- (c) Separation of reversely charged free carriers before there recombination
- (d) Collection photons-generated charge carriers across electrical contacts and their passage through an external circuit to create an advantageous electric current [1][82].

In order to improve efficiency, the materials must be adjusted to include band gap energies for photons in the visible range, which have the most energy accessible from the sunlight. The spectrum from infrared (IR) to ultraviolet (UV) covers a range of about 0.5 to 2.9 eV. For instance, red light has an energy of about 1.7 eV, and blue light has an energy of about 2.7 eV. Productive PV semiconductors have band gap energies ranging from 1.0 to 1.6 eV. Band gaps in semiconductors are in the range of 1-3 eV as silicon, which the band gap is 1.1 eV [81].

3.2.2 Theory of Heterojunction Solar Cell

Heterojunction solar cells attract a significant attention in the photovoltaic application owing to their potential to achieve a high power conversion

efficiencies accompanied by cost-effective materials and uncomplicated processes [85]. Heterojunctions have appeared as a substantial in next-generation solar cells to facilitate charge collection and separation, including intermediate band solar cells, organic solar cells, and thin-film solar cells. Furthermore, heterojunctions make it possible to formation a p-n junction where the semiconductor of interest cannot be selectively doped n-type or p-type [86].

Generally, a p-n junction can made it by using a single semiconductor material, which is doped with a properate elements to form an n and p regions. It means that, the semiconductor is basically based on a single element such as Si, or a single compound semiconductor as GaAs. However, if a p-n junction is established between two dissimilar semiconductor materials, then a heterojunction is created [83]. For example of this, a p-type of Si on one side of the junction and an n-type of ZnS or ZnO thin film on the other side. Each has its own lattice structure together with different lattice constants and band gap that are chosen based on their individual and common properties as shown in Figure 3.2, which is related to the band gap energy of both ZnS/Si and ZnO/Si heterojunction cells. In this case, the Fermi level must be the same on both sides in thermal equilibrium [33]. Cut out lattice mismatch will cause dislocations at the interface and results in electrical defects like interface traps [39].

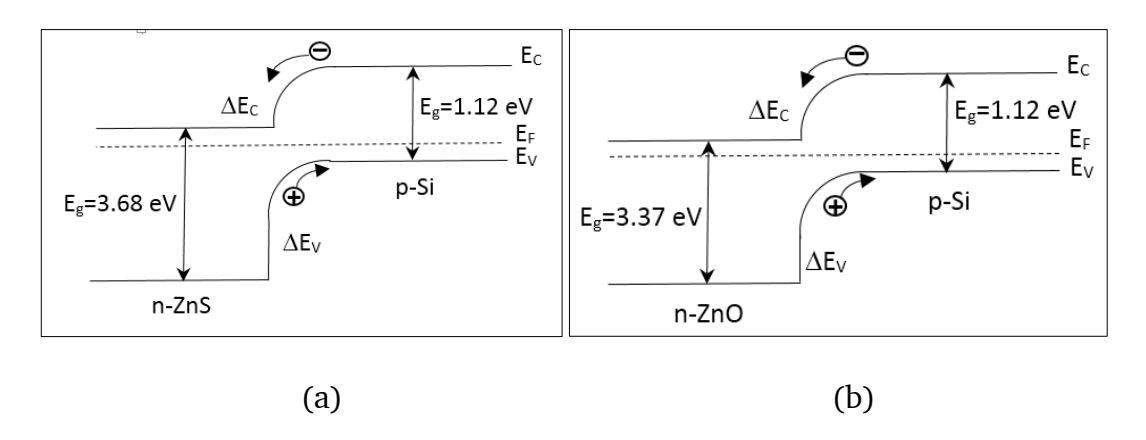


Figure 3.2 (a) Energy band diagram of n-ZnS/p-Si heterojunction in equilibrium [87], (b) schematic diagram of n-ZnO/p-Si heterojunction in equilibrium [25]

3.2.3 Light Absorption and Electron-Hole Generation

The concept "generation" is defined as a procedure that increases the density of either free electrons, holes, or both. In order to complete this process, it requires

a minimum generation energy, which is equivalent to the band gap energy E_g [6]. Photon absorption in solar cell excites the electros from the initial energy level E_i to a higher energy level E_f , it means that photon energy is equal to the difference of E_f and E_i ($E_f - E_i = hv$). Indeed, a carrier generation in solar cells is a process where electron-hole pairs are created through exciting an electron from the valance band to the conduction band, thereby creating a hole in the valance band as presented in Figure 3.3 [84].

The degree of light absorption is known by the absorption constant $\alpha(\lambda)$, which is depend strongly on the wavelength of the incident light. On behalf of the photon energy, hv the absorption coefficient $\alpha(hv)$ can be defined as the relative rate of decrease in light intensity L(hv) along its path of a propagation such that [88].

$$\alpha = \frac{1}{L(h\nu)} \frac{d[L(h\nu)]}{dx} \tag{3.2}$$

Optical absorption can be classified into intrinsic and extrinsic absorption. In intrinsic, the energy of each absorbed photon is consumed by raising an electron from the valance band to the conduction band by creating an electron-hole pair. While in extrinsic, the absorption is through a deep location states. Intrinsic absorption occurs in both direct and indirect band gap materials.

In direct band gap materials, the conduction band (CB) minimum and valance band (VB) maximum occur at the same value of crystal momentum k, and momentum is conserved when an electron is promoted from the top of the VB to the bottom of the CB. For this material, the variance of absorption coefficient α with incident phton energy $h\nu$ obyes the following formula which is called Tauc formula.

$$\alpha(h\nu) = A[h\nu - E_g]^m \tag{3.3}$$

where h is Planck's constant. ν is the frequency of the incident photon, A is a constant associated with the effective mass related to the valance band and conduction band, E_g represent the energy band gap and m is a constant relying on the transition type of the optical absorption process and it is theoretically equal to 2 and $\frac{1}{2}$ for indirect and direct allowed transitions, respectively [32] [60]. For

indirect transitions, the CB minimum and VB maximum do not occur at the same value of k and consequently momentum is not conserved, therefore, phonons are involved in order to conserve momentum [39].

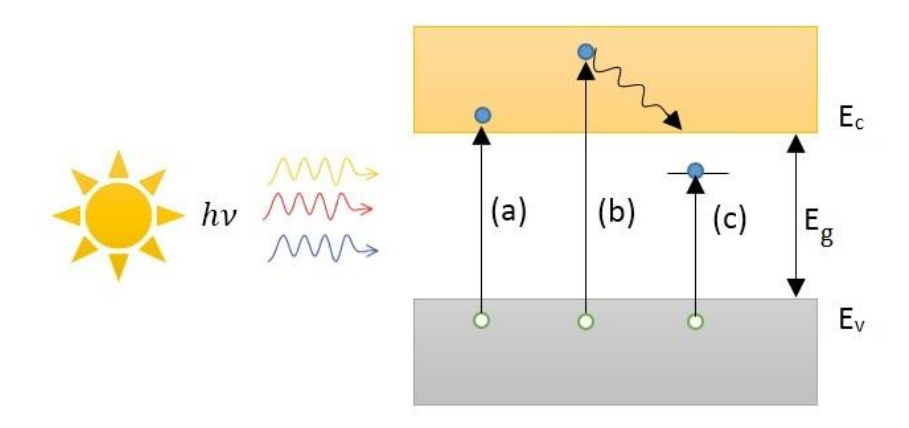


Figure 3.3 Photon transitions in semiconductor at (a) $h\nu = E_g$, (b) $h\nu > E_g$, (c) $h\nu < E_g$

3.2.4 Separation of Photogenerated Carriers

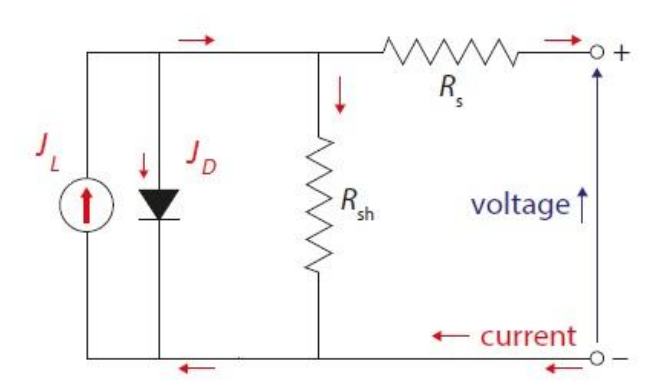
In solar cell, to generate an electrical current, electrons and holes should be separated to avoid the electrons to fall back to its initial energy state and recombine with holes through the recombination process [89]. It means that, electron-hole pairs have a finite lifetime τ in order to be carried off into the external circuit, therefore, an electric field must be exist in account for free carriers to be separated and drawn out through the front and back contacts before recombination. However, the time required to reach these charge carriers to the contacts must be smaller than their lifetime.

3.2.5 Collection of Charge Carriers at the Terminals of the Junction

When photons with energies larger than the band gap of a semiconductor, they fall down into the depletion reigon to create a free electron-hole pairs. Due to the existing of internal electric field, the electrons will attracted from p-type region (Si) into the n-type region (ZnS or ZnO) and out the front contact. While the holes will attracted from the n-type towards p-type and out the back contact. These electrons will leave the solar cell across the electrical contacts to recombine with the holes that have created in the valence band and the chemical energy of the electron-hole pairs has been converted to electric energy [1] [90].

3.3 Equivalent Circuit of Solar Cell

Commonly, solar generator convey DC voltage or current. Several of the small applications are formed for DC supply, but most other applications demand AC current. Therefore, an inverters are utilized to convert DC current into AC, which required for commercially applications. The unit of a solar PV system is the solar PV cells, which fundamentally consist of a p-n semiconductor junction. When the cell is exposed to the solar spectrum, the photons which have energies less than E_g make no contribution to the cell output. While the photons with energies higher than E_g contribute with an electric charge to the cell output and hence a DC current is generated as well as the surplus energy over ${\cal E}_g$ is lost as heat [91]. In photovoltaic cell, the quantity of current generated by photon excitation at specific temperatures is affected by the intensity of the incident light and by the wavelength of the incident light [5]. In order to understand the working principle of a solar cell, it is convenient to establish a design, which is electrically equivalent. Commonly, the simplest configuration of PV cell is consist of a constant current source and parallel connected diode. In case there is no light exist to generate any current, the PV cell works as a diode. The constant current behaves as a generator to push the electrons to the external circuit. The ideal equivalent circuit of the solar cell design is given in Figure 3.4, the source I_L (photocurrent) results from the excitation of excess carriers by solar radiation due to the photovoltaic effect,



 I_D is the diode current of a solar cell [39]. Virtually solar cells are not ideal,

therefore, shunt and series resistance component are gathered to the equivalent

circuit.

Figure 3.4 Equivalent circuit diagram of solar cell [5]

The output current of a photovoltaic cell is equal to the difference of photogenerated current density, dark current density, and shunt current density.

$$J(V) = J_L - J_D - J_{SH} (3.4)$$

Where J_D is a dark current of a simple forward-biased diode. While the voltage across these components given from the flow of currents.

$$V_D = V + JR_S \tag{3.5}$$

Where V_D is the voltage across shunt resistance and diode, V is the output terminal voltage, and JR_S is the voltage across the series resistance. The diode current is given by.

$$J_D = J_0 \left[exp \left(\frac{qV_D}{\eta kT} \right) - 1 \right]$$
 (3.6)

Here J_0 is called diode saturation current density, q is the charge of electron = 1.6×10^{-19} C, η is the ideality factor, k is the Boltzmann constant and T is the absolute temperature in Kelvin. The current flows by shunt resistance can be calculated from Ohm's law.

$$J_{SH} = \frac{V_D}{R_{SH}} \tag{3.7}$$

The net output current density of a solar cell can be given by substitute equations 3.5 and 3.6 in equation 3.4 to obtained the basic equation that described the J-V characteristic for the solar cell [37].

$$J(V) = J_L - J_0 \left[exp\left(\frac{qV_D}{\eta kT}\right) - 1 \right] - \frac{V + JR_S}{R_{SH}}$$
(3.8)

3.4 Basics Parameters and Device Characterization

3.4.1 The Current Density-Voltage Characteristics

The fundamental characteristics of a p-n heterojunction solar cell are obtained via analyzing the current density-voltage measurements (*J-V*) behavior under dark and illumination conditions. The characteristic curve of *J-V* is the graphical

representation of the operation of a photovoltaic cell. In dark conditions, a solar cell has comparable electrical characteristics as of diode. However, when light hits on the solar cell, electrical power will be introduced and *J-V* curve falls into the fourth quadrant. Then, the illuminated cell added to the dark diode and the diode equation can be written as.

$$J(V) = J_0 \left[exp \left(\frac{qV_D}{\eta kT} \right) - 1 \right] - J_L \tag{3.9}$$

Typically *J-V* characteristics can be measured after illuminating the solar cell in standard operation, namely standard testing conditions (STC) of air mass (1.5 AM) at 25°C [84]. The *J-V* characteristics of the solar cell under dark and illumination are explained in Figure 3.5.

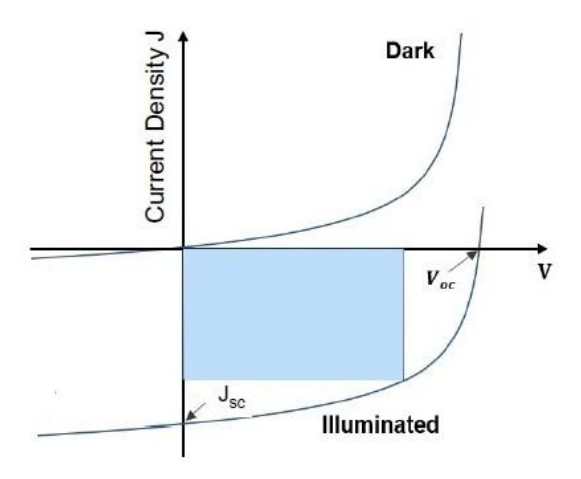


Figure 3.5 The *J-V* characteristics of a solar cell in dark and under illumination [93]

3.4.2 Short Circuit Current Density

The maximum current density flow across the solar cell at zero load condition (R_L =0) is defined as short-circuit current density (J_{SC} in mA/cm^2). The short-circuit current density will be at the largest value of J_{SC} when the voltage of solar cell equal to zero, where the entire current is extracted. This value depends mainly on the amount of light entering the cell and spectrum, area of the solar cell, optical properties as well as contributing to the generation of the current [84].

It's clear that when the band gap decreases, the short circuit current density increases, due to the more photons have the energy required to create as electronhole pairs [92]. The graphical representation of short circuit current density is shown in Figure 3.5.

3.4.3 Open Circuit Voltage

The open circuit voltage (V_{oc} in Volt) refers to the voltage obtained at one-sun illumination, when no current is extracted. It means that, the maximum voltage is taken from the solar cell at ($R_L = \infty$) is known as open-circuit voltage. If a solar cell is an open circuited and no load is connected through the solar cell, then current density will be zero while the voltage will be at the maximum value. The open circuit voltage can be derived by setting the net current to zero and obtain the following equation.

$$V_{oc} = \frac{\eta kT}{q} \ln \left(\frac{J_L}{J_0} + 1 \right) \qquad at \ J = 0$$
 (3.10)

 V_{oc} is determined by saturated current density J_0 and light generated current density J_L . Where J_0 relies on recombination in the solar cell, therefore, V_{oc} is a measure of the quantity of recombination in a solar cell. The representation of V_{oc} is given in Figure 3.6.

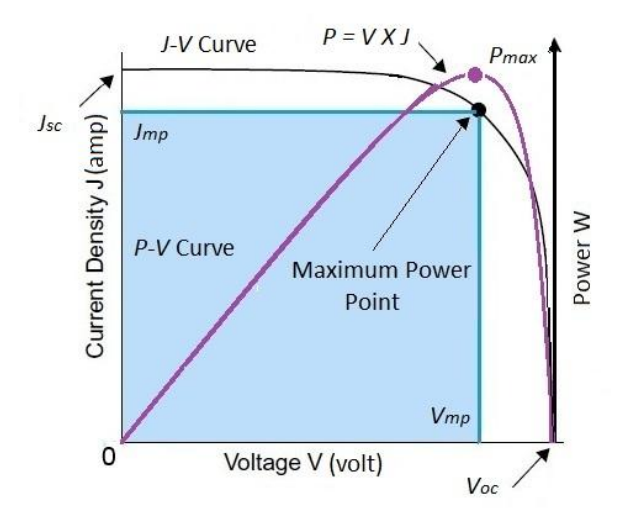


Figure 3.6 The *J-V* characteristic of a solar cell under illumination. The short circuit current J_{sc} and the open circuit voltage V_{oc} are shown. The maximum power point is also illustrated [94]

3.4.4 Fill Factor

The fill factor (*FF*) is a parameter that determined the performance of the solar cell and can be defined as the ratio between actual power to the theoretical power in case both open circuit voltage and short circuit current were in maximum value. It is a measure of how "square" the output characteristic are. Typical fill factor in range 0.5-0.82, FF can be represented as a percentage % and given by equation [80].

$$FF = \frac{P_{max}}{V_{oc} J_{sc}} = \frac{V_{mp} J_{mp}}{V_{oc} J_{sc}}$$
(3.11)

Where P_{max} is the maximum power density and it is represented by the rectangle area and can be calculated from the product of the V_{mp} and J_{mp} as shown in Figure 3.6 [33].

In real devices, maximum power can not be extracted through operating the solar cell in either short or open circuit condition. However, the ideal solar cell is to obtain a maximum power value, whereas ensuring that V_{mp} and J_{mp} , are so close to the short circuit current and open circuit voltage [95].

3.4.5 Maximum Power Point

The power output for any operating point is equal to the area of the rectangle as can be seen from Figure 3.6, which is equal to the product of voltage by the current and given by.

$$P_{out} = V_{out} J_{out} (3.12)$$

In case of short and open condition there is no power is generated. Therefore, the maximum power point P_{max} can be defined as a point at which the product of current density J_{mp} and voltage V_{mp} is maximized [92]. In terms of fill factor, the maximum power point can be written as:

$$P_{out} = V_{oc}J_{sc}FF \tag{3.13}$$

3.4.6 Power Conversion Efficiency

The high-efficiency thin film solar cell are very important in order to reduce cost and to increase lifetime of the cell. The power conversion efficiency (*PCE*) of the

solar cell can be defined as the ratio of the maximum output power P_{max} of the solar cell to the incident light power on the solar cell P_{in} . P_{out} can be used to be P_{max} because the solar cell can be worked up to its maximum power to gain maximum efficiency as following:

$$PCE; \eta = \frac{P_{max}}{P_{in}} = \frac{V_{mp}J_{mp}}{P_{in}} = \frac{V_{oc}J_{sc}FF}{P_{in}}$$
 (3.14)

Where P_{in} is the total radiation power incident on the cell. Typically, the PCE; η of a solar cell can be enhanced by raise V_{oc} , J_{sc} and FF and these parameters are measured under standard test condition AM 1.5, a cell temperature of 25°, and incident power density of 1000Wm⁻² [5] [94].

3.4.7 Series and Shunt Resistance Effects

Series resistance has a significant affect to the fill factor by lowering the value of FF from its ideal. The main contributions to the series resistance R_S along the current path are the bulk resistance of the semiconductor materials, the bulk resistance of the metallic contacts as well as interconnections, and the contact resistance between the metallic contact and the semiconductor. The bulk resistance can be define as the product of the resistivity and the thickness of the components [44].

Whereas the shunt resistance R_{SH} is generated from leakage across the p-n junction which is come from defects in the junction [92].

This chapter introduce the experimental details by using three different methods involving chemical bath deposition CBD, spray pyrolysis, and spin coating technique, which have been employed to prepare both ZnO and ZnS thin films in order to fabricate n-ZnS/p-Si and n-ZnO/p-Si heterojunction solar cells.

4.1 Deposition of Doped and Undoped ZnS Thin Films Using CBD Technique

Chemical bath deposition is a convenient technique that has been used for many years to deposit semiconductor thin films, which is enormously attractive since it is low cost, low evaporation temperature and easy coating of a large area [72] as we mentioned in section 2.6.1.

In this study, undoped (with double and 4 –times molarity) and Na doped ZnS thin film were deposited by CBD on a glass and FTO substrates. In the following sections, the reaction mechanism and preparation setup will discuss.

4.1.1 Reaction Mechanism

Basically, the substantial CBD process has include mass transport of reactants, adsorption, surface diffusion, reaction, nucleation as well as growth. ZnS thin films can be produced by disintegration of thiourea $[CS(NH_2)_2]$ as a source of sulfide $(S^2$ ion source) in an alkaline solution as well as ammonia that can be used as a complex agent. The deposition process is established on the slow release of Zn^{2+} and S^{2-} ions within the precursor solution, that condensed on an ion-by-ion basis on the substrate, is properly mounted in a reaction solution. ZnS thin film exists when the ionic product of Zn^{2+} and S^{2-} ions surpasses the solubility product of ZnS. The chemical reaction mechanism related to the deposition of ZnS thin film can be presented as follows [96].

$$Zn^{2+} + 2Oh^{-} \rightarrow Zn(OH)_{2}$$

$$NH^{4+} + Oh^{-} \rightarrow NH_{3} + h_{2}O$$

 $Zn(OH)_{2} + 4NH_{3} \rightarrow [Zn(NH_{3})_{4}]^{2+} + 2OH^{-}$
 $CS(NH_{2})_{2} + 2OH^{-} \rightarrow S^{2-} + CN_{2}h_{2} + 2h_{2}O$

Finally, the ZnS films are formed on substrates according to the relation

$$[Zn(NH_3)_4]^{+2} + S^{2-} \rightarrow ZnS_{(s)} + 4NH_3$$

4.1.2 Preparation of Bath Solution and Cleaning Process

In this work, ZnS films were deposited on glass, FTO and Si from aquous solution with the size of (1 cm^2) . Before the deposition, the substrates were cleaned by distilled water, acetone, and ethanol washed again with distilled water, finally dried with N_2 gas. This treatment is vitally important to attain a uniform and continuous film layer [32]. Typically chemical bath deposition component, which is used in our study, is illustrated in Figure 4.1.

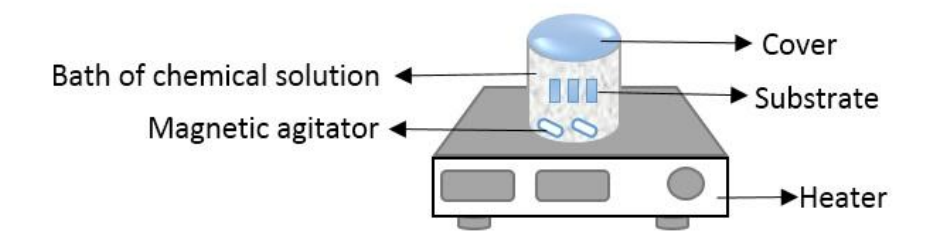


Figure 4.1 Chemical bath deposition (CBD) system [31]

The reaction solution for the deposition of ZnS films consists of (0.02 M) zinc acetate dihydrate $\text{Zn}(\text{CH}_3\text{CO}_2)_2$, as a zinc source dissolved in 10 ml with distilled water, (0.0608 M) tri-sodium citrate dihydrate $\text{Na}_3\text{C}_6\text{H}_5\text{O}_7$ in 20 ml of distilled water, (0.0377 M) of sodium chloride NaCl in 10 ml of distilled water, which is used as a dopant source. In addition, (0.0604 M) of thiourea $\text{CS}(\text{NH}_2)_2$ in 10 ml of distilled water, as a sulfur precursor source. By using a magnetic stirrer (agitator), each solution was stirred for 20 min. After mixing all of them, add 200 ml of distilled water to the reaction solution and pH was adjust to 10 by adding an appropriate amount of ammonia NH_4OH as a complex agent.

Then, the previously cleaned glass, FTO and Si substrates were immersed and fixed vertically to the wall of the beaker containing the reaction solution by using

bands and the solution was kept under stirring at 80 $^{\circ}$ C for 1 h. The substrates were washed in tap water after they were removed and then rinsed in distilled water to remove soluble impurities and then dried by N_2 gas. The films grown on the back side were removed by cotton swabs dipped in concentrated HCl in order to enhance the optical absorption [97].

In this work, Na doped ZnS films are deposited at first, then for undoped ZnS films, the molarity of the solvent materials was doubled twice from the origin in order to obtain different precursor solutions as shown in Table 4.1.

Table 4.1 Percentage of solvent materials

No.	Precursor Solution	Doped	Undoped		
		Molarity (M)	Double Molarity (M)	4-Times Molarity (M)	Distilled Water
1	Zn(CH ₃ COO) ₂	0.02	0.04	0.08	10 ml
2	Na ₃ C ₆ H ₅ O ₇	0.0608	0.1216	0.2432	20 ml
3	CS(NH ₂) ₂	0.0604	0.1208	0.2416	10 ml
4	NaCl	0.0377			10 ml

4.2 The Deposition of ZnS Thin Films Using Spin Coating Technique

As compared to other preparation methods, the spin coating method for deposition of ZnS films is chosen due to its relative simplicity and has a general advantage of large area deposition and uniformly of the film thickness.

In this study, ZnS were synthesized using sol- gel technique by adopting spin coating methods. Generally, sol-gel processing includes four key steps; all steps

contribute to the framework of the gel and the effectiveness of its properties and hence the corresponding application. These steps can be concluded as

- Sol preparation: A colloidal suspension is created as a result of the dispersion of solid nanoscale particles, concluded from a precursor material, within a solvent.
- Sol to gel transition: Branching particles and cross-linking happen when the addition of an acid or a base catalyst is added, which begins with polymerisation to form an interconnected chain structure.
- Ageing of the gel: The gel is aged in its origin solution in order to increase the mechanical strength of the gel.
- Drying of the gel: The solvent is extracted from the pores of the gel in a way deterrent of gel cracking [74].

4.2.1 Film Preparation and Processing

Zinc precursor solution was constructed by dissolving (0.2 M) of zinc acetate dehydrate $Zn(CH_3COO)_2.2H_2O$ and (0.2 M) of thiourea $CS(NH_2)$ in 5 ml of ethanol C_2H_5OH , which was choosen as a starting solvent, then (methanol CH_4O , 2-propanol $CH_3CH(OH)CH_3$ (IPA) or 2-methoxyethanol $C_3H_8O_2$) were applyed also as a solvent materials in four different beakers. Normally, diethanolamine $C_4H_{11}NO_2$ (DEA) was used as a stabilizer in order to keep metal ions in a homogeneous solution without undergoing precipitation [98]. Each complex solution was stirred with a magnetic stirrer for 1 h at room temperature and atmospheric pressure to obtain a clear and homogeneous solution. After that, those were aged for 24 h at room temperature to form the sol before their use as coating precursors [28]. Figure 4.2 presents the process using the spin coating deposition technique. Before the deposition, the substrates were properly cleaned using distilled water, ethanol, acetone and distilled water again to remove all contamination that could affect the features of the thin film.

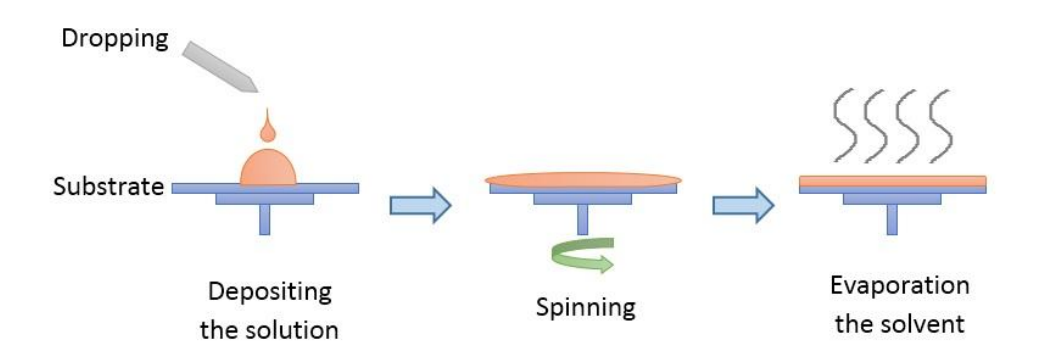


Figure 4.2 The process of spin coating deposition technique

The obtained sol was spin coated on glass and FTO substrates at 500 rpm with rotation time 30 sec per sample, and have undergone five layer deposition. After that, the substrates were removed from the spin disc and placed on the hot plate for 1 min at 100 °C after each layer processing. Finally, the samples were annealed at temperature 400 °C in furnace for 1 h. Then the furnace is switched off and left the samples cool down in order to be ready to analyze.

Figure 4.3 represents the flow chart of ZnS thin films were deposited on glass and FTO substrates by using spin coating trchnique.

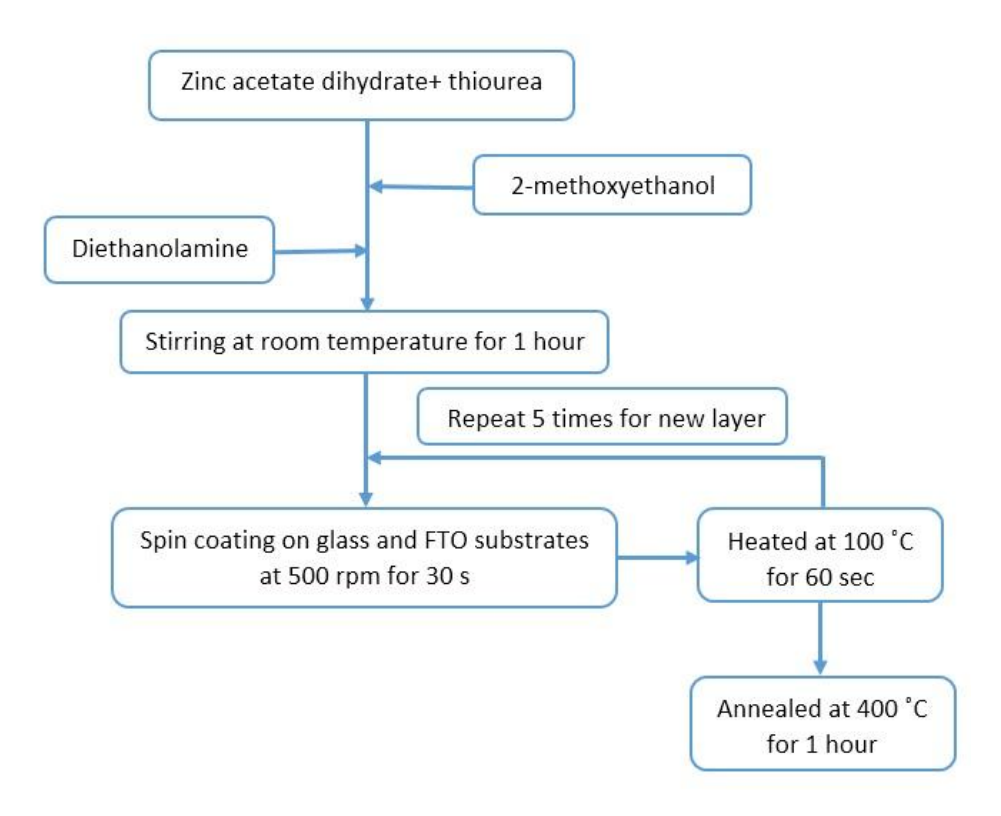


Figure 4.3 Flow chart diagram of the synthesis of ZnS thin film

4.3 Deposition of Doped and Undoped ZnS and ZnO Thin Films Using Spray Pyrolysis Technique

The ZnS and ZnO thin films were deposited using a cost-effective and simplified spray pyrolysis technique [19] [56], which is a processing technique being considered in research to prepare thin and thick films. In the traditional spray method, ordinarily, a carrier gas such as N₂, O₂, or air is used to spray the precursor solution. Nevertheless, in our work, a cheap and uncomplicated spray technique has been synthesized by using a perfume atomizer. Indeed, perfume atomizer prevents the deposition of large droplets that usually happen in standard spray deposition, enhances wet ability between sprayed microparticles and the formerly deposited layers. [99][100][101].

4.3.1 Spray Pyrolysis Structure

In this present work, we employ a glass, FTO and p-type silicon wafer (111) as substrates with area 1.0 cm². The glass, FTO, and Si substrates were cleaned by detergent followed by distilled water, alcohol, and once more distilled water, respectively. Finally, the cleaned substrates were dried in air. Subsequent to these treatments, substrates show good hydrophilic property, which is vitally important to obtain uniform and continuous film layer [32].

The atomizer perfume was kept at a constant distance from the substrate (35 cm approximately) for all the samples. A heater is used as a heat source to provide a temperature about 350-400 °C, which is controlled by a temperature controller. A thermocouple connected to temperature controller is utelized to regulate the growth temperature [102]. Figure 4.4 illustrate the simplified scheme for spray pyrolysis deposition, start with the atomization of the precursor solution then aerosol convey of the droplet and finally decomposition of the precursor to set film growth.

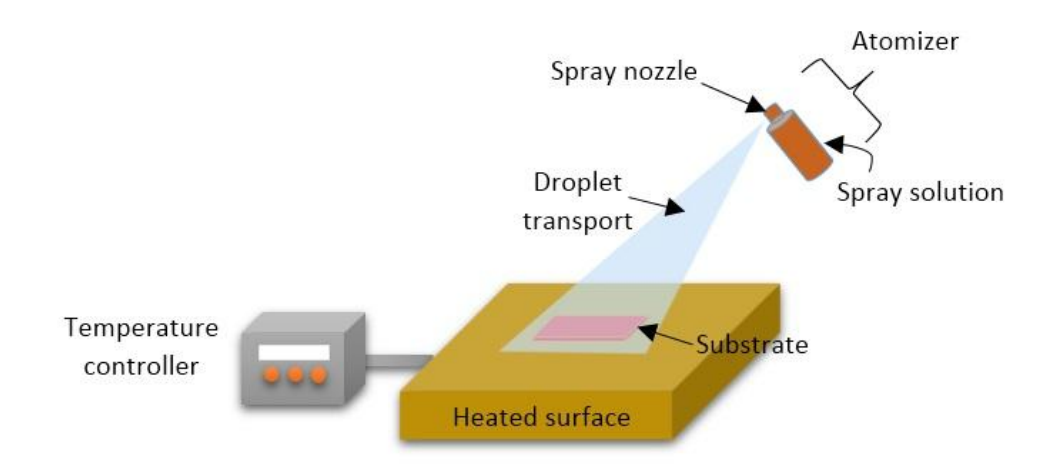


Figure 4.4 Schematic of spray pyrolysis deposition technique [77]

4.3.2 Fabrication of ZnO via Spray Pyrolysis

In preparing the precursor solution of the ZnO, zinc chloride ZnCl₂ or zinc acetate dihydrate Zn (CH₃COO)₂.H₂O was applied as a source of zinc. 0.05 M ZnCl₂ aqueous solution was dissolved in 100 ml of distilled water and was stirred at room temperature for 30 min in order to obtain a homogeneous precursor solution.

The proposed growth mechanism for the ZnCl₂ or Zn(CH₃COO)₂ can be illustrated by the following chemical reactions [103].

$$ZnCl_2 + H_2O \rightarrow ZnO + HCl$$

Zn
$$(CH_3COO)_2.H_2O \rightarrow ZnO + CH_3COOH, CH_3COCH_2, CO_2$$

To increase the electrical conductivity of the ZnO thin films, it was required to insert a dopant into ZnO crystal lattice. Sodium tetraborate $Na_2B_4O_7.10H_2O$ and indium chloride $InCl_3$ were used as Na and In source, respectively. In our study, the spray solution was prepared by mixing 0.05M of $ZnCl_2$ with 1% and 5% of $Na_2B_4O_7.10H_2O$ in 100 ml distilled water at room temperature.

4.3.3 Fabrication of ZnS via Spray Pyrolysis

Undoped and Na doped ZnS thin films were grown on glass and p-type Si substrates by spray pyrolysis. The spray aqueous solution was prepared by mixing 0.05 M zinc chloride $ZnCl_2$ as a Zn source and 0.05 M thiourea $CS(NH_2)_2$ as a S source. $NaCl_2$ was added into solution in an appropriate concentration to achieve

1%, 5%, 10% and 15% Na doped ZnS films to cover a wide doping range. Solutions were stirred at room temperature for 1 h in order to ensure homogeneity and sprayed onto the substrates, as we mentioned in Figure 4.4 in privous section.

4.3.4 Growth ZnS and ZnO in Specific Temperature

The films were deposited on glass, FTO, and p-type Si substrate for obtaining thin films and ZnS/p-Si heterojunctions at a stationary substrate temperature of 350°C, which is measured during the experiment by thermocouple. A thermocouple was in contact with the glass substrate throughout the experiment. Before being sprayed, the substrates were kept on a hot plate until they reached a required temperature to grow undoped and doped ZnS or ZnO thin films. The deposition temperature was preserved during the experiment at 350°C for each sample.

The interrupted spray cycle in this study was arranged by two steps: the first one was spraying for 1 second and the second step was waiting for 3 seconds; therefore, this interval enables the substrates to reach the required temperature until starting the next spray [104]. After that, the annealing process was carried out at 350°C for 30 min. All the coated substrate were allowed to cool down naturally.

In order to calculate the thickness, it needs to weigh all the glasses substrate before and after the deposition. The difference is equal to the total mass of the film and find the total area of the film using the following relation:

$$Thickness \times area = volum \rightarrow Thickness \times area = \frac{mass}{density}$$

$$Thickness = \frac{mass}{(area \times density)}$$

4.4 Measuring Instruments and Characterizations

4.4.1 Structural Properties

The lattice parameters of crystalline materials are precisely measured by X-ray diffraction [105]. In this study, XRD analysis of the ZnS and ZnO samples substrates were carried out using Philips Paralytical X-ray diffractometer with Cu K_{α} radiation ($\lambda = 1.54056$ °A). Data were gathered in the 2θ range of 5° - 80° .

4.4.2 Morphological Properties

Morphological properties of thin films were carried out by scanning electron microscopy FEI-Quanta FEG 250. The thickness of the films was calculated by the weighing method. In order to calculate the thickness of the samples after the necessary cleaning of these substrates, it needs to weigh all the glass substrates before and after the deposition process. The difference between these two weighing results is the mass of the films.

4.4.3 Optical Charaterisation

The optical transmittance provides a beneficial information about the optical band gap of the semiconductor that are used in this study. The transmittance spectra of thin films were measured by using Shimadzu UV-Vis 1280 spectrophotometer. The measurements were carried out in the range of wavelength 320-1100 nm in reference to the glass and FTO substrates. In order to verify that all the active substrates are ready, it is important to run an initial test before taking measurements. The initial test including a baseline test with a glass substrate that inserted into a convenient place to check the optical properties like transmittance and the wavelength range required. The band gap energy of growth ZnS and ZnO are calculated from the absorption spectrum using the relation 3.3 in chapter 3, which is represent the relation between absorption coefficient and incibent photon energy.

4.4.4 Electrical Properties

The schematic diagram of n-ZnS/p-Si and n-ZnO/p-Si heterojunction is shown in Figure 4.5. ZnS/Si and ZnO/Si heterojunction cells were fabricated in metal (In)/ZnS or ZnO /Si/ metal (Ag) structure. ZnS, ZnO thin films deposited onto Si substrate then silver back contact onto Si and then grid shaped indium front contact onto ZnS were deposited by electron beam evaporation.

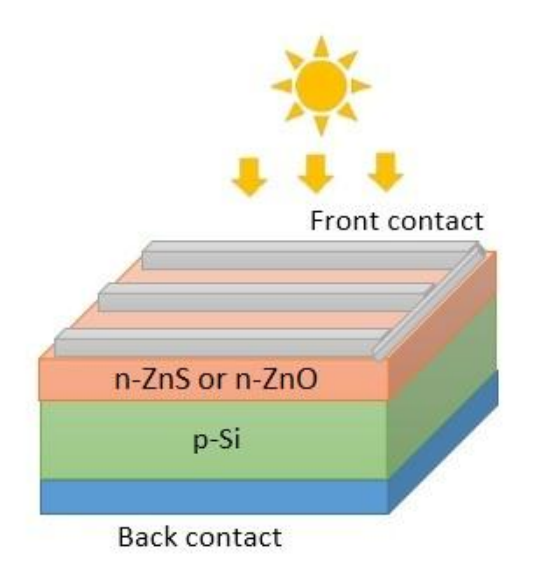


Figure 4.5 Schematic diagram of n-ZnS/p-Si or n-ZnO/p-Si heterojunctions

Conduction type of ZnS and ZnO films are determined by hot probe method [106] and the resistivity of the films were determined by Van der Pauw technique [107]. Current-voltage characteristics of the cells were measured by Air mass 1.5 and under 100 mW/cm² illumination. Open voltage (V_{oc}) short current density (J_{sc}) fill factor (FF) and power conversion efficiency (PCE; η) of the cell were calculated.

In this chapter, we will present the results of ZnS and ZnO films prepared by CBD, spin coating, and spray pyrolysis technique including structural properties, surface morphology, optical properties, and electrical properties. Besides, the results related to the ZnO/Si heterojunction and the Na doped ZnS/Si heterojunction that are prepared by spray pyrolysis technique will be discussed.

5.1 Experiments Done by CBD Technique

ZnS thin films have been grown on glass and FTO substrate via chemical bath deposition. Zinc acetate, thiourea, ammonia and tri-sodium citrate (and sodium chloride for Na doped ZnS) were used to prepare ZnS (see section 4.4.1). In the following sections, we will introduce the optical properties related to the work done by chemical bath deposition technique.

5.1.1 Investigation the Impact of Thermal Treatment Time on the Optical Properties of Na Doped ZnS Deposited on Glass Substrate

The optical transmittance versus wavelength spectrum in the range 300-1100 nm of unannealed and annealed Na doped ZnS films deposited on a glass substrate were examined. This study has demonstrated the significance of post deposition annealing time at (30-60-90) min in the atmosphere at 450°C as shown in Figure 5.1 (a). The transmittance spectra of unannealed Na doped ZnS films exceeds 90% in near infrared and ultraviolet region, while they have 80-90% transmittance in the visible region. The annealed transmittance at different times for all films has an interference between them that is showed a significant improvement in the crystallinity and uniformity of the grown films. Moreover, the annealed samples are transparent in the visible region and absorb light in the ultraviolet region when have increased annealing time due to improved crystallinity of the ZnS thin films. It can be realized that the transmittance spectra of all annealed samples have

similar behavior and show low and high percentages in UV and visible regions of light, respectively [108].

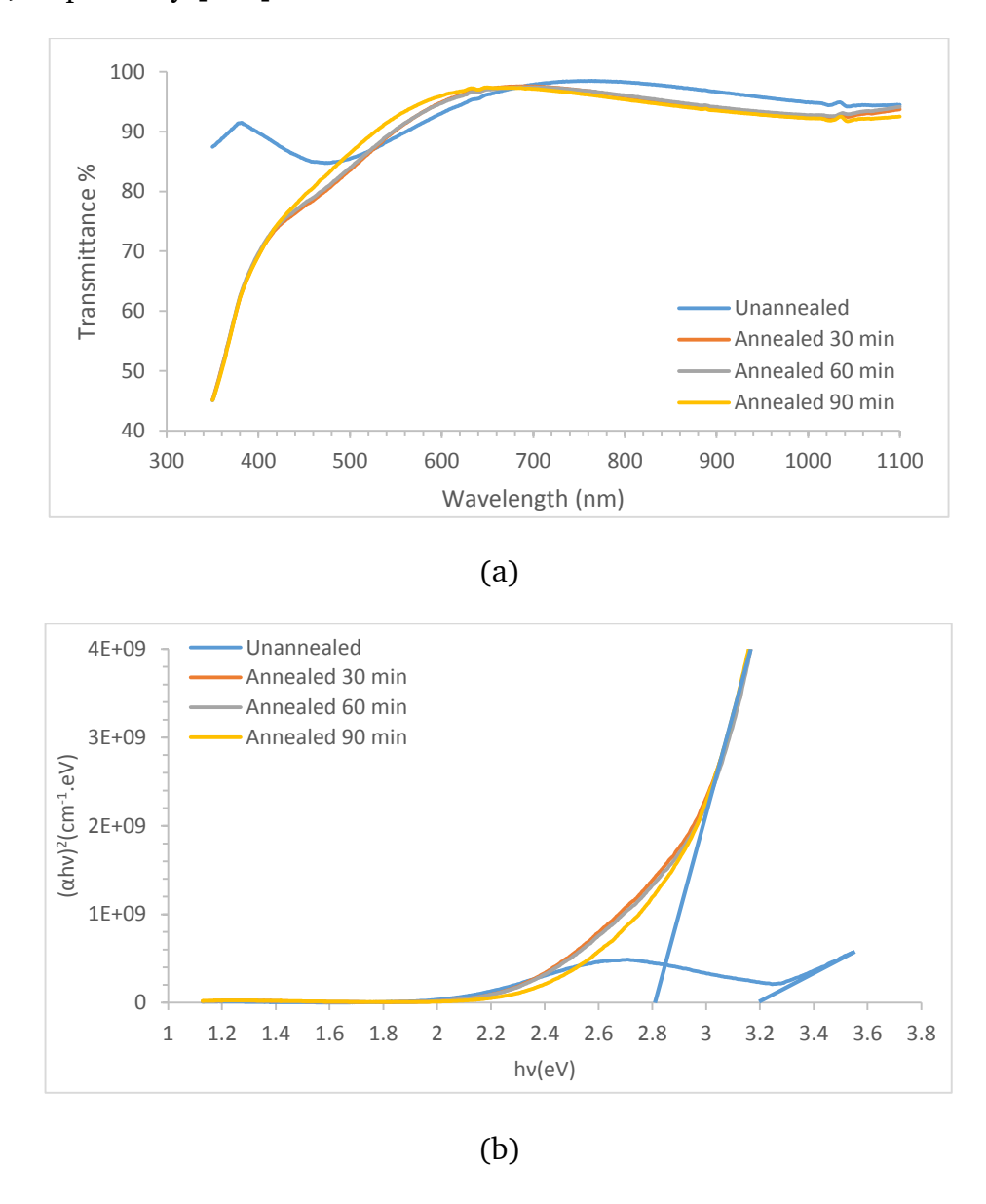


Figure 5.1 (a) Transmittance spectra and (b) plots of $(\alpha hv)^2$ as a function of photon energy of unannealed and annealed Na doped ZnS thin films

Figure 5.1(b) clarifies the effect of annealing time on the absorption measurements of ZnS sampls which have been unannealed and annealed at 30, 60, 90 min. It has been observed that the absorption value did not change as much as with the increasing annealing time. The decrease in band gap of ZnS films after annealing may be referred to as improvement in the crystals and change grain size of films with annealing temperature. Moreover, this reduction could be attributed

to a change in stoichiometry with the absence of Zn by evaporation. These results are in agreement with the Yildirim *et. al.* [109].

5.1.2 Thermal Treatments Effectiveness on the Optical Properties of Undoped ZnS with Double Molarity Deposited on Glass Substrate

The optical properties of ZnS films with double molarity in the range of 300-1100 nm were determined using a UV-Visible spectroscopy.

Figure 5.2 (a) demonstrates the transmittance spectra of unannealed and annealed ZnS thin films at 450°C for 30 min at the same atmosphere.

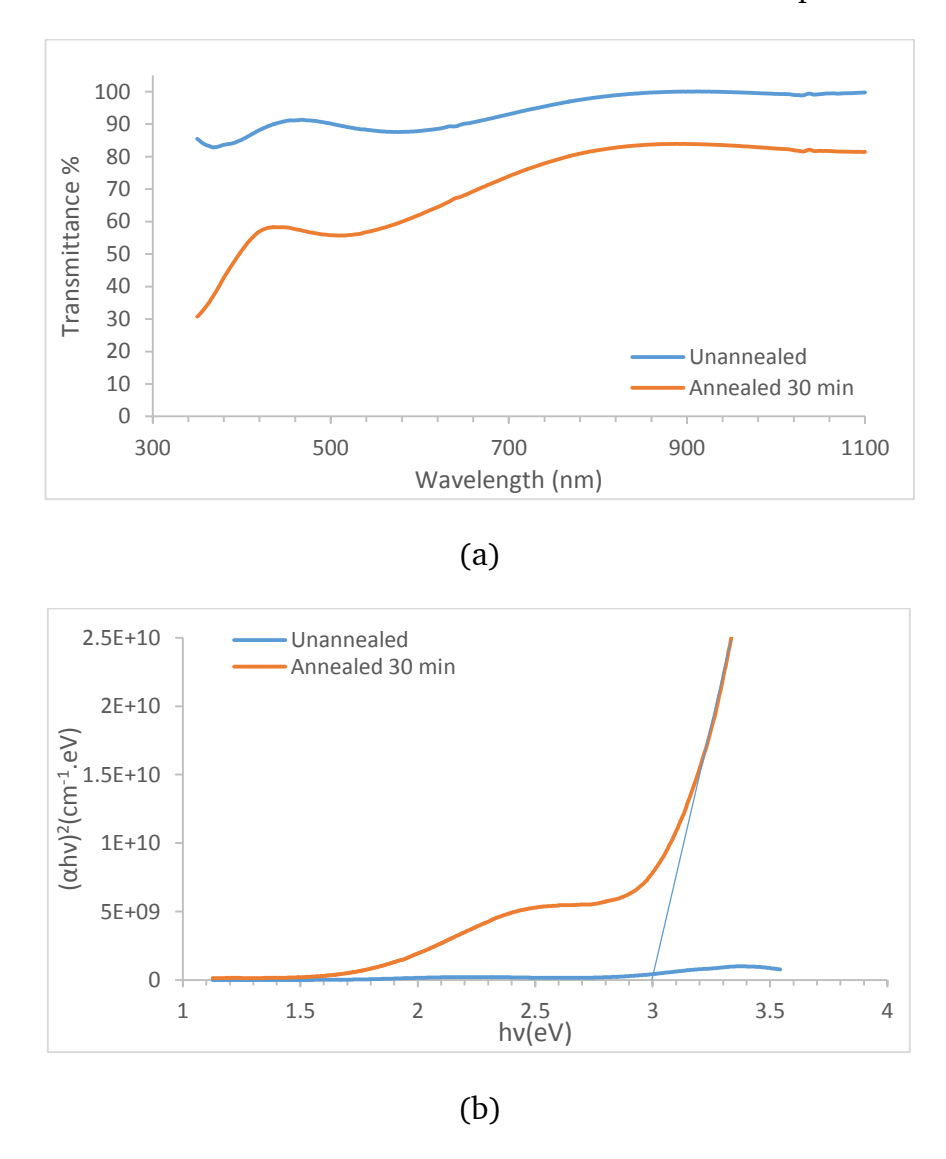


Figure 5.2 (a) Transmittance spectra and (b) plots of $(\alpha h v)^2$ as a function of photon energy of unannealed and annealed Na doped ZnS thin films with double molarity

The unanneled ZnS film shows a good transmittance in all the wavelength range. After annealing treatment, it can be observed that an absorption in UV region and the average transmittance in the visible and infrared region between 60-80%. This may attributed to the good homogeneity in the grain shape and size after annealing treatments.

The optical transmittance provides significant information about the optical band gap of the semiconductor where it stretched the liner part and intercepts at $\alpha^2 = 0$ to find E_g from $h\nu$ value. Figure 5.2 (b) illustrates $(\alpha h\nu)^2$ as a function of $h\nu$ of the unannealed and 30 min annealed ZnS thin film at 450°C.

According to this figure, the band gap energy of the annealed film is 3.00 eV. While in unannealed film, it can be seen the line was nonuniform and cannot determine the band gap energy of unannealed ZnS film.

5.1.3 Optical Properties of Undoped ZnS with 4-Times Molarity Deposited on Glass Substrate

Figure 5.3 (a), shows the optical transmittance of undoped ZnS with times molarity in the wavelength range 300-1100 nm. It can be observed that the transmittance increases gradually from UV at 60% to IR at 90% and the higher transmittance is noticed in IR region.

This result are much better than previous section for unannealed double molarity that show high transmittance in UV region.

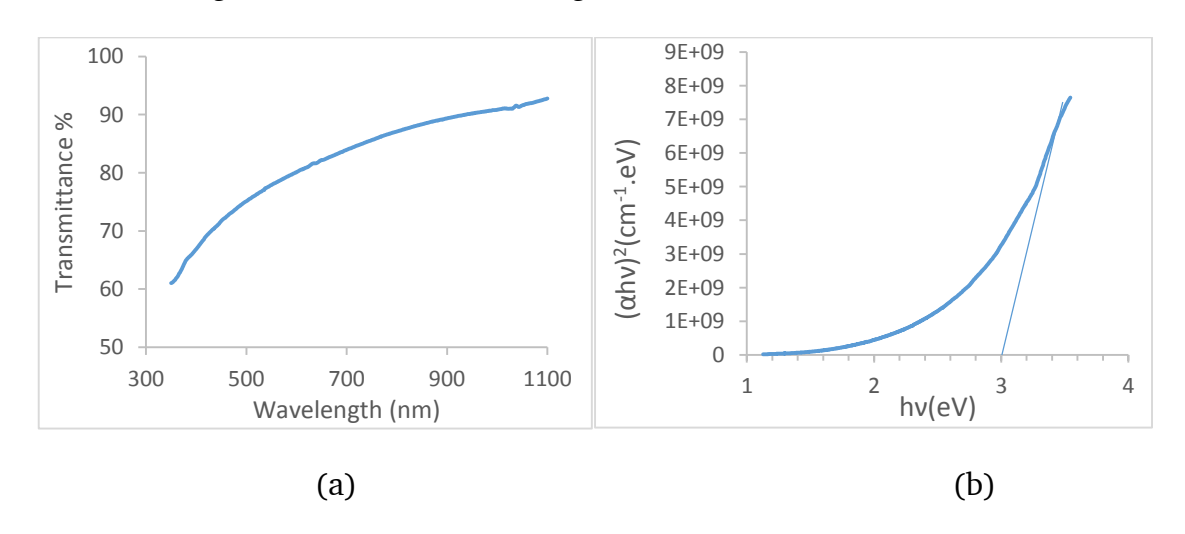


Figure 5.3 (a) Transmittance spectra and (b) plots of $(\alpha hv)^2$ as a function of photon energy of Na doped ZnS thin films with 4-times molarity

The absorption coefficient was illustrated in Figure 5.3 (b), the band gap value were regulated from the intercept of the straight line part of the $(\alpha hv)^2$ against the hv. The band gap value was observed as 3.00 eV, and it was lower than bulk value of hexagonal ZnS thin film.

5.1.4 Influence of Thermal Treatment on the Optical Properties of Na Doped ZnS Deposited on FTO Substrate

Figure 5.4 (a and b) represents the optical properties of unannealed and annealed Na doped ZnS deposited on fluorine tin oxide FTO.

The results show the optical transmittance for unannealed films is higher than once for annealed ZnS films and exceeds 90% for IR region. From Figure (b), the band gap energy for unannealed and annealed for Na doped ZnS films were 3.10 eV and 3.00 eV respectively.

It can be observed that the band gap of Na doped ZnS films deposited on FTO substrate decreases when the samples were annealed. Furthermore, the results confirm that that the annealing temperature has no significant effects on the optical properties of the ZnS film.

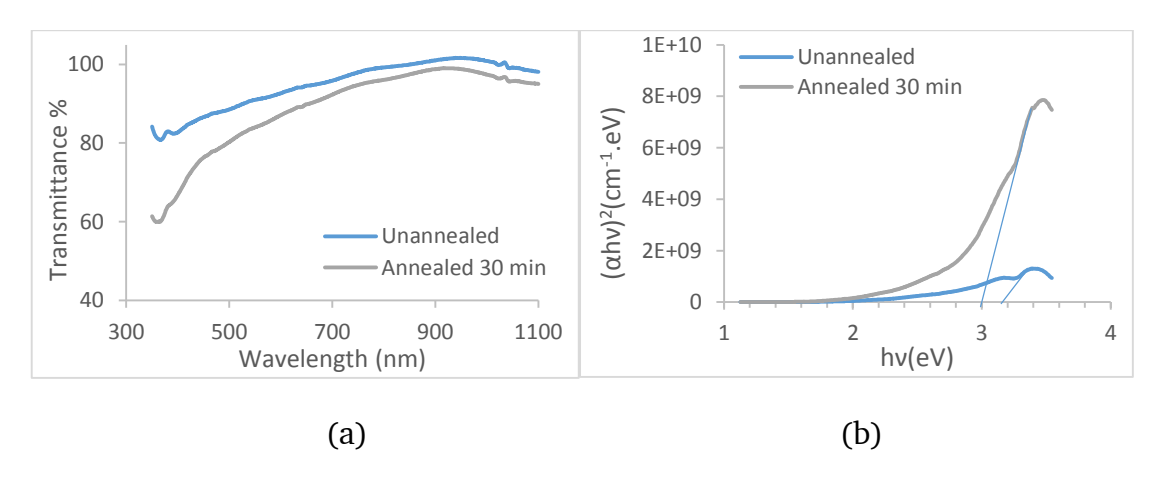


Figure 5.4 (a) Transmittance spectra and (b) plots of $(\alpha hv)^2$ as a function of photon energy of Na doped ZnS thin films deposited on FTO substrate

5.1.5 Effect of Annealing on the Optical Properties of Undoped ZnS with Double and 4-Times Molarity Deposited on FTO Substrate

Figures 5.5 (a) and 5.6 (a), show the transmittance spectra of ZnS films deposited on FTO substrate with double and 4-times molarity in the range of 300-1100 nm. Depending on these figures the transmittance spectra of unannealed samples related to the double and 4-times molarity presents a good and high transmittance in UV and visible region compared with the annealed samples.

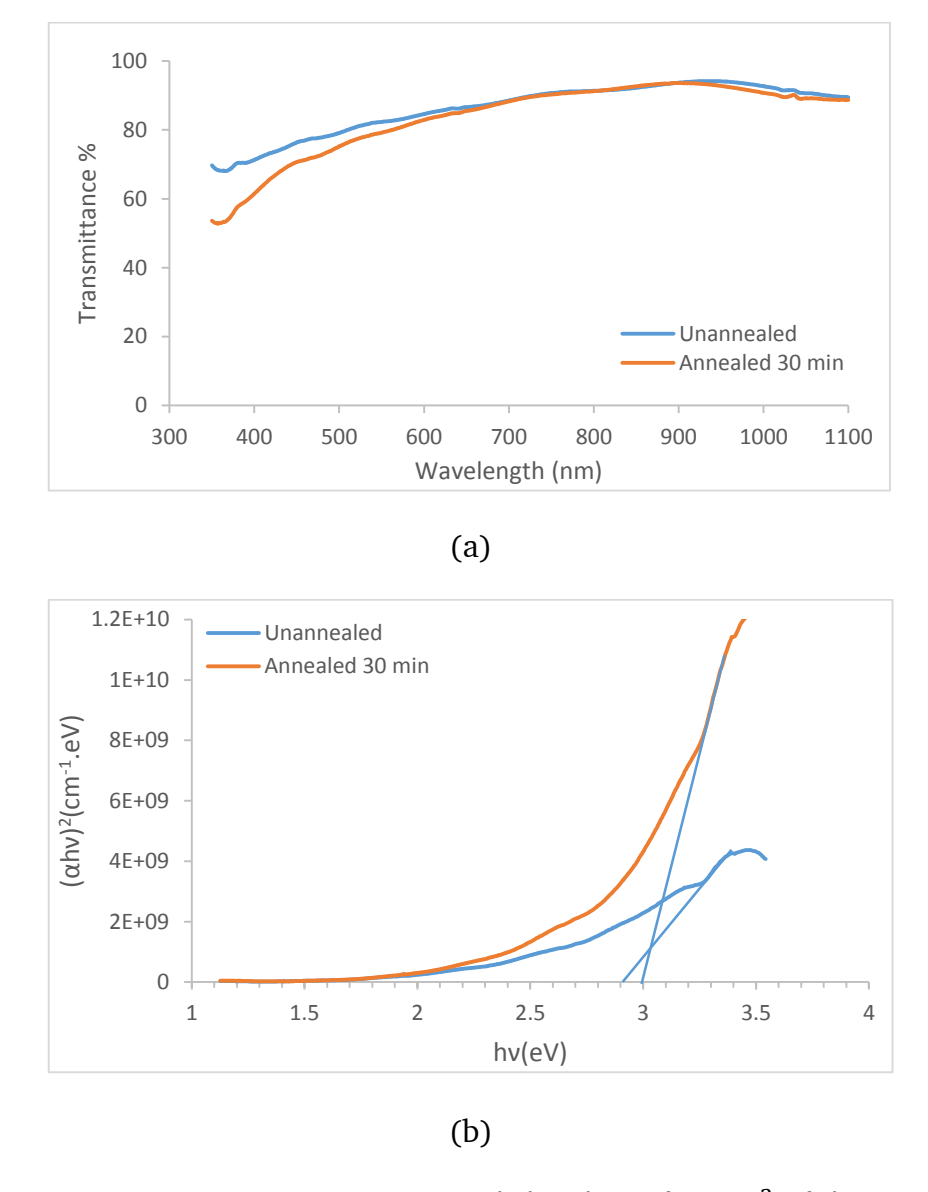


Figure 5.5 (a) Transmittance spectra and (b) plots of $(\alpha h \nu)^2$ of the unannealed and annealed Na ZnS thin films with double molarity deposited on FTO substrate

Figure 5.5 (b) and 5.6 (b) shows the band gap energies for ZnS samples. Corresponding to these graphs, the band gap energy of the unannealed ZnS film at double and 4-times molarity precursor solution is 2.9 eV for both of them. While in the case of annealed ZnS samples, the band gap energy at double molarity was 3.00 eV and at 4-times molarity was 3.10 eV.

It can be noticed that the annealing treatment of 4-times molarity is better than double molarity, this may be indicated to increase in the crystallite size and crystalline quality of ZnS.

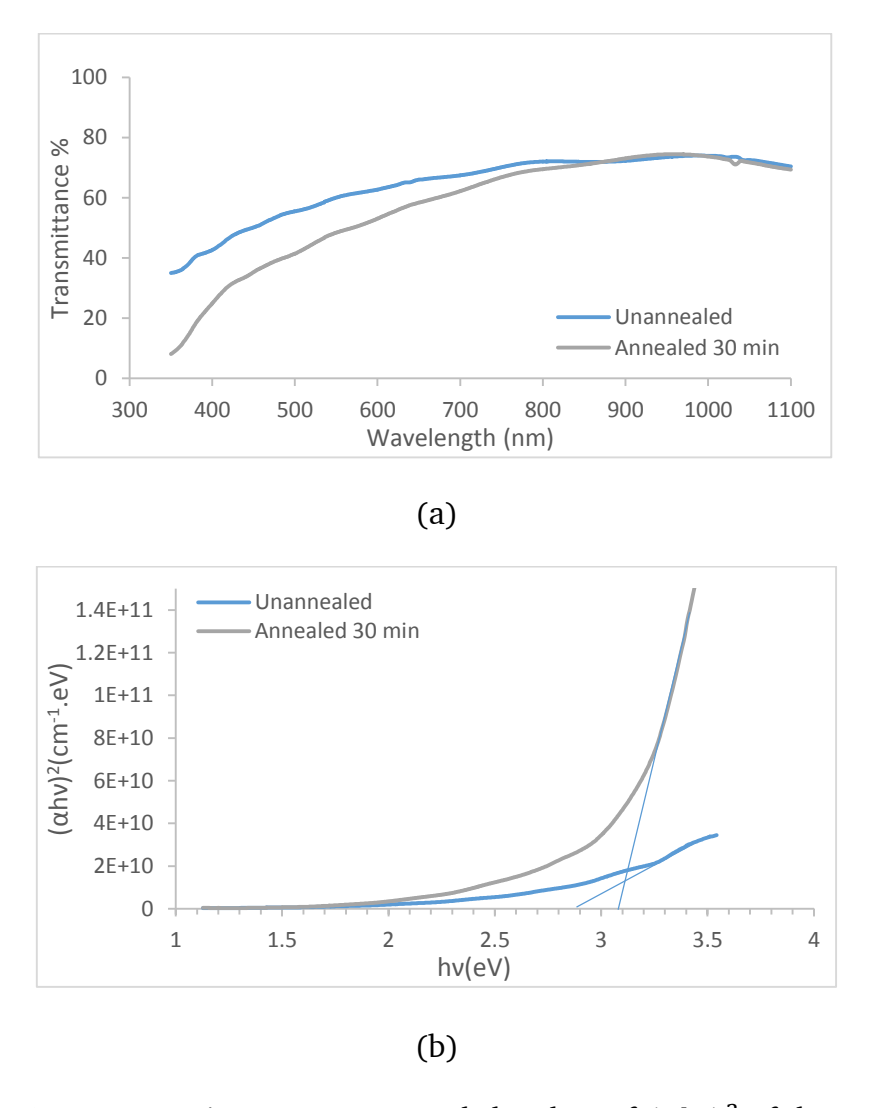


Figure 5.6 (a) Transmittance spectra and (b) plots of $(\alpha h \nu)^2$ of the unannealed and annealed Na doped ZnS thin films with 4-times molarity deposited on FTO substrate

5.2 Experiment Done by Spin Coating Technique

It was experimentally established that the synthesis of coating solution plays a substantial role in preparing high-quality ZnS thin films. In this study, it was found that after aging the four precursor solutions (as has mentioned in section 4.3.1), the growth of ZnS thin films from 2-methoxyethanol solvent was used as a coating complex solution, which remained clear and homogeneous sol. While other solvent was nonhomogeneous and not used because they did not react easily to form a polymer precursor solution, which is very important to convert sol in to gel and it may be attributed to humidity that was presented in the lab. The films obtained were transparent, homogeneous and crack-free.

5.2.1 Optical Properties

The optical properties of ZnS thin film were determined from transmittance measurements using UV-Vis spectrophotometer in the range of wavelength 350-1100 nm on various nature substrates (glass, FTO and Si). The transmittance spectra presented intensive absorption in the UV region. The behavior of the curve shows a good homogeneity of the ZnS thin films, the optical transmittance exceeds 87% of five layers. ZnS film and has good transparency in the visible region, which has significant interest for the application of respective films for instant transparent conductive electrodes and solar cell windows [71].

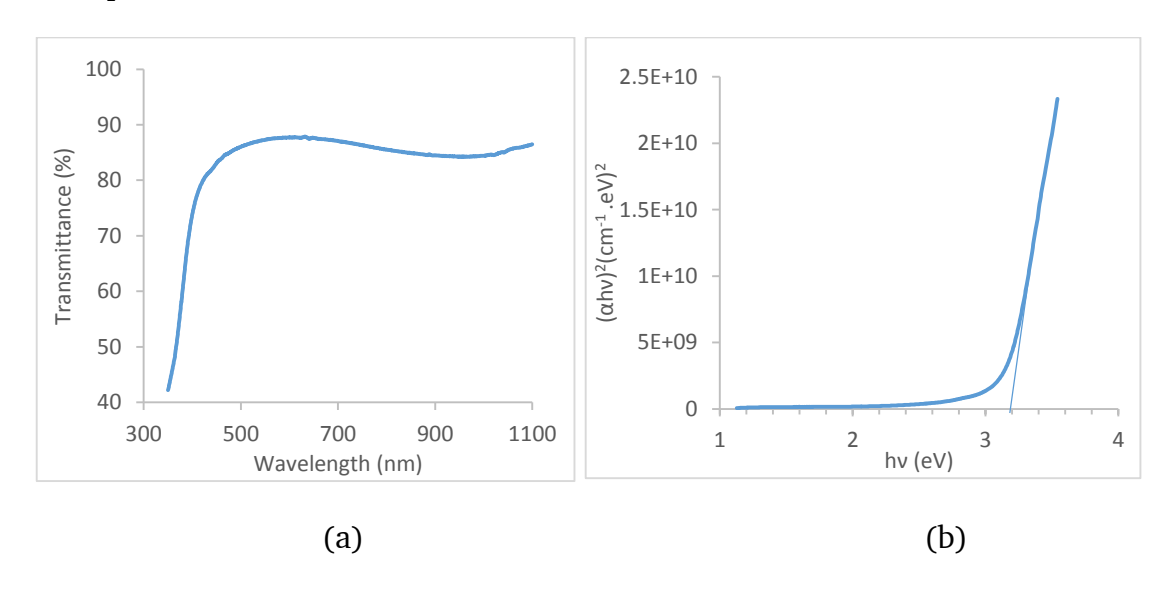


Figure 5.7 (a) Transmittance spectra (b) absorption coefficient of ZnS thin film prepared by spin coating

The plot in the absorption edge was linear, which emphasizes that ZnS is a direct band gap semiconductor [93]. The optical energy band gap of the films was calculated by using the formula that has mentioned in section 3.2.3.

Figure 5.7 (b) shows the variation of $(\alpha h v)^2$ agains thv, and the band gap was specified on behalf of extrapolating the stright line to the energy at $\alpha = 0$. We note that the ZnS layer deposited on the glass substrate has a small value of the optical gap 3.2 eV compared with the typical value.

The small value of band gap is attributed to increase in thickness of ZnS deposited as a five layer, which leads to decrease in band gap.

5.3 Experiments Done by Spray Pyrolysis Technique

5.3.1 Impact of Film Thickness on the Optical and Electrical Properties of ZnO Thin Films

In this study, we investigate the effect of thickness on the optical and electrical properties of ZnO thin films deposited onto a hot glass substrate and the temperature was kept for all samples at 350°C.

5.3.1.1 Optical Properties

The effect of film thickness on the optical properties was examined by UV-Vis measurements. Figure 5.8 (a, b, c and d) represents an absorption coefficient $(\alpha h v)^2$ of ZnO film as a function of photon energy. The band gap values for the samples at different thicknesses (100, 200, 300, and 400) nm were obtained as 3.24 eV, 3.32 eV, 3.52 eV and 3.60 eV, respectively.

It can be seen, when the film thickness increase, the achieved band gap values increase. This may be attributed to the decrease of a localized state in the band gap and more electron-hole pairs production.

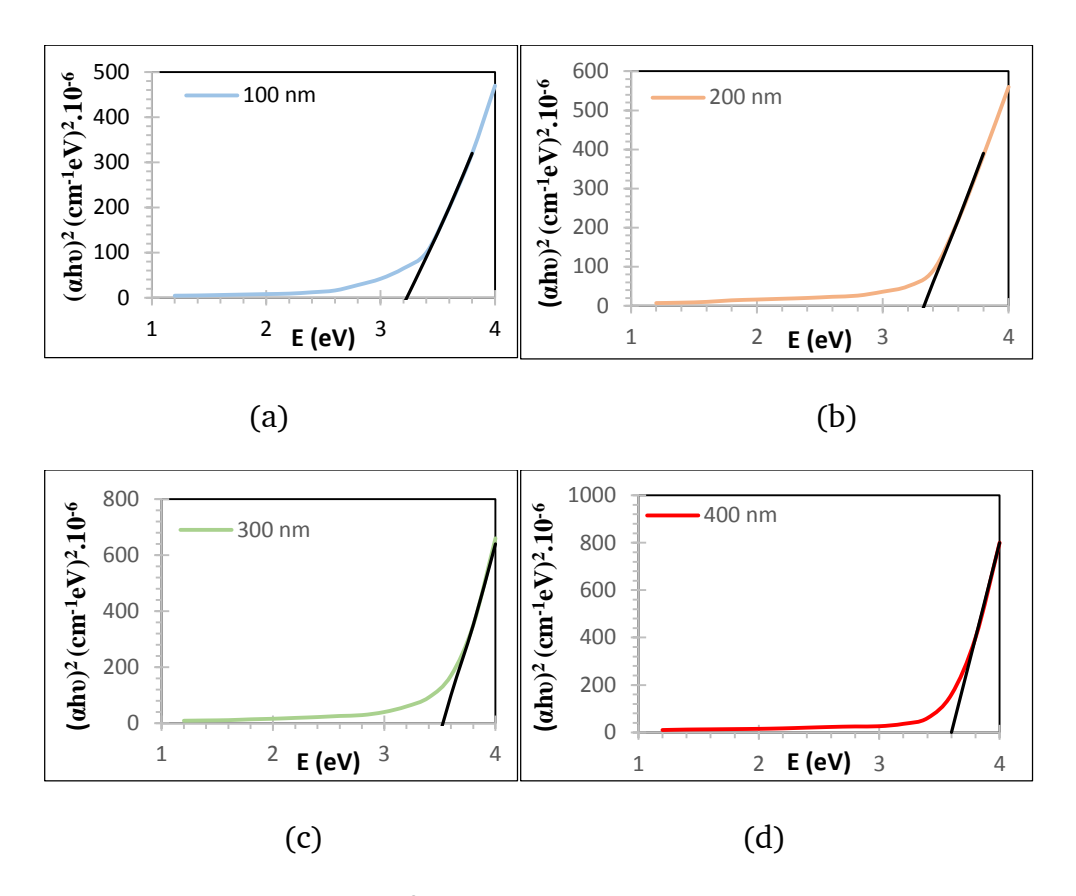


Figure 5.8 Plots of $(\alpha h \nu)^2$ as a function of $h \nu$ for ZnO films at different thicknesses

5.3.1.2 Electrical Properties

The resistivity of the ZnO films at different thicknesses was investigated. It can be seen that theresistivities was increased with the thickness increases. The resistivities in the range of thicknesses (100, 200, 300, and 400) nm were 20.64, 20.84, 21.20, and 21.78 Ω .cm. Depending on the results; we found that the resistivity has the direct effect to the thicknesses increasing.

5.3.2 The Effect of Thermal Treatment Time on Optical Properties of Undoped and Na Doped ZnS Thin Films

In the following sections present the optical properties of unannealed and annealed behavior of Na doped and undoped ZnS films. It was shown that the annealing treatment has a different effect on the transmittance of the ZnS films. The increases of transmittance with the increasing of annealing time may be attributed to decreasing optical scattering caused by defects of film crystallites, it means that crystallite boundaries reduces when crystallites size increses [71].

However, the best results were achieved from the band gap of pure ZnS with (0.05M) as 3.00 eV and 10% Na doped ZnS with (0.025) M as 3.30 eV.

5.3.2.1 Undoped ZnS (0.05 Molarity)

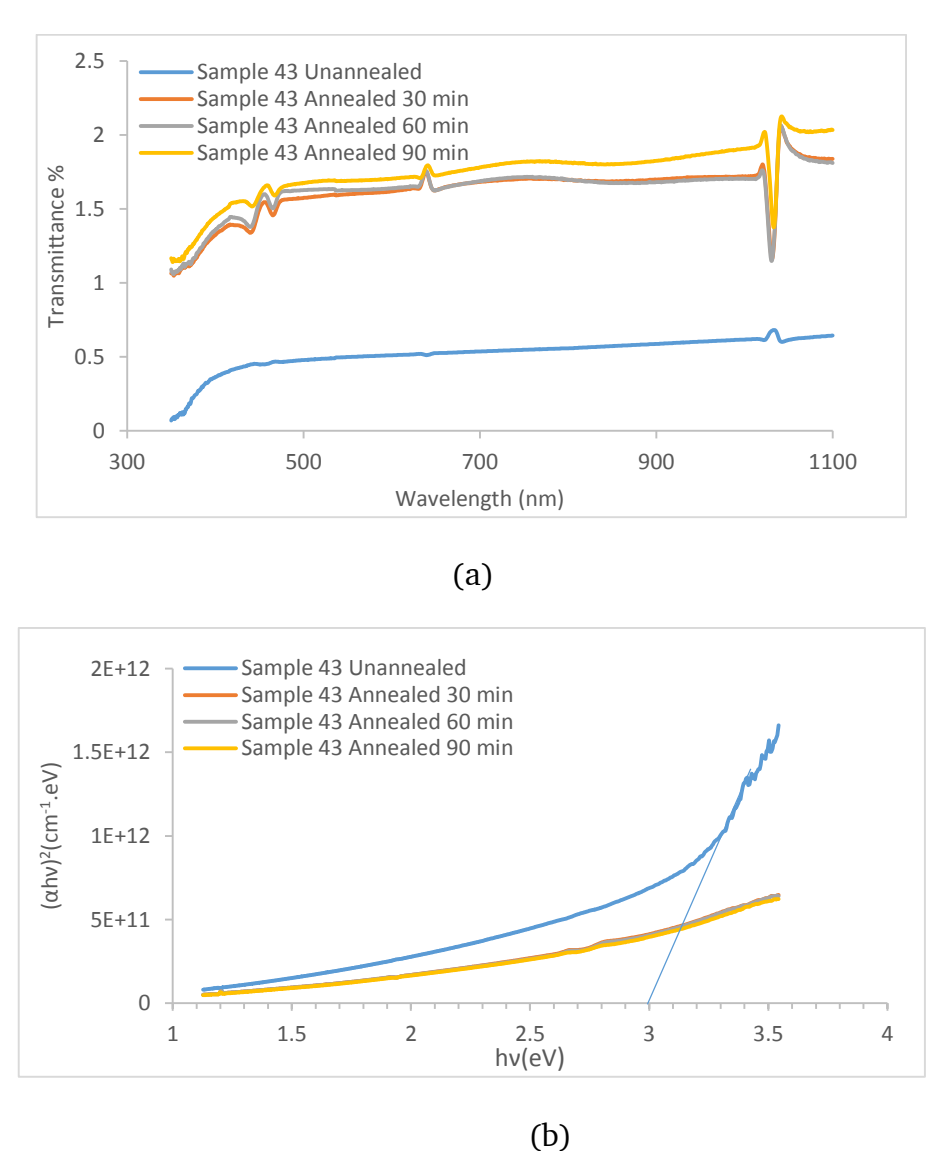


Figure 5.9 (a) Transmittance spectra (b) absorpance of undoped ZnS thin films before and after annealing at 450 $^{\circ}$ C

5.3.2.2 1%Na Doped ZnS (0.05 Molarity)

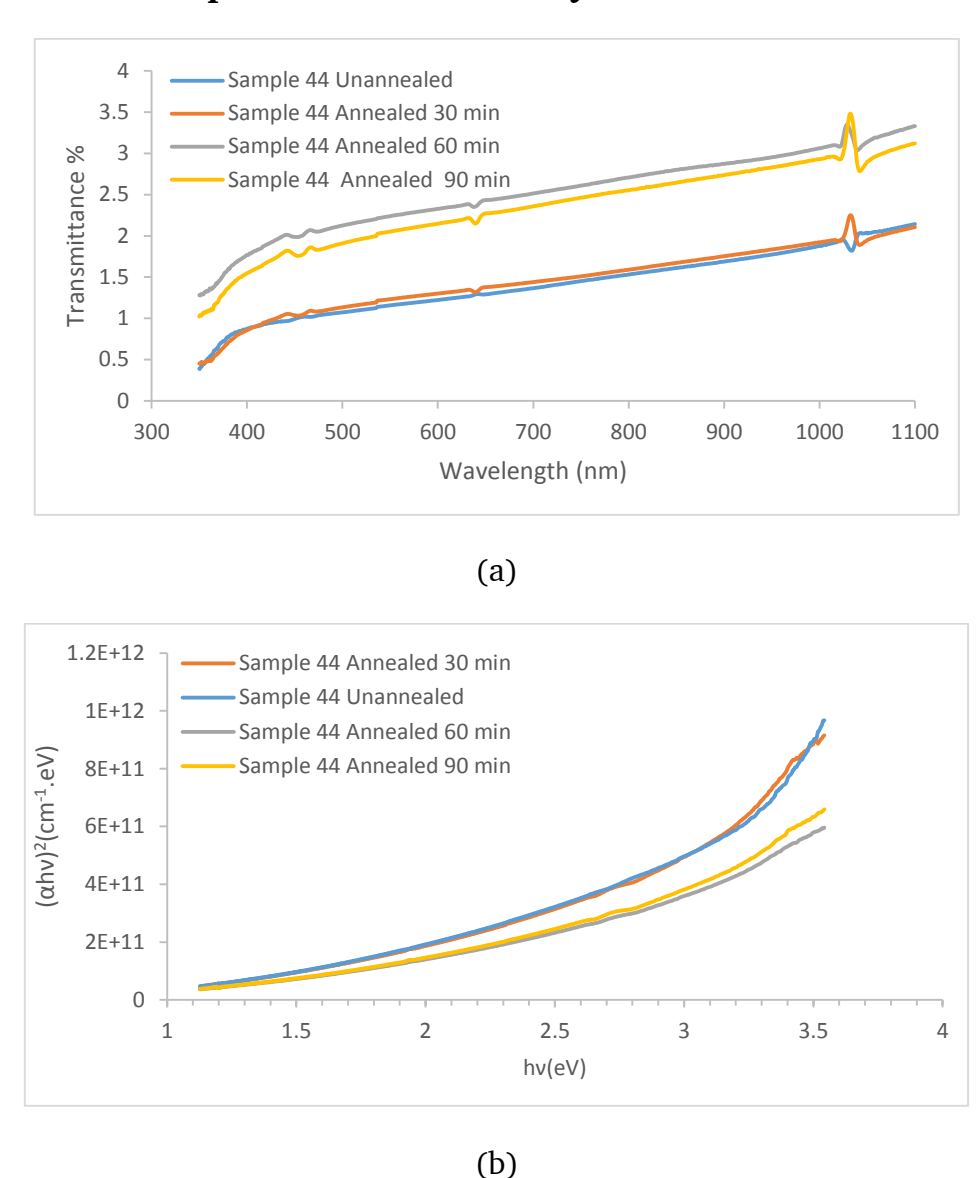
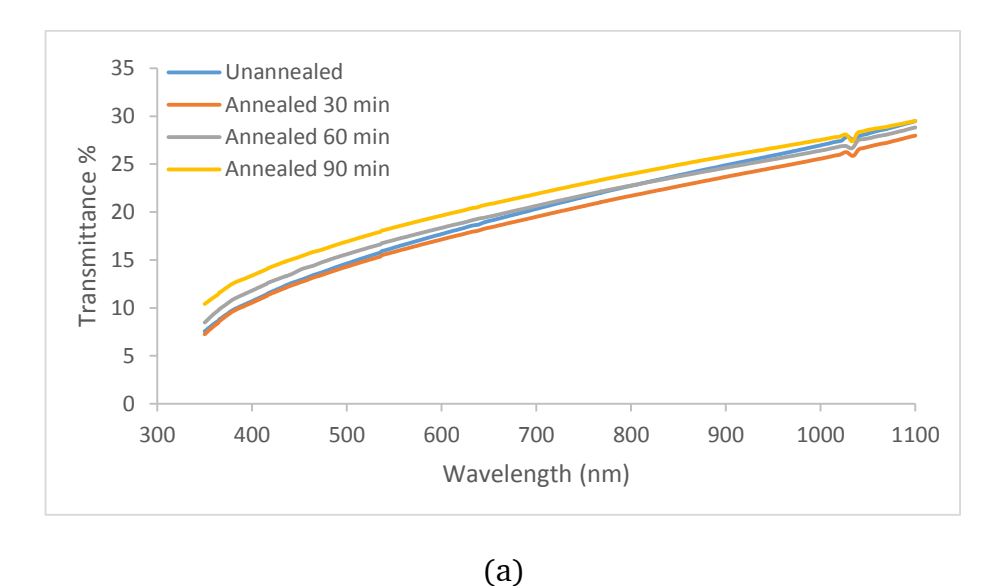


Figure 5.10 (a) Transmittance spectra (b) absorpance of 1% Na doped (0.05 M $ZnCl_2$ +0.05 M of $SC(NH_2)_2$) of ZnS thin films before and after annealing at $450^{\circ}C$

5.3.2.3 1%Na Doped ZnS (0.025 Molarity)



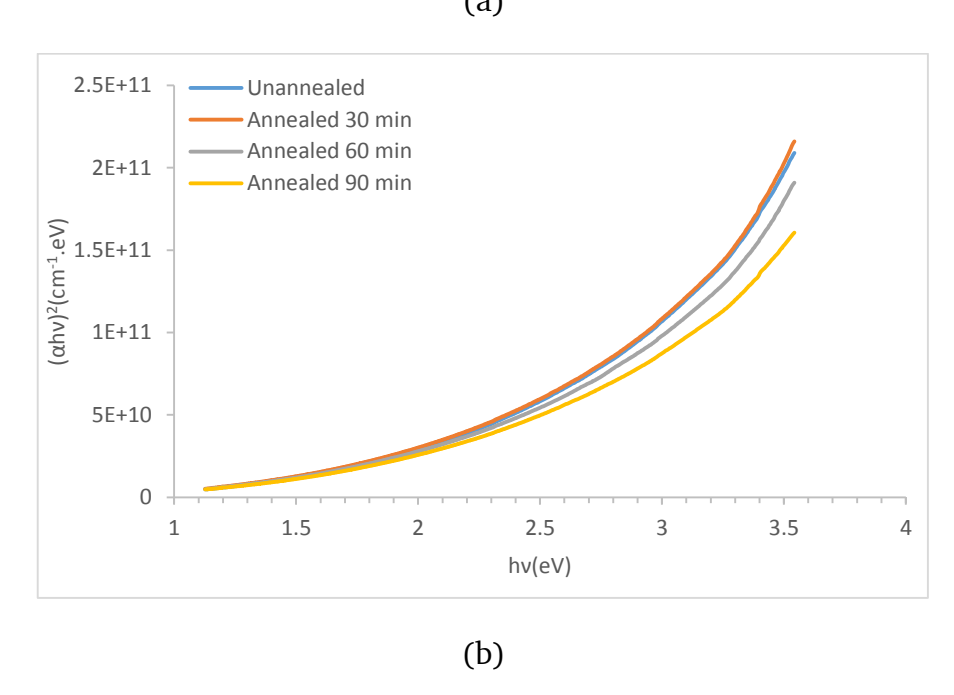


Figure 5.11 (a) Transmittance spectra (b) absorpance of ZnS (1% Na doped 0.025 M of ZnCl₂+0.025 M of SC(NH₂)₂, before and after annealing at 450 $^{\circ}$ C

5.3.2.4 5%Na Doped ZnS (0.025 Molarity)

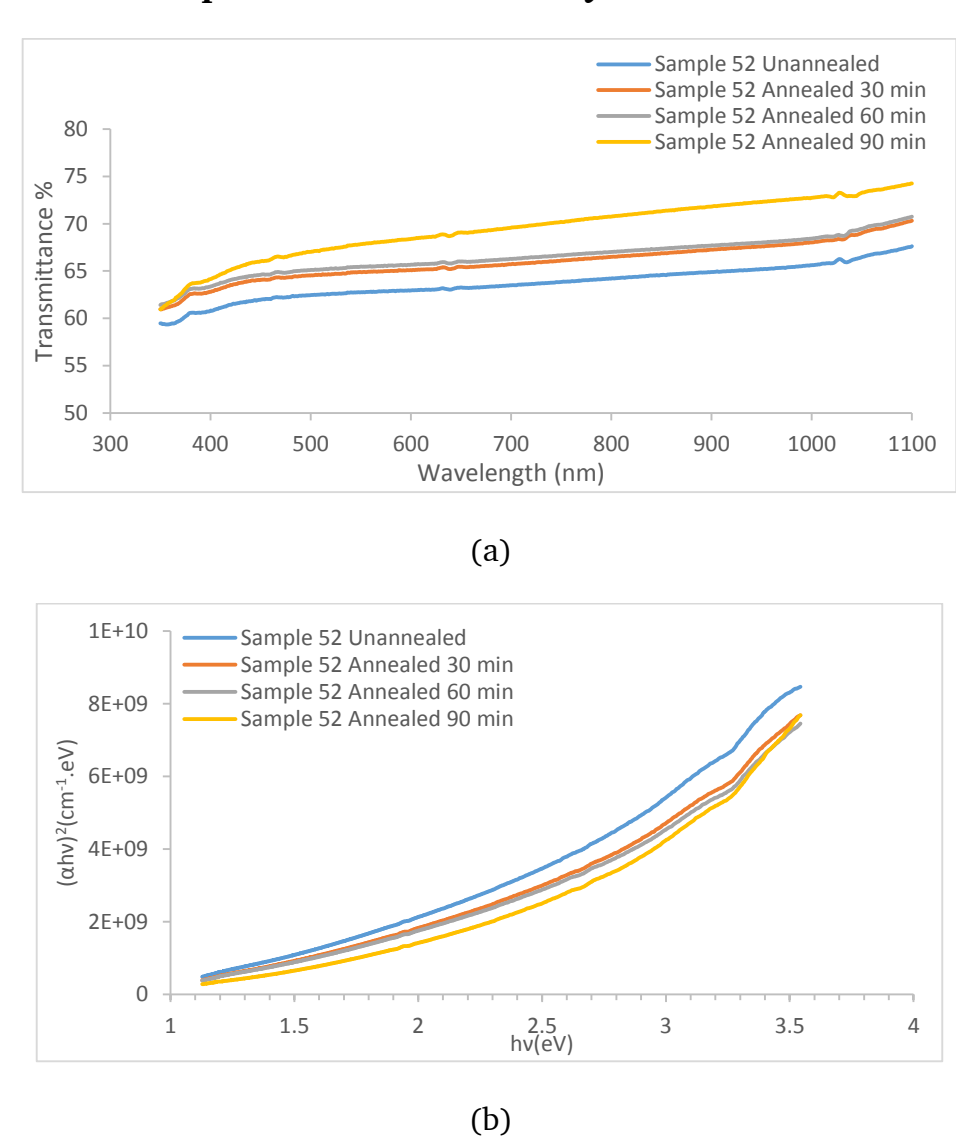
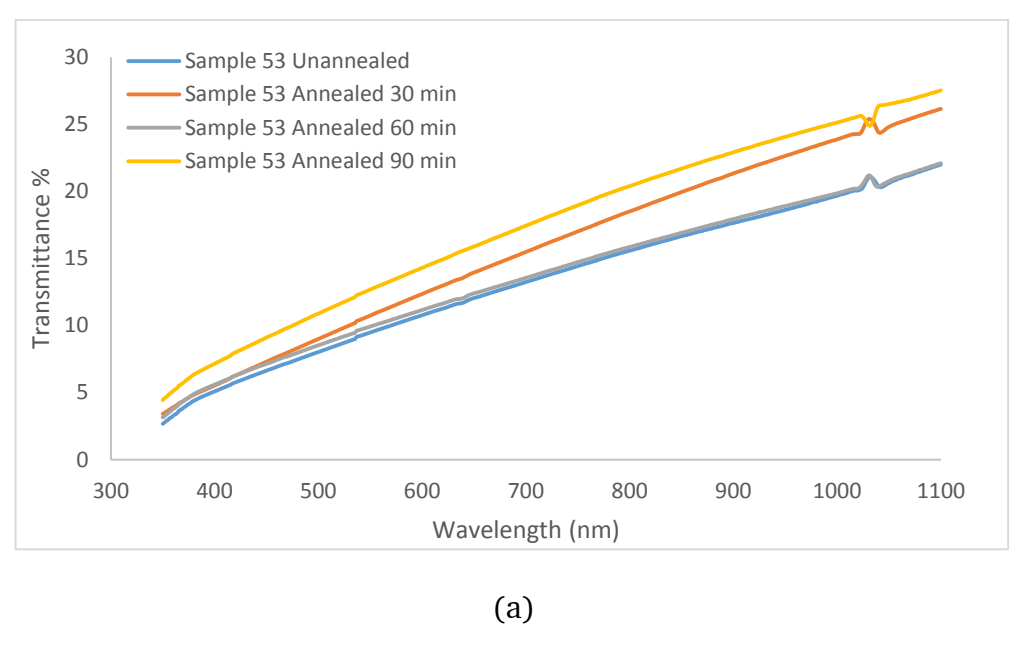


Figure 5.12 (a) Transmittance spectra (b) absorpance of ZnS (5% Na doped 0.025 M of $ZnCl_2+0.025 \text{ M}$ of $SC(NH_2)_2$), before and after annealing at 450 °C

5.3.2.5 10%Na Doped ZnS (0.025 Molarity)



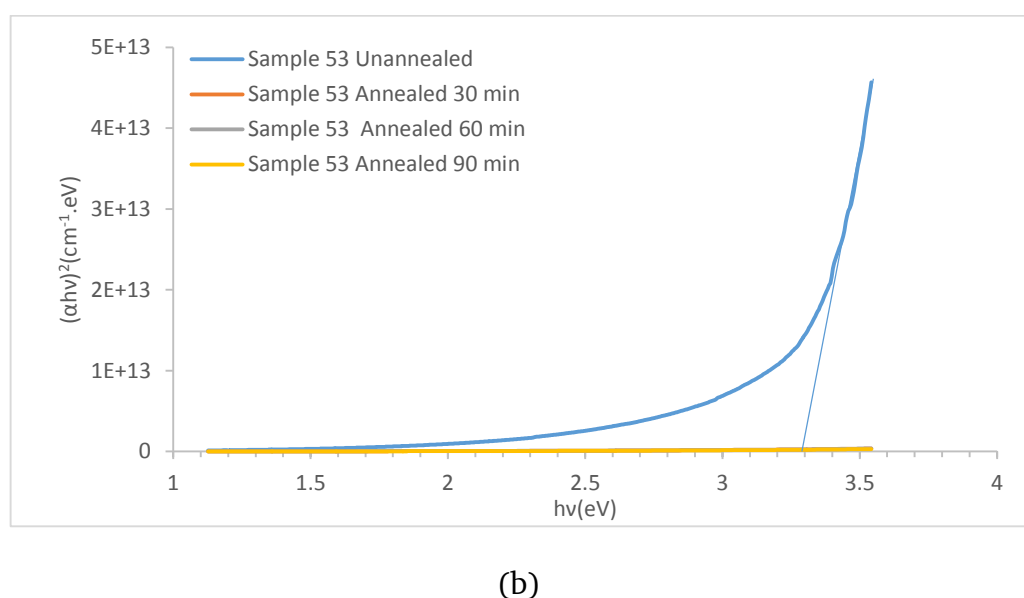


Figure 5.13 (a) Transmittance spectra (b) absorpance of ZnS (10% Na doped 0.025 M of ZnCl₂+0.025 M of SC(NH₂)₂, before and after annealing at 450 °C

5.3.3 Influence the Amount of Precursor Solution on the Optical Properties of ZnO Thin Films

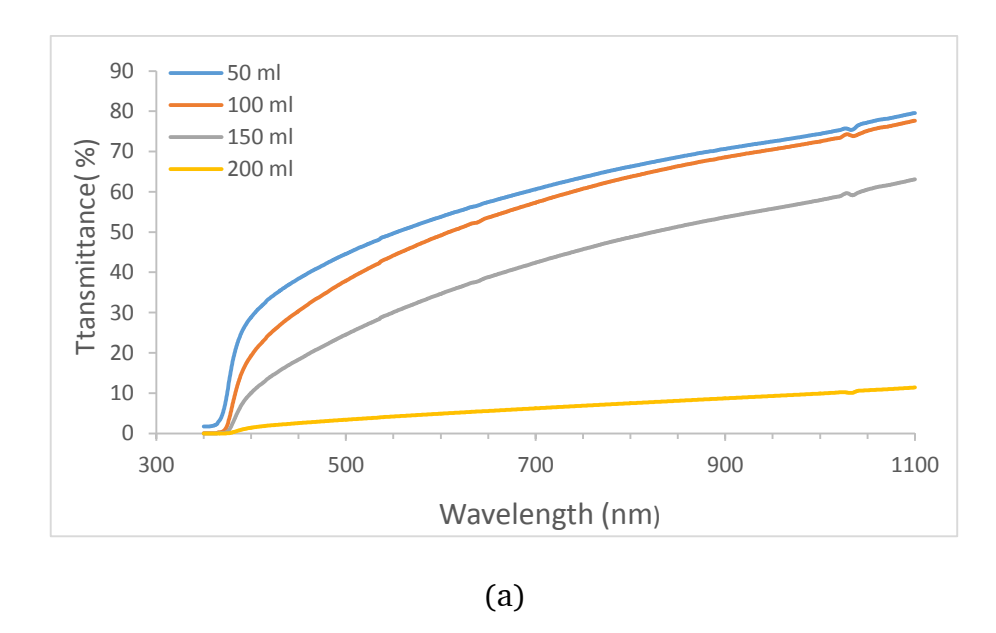
In this study, the effect of the varying amount of precursor solution on optical properties of ZnO thin films was investigated.

The ZnO films of various amount of spraying solution deposited onto preheated glass substrate with perfect adherence, and visual transparency was acquired at

temperature $T = 350^{\circ}C$ and the transmittance in the wavelength range 300-1100 nm. The transmittance spectra and absorbance of ZnO thin films grown with different amount of precursor growth solution (50, 100, 150 and 200 ml) to obtain different transmitions are presented in Figure 5.14.

The optical transmittance spectra of the ZnO films give the transparency in the visible range, the transmittace changed according to the films spray solution volum. As can see on Figure 5.14 (a), the transmittance of ZnO thin films with 50 and 100 ml are determined over 75% while with 150 ml the transmittance is lower than 60% in visible light region. Nonetheless, the transmittance at 200 ml is up to 10, which is so low compared with other molar concentration.

Similar result was found by Efkere *et. al.*, who was stated that increasing ZnO film amount of precursor solution lead to the decrease in band gap [64]. We can conclude that the transmittance is decreases with increasing the precoursor molar concentration.



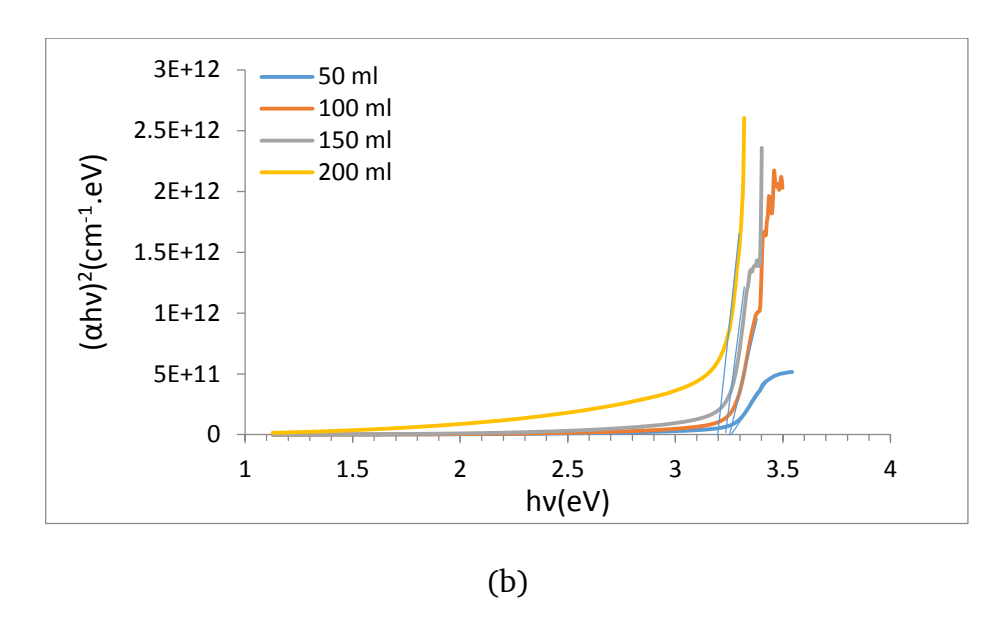


Figure 5.14 (a) Transmittance spectra and (b) absorpance of ZnO thin film (0.05) M of zinc acetate dihydrate at different amount of precursor solution

The optical absorption of ZnO thin films with different amount of precursor solution were figured out from Tauc plot (see equation 3.2) by extrapolation of the straight section of the versus photon energy as mentioned in Figure 5.14 (b). It can be seen the optical band gap decreases from 3.27 to 3.20 eV when precursor of growth solution was increased. This may attributed to increase in crystallite sizes with the increasing the amount of precursor solution [111].

5.3.4 Optical Properties of ZnO Prepared by Different Precursor Solutions

ZnO thin films were prepared using zinc acetate and zinc chloride by spray pyrolysis technique on glass substrate at 350 °C.

Uv-vis measurements were used to investigate the effect of precursor solution on optical properties. The optical transmittance for ZnO films is given in Figure 5.15 (a) as a function of wavelength in the range 350 to 1100 nm. In this study, ZnO film which is produced using zinc acetate were not found to be high transparent It was found that the optical transmittance in the visible region reach to over 50 % when zinc acetate dihydrate was used as a precursor solution. While the optical transmittance was exhibited worse and nonuniform when zinc chloride was used as a precursor solution. The main reason for the poor transparency of these

samples may be that its rough surface scattered and reflected light [112] at the grain boundaries, which is mentioned in the study of Bacaksiz *et al* on the ZnO thin films [79].

These films, which is prepared by zinc acetate dihydrate as a precursor solution, can be applied as UV-protective films for optoelectronic devices since these films have transmittance less 20% in UV region [28].

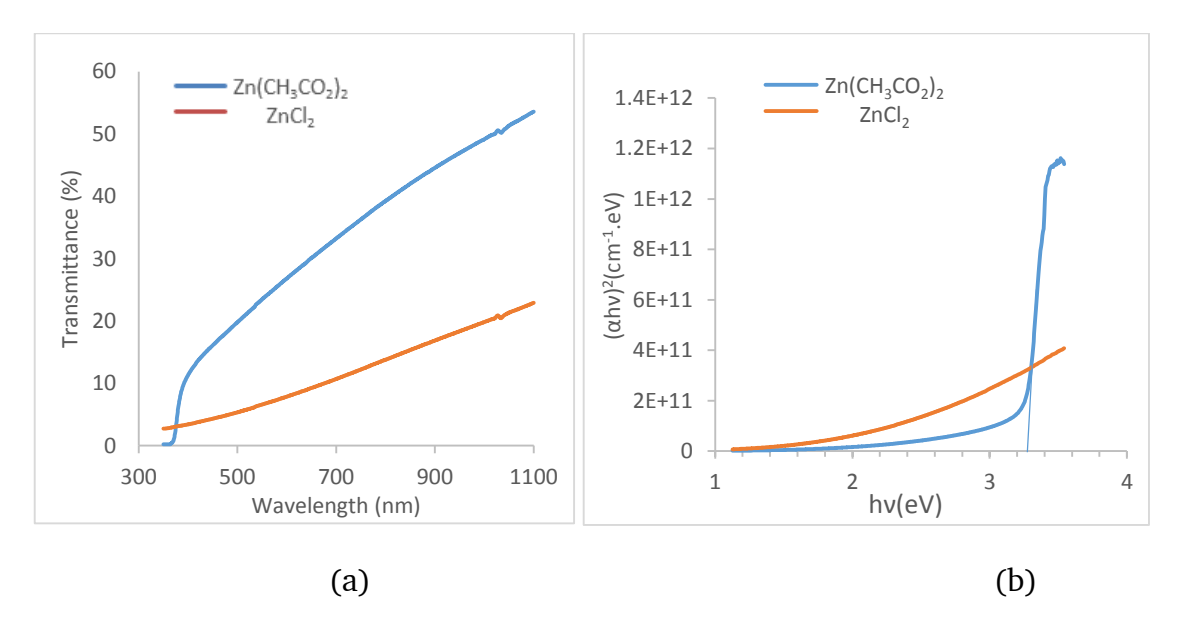


Figure 5.15 (a) Transmittance spectra and (b) absorption of ZnO thin film prepared by zinc acetate and zinc chloride

Figure 5.15 (b) represent the square of absorption coefficient $(\alpha h v)^2$ is plotted as a function of photon energy (hv). The extrapolated values of the optical band gap is approximately 3.3 eV for ZnO synthesized using precursor zinc acetate. Whereas we could not calculate the optical band gap of ZnS using precursor zinc chloride.

5.3.5 The Properties of ZnO Thin Films and ZnO/Si Heterojunction Cells

5.3.5.1 Structural Properties

The crystal structures and crystallization of spray pyrolysis derived ZnO thin films deposited on glass and p-Si substrates were investigated by X-ray diffraction. Figure 5.15 shows the diffraction patterns of ZnO thin film sprayed on glass substrate at 350 °C. The result shows a preferred orientation of (101) with the remarkably highest peak and second peaks of (002), (100), (102), and (103), this

means that our spray pyrolysis process produced polycrystalline ZnO films with a hexagonal wurtzite phase. The peak positions are in good agreement with the data from JCPDS card. It can be seen that no other peaks were detected, revealing that the prepared material is pure ZnO.

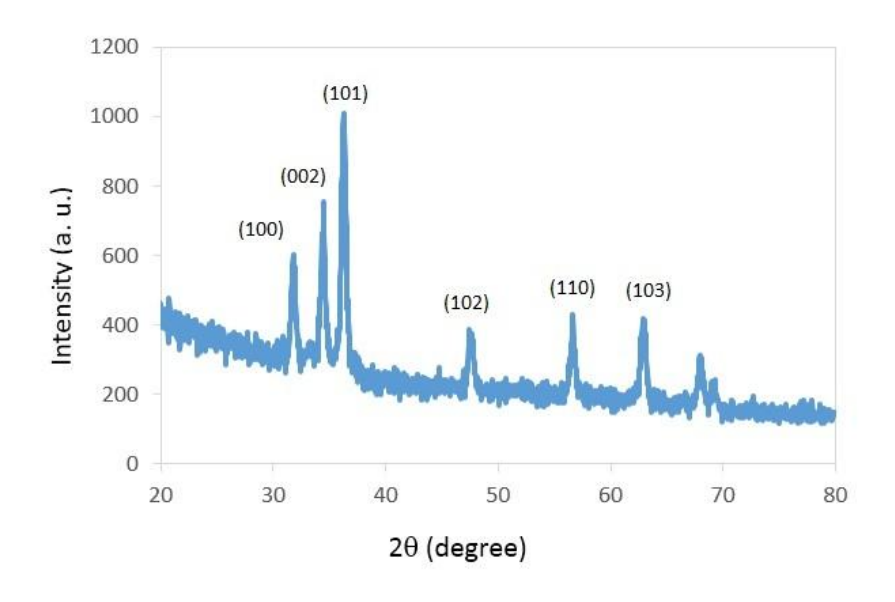


Figure 5.16 XRD pattern of spray pyrolised ZnO thin film

5.3.5.2 Effects of Annealing on the Electrical Properties

The principal function of the photovoltaic cell is to conversion of light into electricity under standard conditions. In this section, the annealing process at 350 °C for 30 minutes was applied after deposition ZnO layer on Si substrate in order to fabricate a junction. ZnO/Si heterojunction was prepared using zinc chloride as a precursor solution and spray pyrolysis technique was used as a deposition technique. The comparison between the electrical properties of both annealed and non-annealed ZnO/Si was investigated.

In the dark condition, the photovoltaic solar cell is regarded as a large diode and constructs the exponential J-V curve. Before illumination, the solar cell gives the smallest value of current density and there were no significant variation in $V_{\rm oc}$ between annealed and non-annealed samples, which is attributed to the minority carriers in dark conditions. While solar cell starts working under illumination condition and current flows as a result of generating the charge carriers by the incident photons. Figure 5.17 illustrates the J-V characteristics of non-annealed

and annealed ZnO/Si heterojunction cells under dark and illumination conditions. It can be seen that the current.

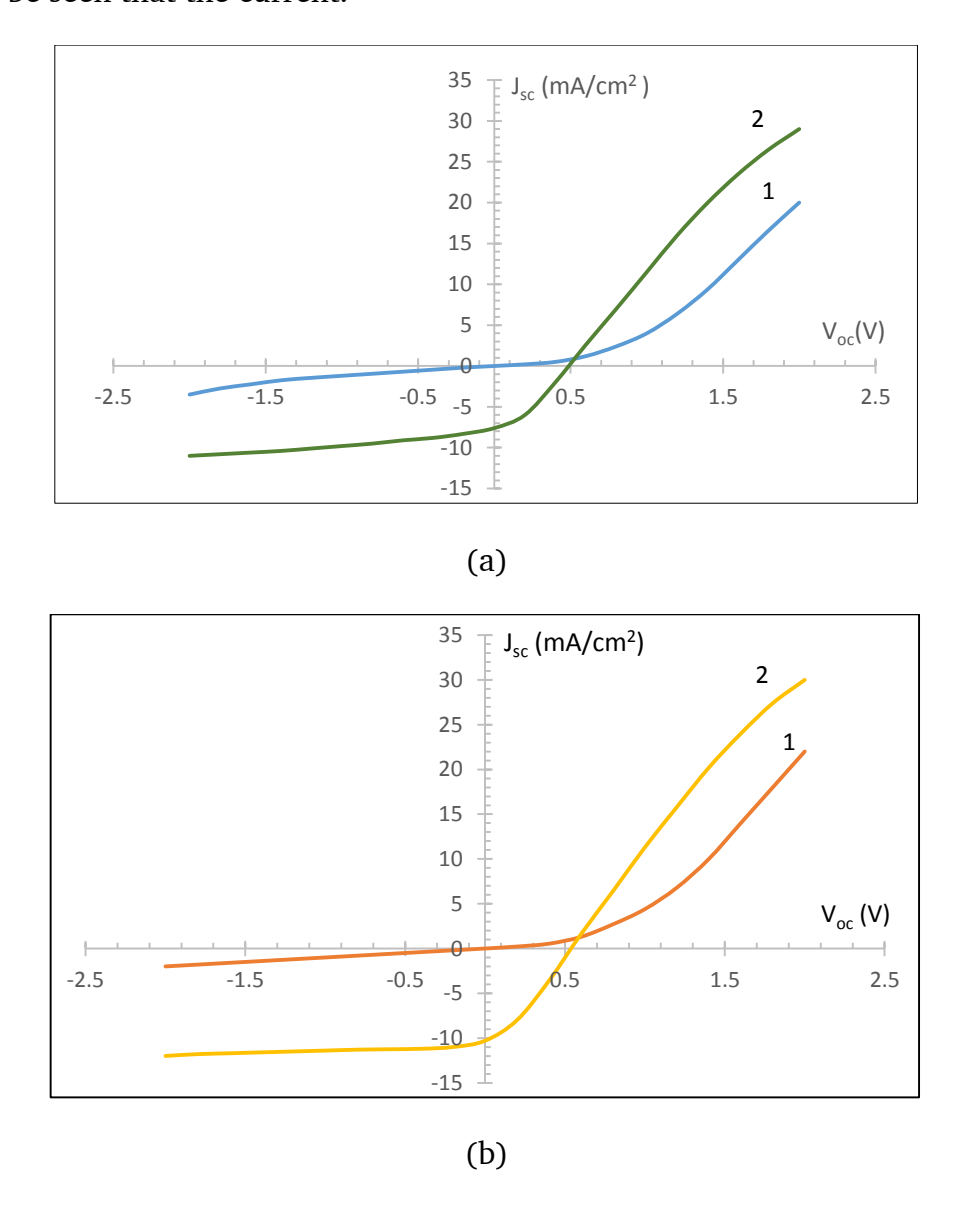


Figure 5.17 *J-V* characteristics of (a) non-annealed ZnO/Si heterojunction cell (b) annealed ZnO/Si heterojunction cell (1: in dark, 2: under illumination)

Figure 5.18 below presents the fourth quadrant current density vs voltage curve of the non-annealed and annealed ZnO/Si heterojunction solar cell under investigation. The information extracted from the measurements were used to determine the photovoltaic parameters such as open circuit voltage V_{oc} , short circuit current density I_{sc} , fill factor FF as well as the conversion efficiency PCE (η) . To calculate the solar cell efficiency, following relation is used.

$$\eta = \frac{P_{out}}{P_{in}} \times 100 \tag{5.1}$$

where $P_{out} = V_{oc} \times I_{sc} \times FF$ and P_{in} is the input power and equal to 100mW/cm². ZnO/Si heterojunction cell gives an open circuit voltage of 0.49 V, a short circuit current density of 7.6 mA/cm², fill factor 0.32 and conversion efficiency of 1.2 %. These values are in the range that mentioned by Chabane *et al* [26].

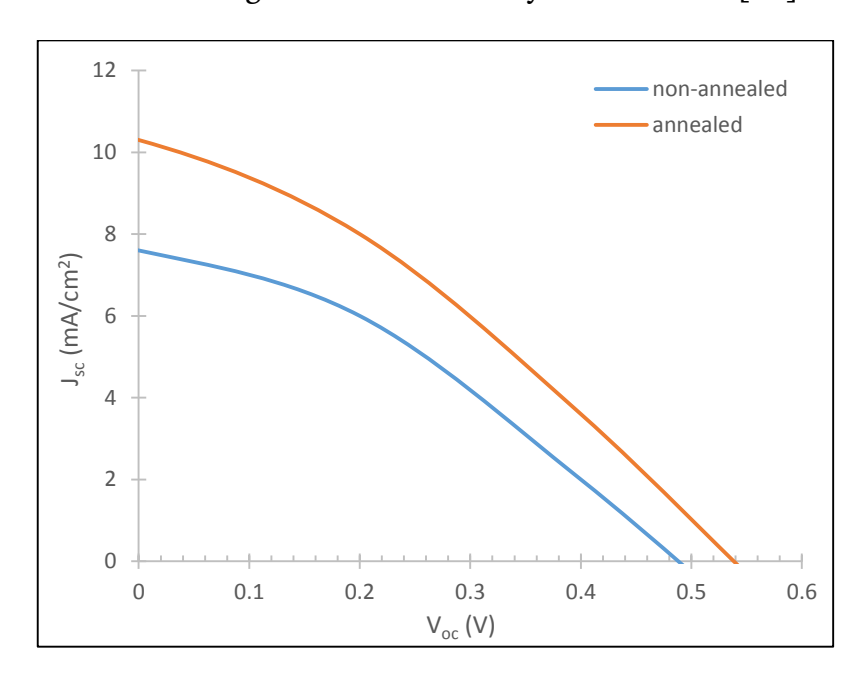


Figure 5.18 J-V characteristics of non-annealed and annealed ZnO/Si Heterojunction cell under illumination

As noticed in figure 5.18 the J_{sc} and V_{oc} considerably increased to 10.3 mA/cm² and 0.54 V respectively after annealing treatment for 30 minutes. The increased in PCE to 1.6 % is mentions that parameters of ZnO/Si heterojunction significantly enhanced after the thermal annealing process. Nonetheless, the FF declined from 0.32 to 0.29 after the thermal treatment was adequate to improve the heterojunction performance. Table 5.1 shows the comparison of the cell parameters of ZnO/Si solar cells declared for non-annealed and annealed process.

Table 5.1 Comparition between non-annealed and annealed ZnO/Si heterojunctopn cells

Annealing Treatment	J _{sc} (mA/cm ²)	<i>V_{oc}</i> (V)	Fill Factor FF	Efficiency (%)
Non-annealing	7.6	0.49	0.32	1.2
Annealing	10.3	0.54	0.29	1.6

5.3.6 The Properties of Undoped and Na Doped ZnS Thin Films and ZnS/Si Heterojunctions Cells

5.3.6.1 Structural Properties

Figure 5.19 shows XRD pattern of ZnS films deposited over glass substrate using 0.05 M zinc chloride (ZnCl₂) and 0.05 M thiourea (CS(NH₂)₂) with different concentration of Na doping that prepared at 350°C. XRD results of undoped and Na doped ZnS thin films, revealed that do not show other phases and the considerable difference in the shape and peak position for the doping concentration.

Three diffraction peaks are observed in all samples, which correlated with the peaks of (111), (220) and (311) at angles of 29°, 48° and 57° respectively, and these results are in agreement with Infahsaeng and Ummartyotin [113]. These peaks match with JCPDS data card no 77-2100 for cubic phase ZnS and the peak at 21.28° corresponds to (101) peak of ZnSO₄ [113, 52] which was not suppress characteristic ZnS peaks. The (111) peak become more broadened and bigger relative intensity peak when Na concentration increase.

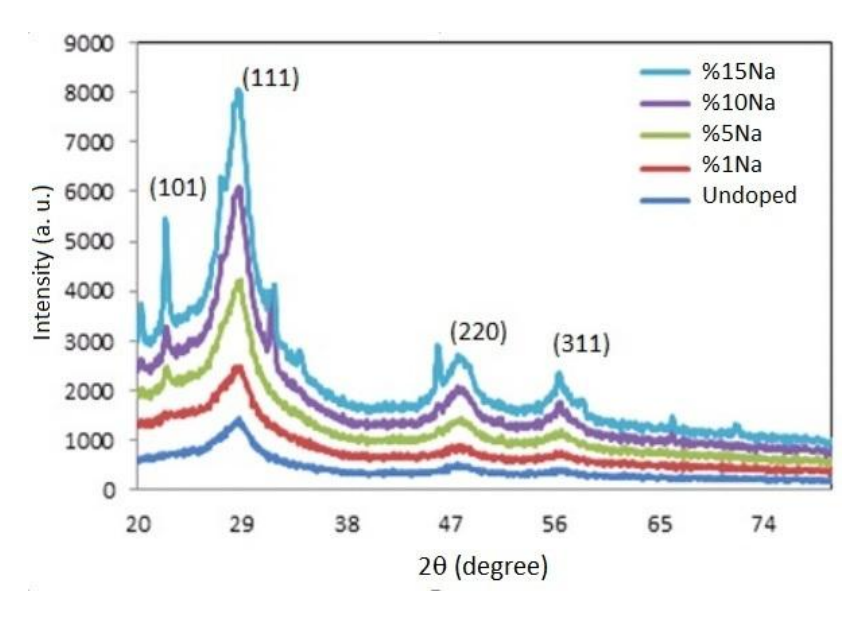
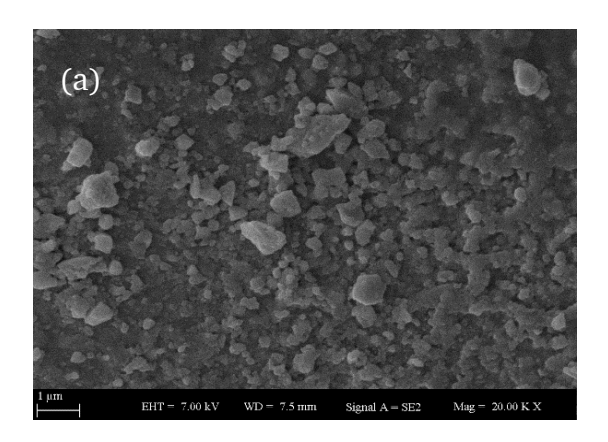


Figure 5.19 XRD patterns of undoped and doped ZnS thin films prepared by spray pyrolysis sprayed at 350°C

5.3.6.2 Surface Morphology

Figure 5.20 presents the top view of the SEM micrograph of undoped and Na doped ZnS on glass substrates by spray pyrolysis technique using 0.05 M zinc chloride (ZnCl₂) and 0.05 M thiourea (CS(NH₂)₂) with different concentration of Na doping that prepared at 350°C. As can be seen in Figure 5.20 (a) the surface morphology corresponding to the undoped ZnS, is relatively more homogeneous and dense with no cracks [114].

From image (b) of the sample with 15% Na dopant, it can be noted an irregular and inhomogeneous surface morphology and indefinite grain boundary of Na were comprehensibly observable from the images with some cracks. Porosity in thin film, which is very important for solar cell grain as Na increase. We can conclude that Na doping has no considerable effect on surface characteristics of ZnS thin films.



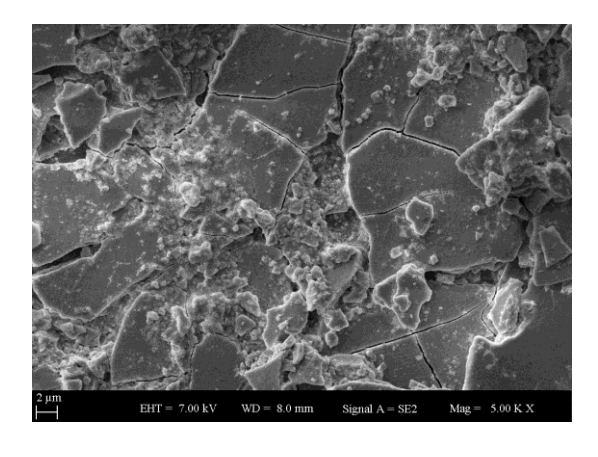


Figure 5.20 SEM images of (a) undoped, (b) 15% Na doped ZnS films were grown on glass substrate at 350°C

5.3.6.3 Optical Properties

The effect of Na doping on the optical properties of ZnS thin films synthesized by spray pyrolysis technique have been studies. Figure 5.21 (a) demonstrates the UV-visible transmittance spectra of ZnS thin films synthesized at various dopant concentration. Generally, the optical transmittance of these films exceeds 60% in the range of 300-1100 nm. Very small decrease in transmittance was observed for 1% Na doped film. Decrease in transmittance was more perceivable for increasing Na concentrations. In addition, it can be said that Na doping decreases the transmittance of ZnS due to the decrease of crystalline quality.

The Tauc's plot of the square of the photon energy absorption coefficients $(\alpha hv)^2$ against a function of energy (hv) is shown in the inset of Figure 3b. Band gap energy of ZnS films determined as explained in section 3.3 in chapter 3. A decrease in band gap energy observed with the values of 3.66 eV for undoped and 3.59, 3.53, 3.49, and 3.42 eV for 1, 5, 10 and 15% Na doped ZnS films respectively as shown in Table 5.1.

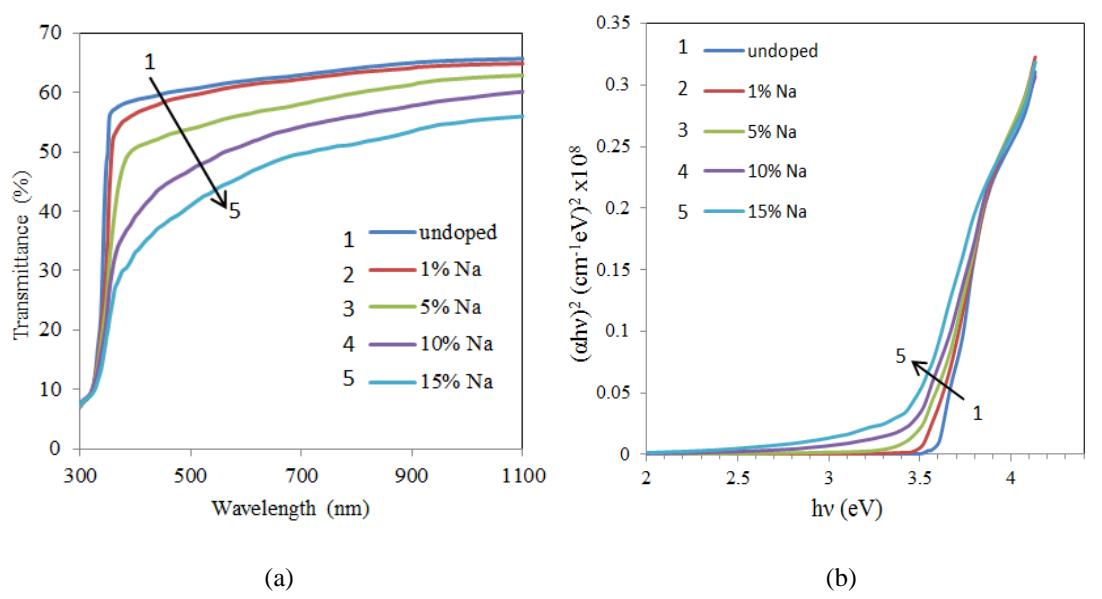


Figure 5.21 (a) Transmittance versus wavelength plots (b) absorption spectra, of undoped, 1%, 5%, 10% and 15% Na doped

5.3.6.4 Electrical Properties

All ZnS thin films were in n-type conductivity. The intrinsic ZnS should be doped in order to reduce resistivity. When the ZnS thin films doped, the resistivity decrease, which lead to increase the difference in Fermi energy between ZnS and

p-Si and hence the performance of the device will improve [44]. In the present work, noticeable decrease in resistivity was determined as Na doping concentration increase. Resistivity of undoped ZnS film was $5.17x10^5 \Omega$.cm where 4.53×10^5 , 3.81×10^5 , 2.56×10^5 and $2.00 \times 10^5 \Omega$.cm for 1, 5, 10 and 15% doped films respectively as illustrate in Table 5. Rate of resistivity decrease was greater than the rate of band gap energy decrease. Owing to this interpretation to this it could be thought that Na behaves as donor dopant in n-type ZnS film [115].

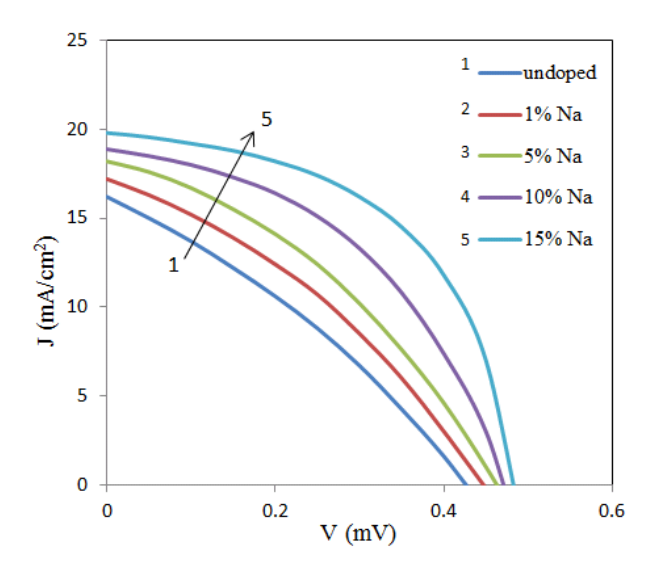


Figure 5.22 Current-voltage characteristics of ZnS/Si heterostructures with doped and undoped ZnS layers under illumination

Figure 5.22 shows the illuminated J-V characteristics of ZnS/Si heterojunction cells with undoped and doped ZnS layers. The functional parameters as open circuit voltage, short circuit current density, fill factor and power conversion efficiency were increase by increasing doping concentration. All the improved parameters are illustrated in Table 5.1 V_{oc} of the cell increased to 482 mV from 425 mV and Jsc was increased to 19.8 mA/cm² from 16.2 mA/cm² gradually with increasing Na doping concentration. FF of the cell increased to 0.53 from 0.32 and as a result of overall improvement in the photovoltaic performance of the cell PCE (η) was increased to 5.06% from 2.20%.

Table 5.2 Parameters of ZnS films and ZnS/Si cells with undoped and Na doped ZnS layers

Na doping concentrations		Undoped	1% Na	5% Na	10% Na	15% Na
ZnS Thin Film Parameters	E _g (eV)	3.66	3.59	3.53	3.49	3.42
	Resistivity (Ω.cm)	5.17x10 ⁵	4.53x10 ⁵	3.81x10 ⁵	2.56x10 ⁵	2.00x10 ⁵
ZnS/Si Cell Parameters	J _{sc} (mA/cm ²)	16.2	17.2	18.2	18.88	19.8
	V _{oc} (mV)	425	446	462	468	482
	Fill Factor	0.32	0.35	0.37	0.45	0.53
	Efficiency (%)	2.20	2.68	3.11	3.98	5.06

5.4 Conclusion

In this thesis, the characteristics and efficiency of solar cells substantially relied on the material used. Therefore, three different fabrication methods including chemical bath deposition, spin coating and spray pyrolysis were carried out to produce high efficiency and cost-effective solar cells. We assume that the properties of ZnS and ZnO films can be improved by adjusting the fabrication techniques and applying some effects such as doping and thermal annealing and; as a result, we can achieve higher efficiency solar cells.

CBD was implemented to grow undoped and Na doped ZnS films over glass, FTO and Si substrates with double and 4-times molarity. The results demonstrate the significant influence of thermal treatment with respect to the time on the optical properties of ZnS films.

ZnS thin films were successfully grown by spin coating techniques that deposited on a glass substrate. Thanks to being low cost, low evaporation temperature and easy coating for a large area. The optical properties of the ZnS film were experimentally tested. The result shows that the low value of the energy band gap is attributed to the applied five-layer deposition.

The optical properties related to the effect of the amount of growth precursor solution of ZnO were investigated. The results present the decreasing of the optical band gap when the amount of solution increases and this can be explained as the increase in crystallite size.

Spray pyrolysis method was used for the fabrication of undoped and Na doped in glass and Si substrates with 1, 5, 10, and 15% doping concentrations. Just as spray pyrolysis methods were carried out for fabrication ZnO/Si heterojunction. XRD patterns displayed that ZnO films and all doped and undoped ZnS films were in a cubic structure. By means of optical and electrical properties, the results display the band gap energy and resistivity of ZnS films decreased when the doping concentration increase.

Several parameters that affected the performance of a photovoltaic cell including efficiency were explained. Efficiency of ZnS/Si heterojunction cells increased to 5.06% from 2.20%. This significant overall improvement of device performance as a result of increasing J_{sc} to 19.8 mA/cm² from 16.2 mA/cm², V_{oc} to 482 mV from 425 mV and FF to 0.53 from 0.32. These improvements can be attributed essentially to resistivity decreases of ZnS layer with Na doping. ZnO/Si heterojunction solar cell was investigated with the characterization of open circuit voltage of 0.49 V, a short circuit current density of 7.6 mA/cm², fill factor 0.32 and conversion efficiency of 1.2 %.

It was found that the efficiency of undoped and Na doped ZnS/Si is larger than undoped ZnO/Si under the same conditions

- [1] I. M. Dharmadasa, Advances in Thin –Film Solar Cells, Pan Stanford Publishing, Singapore, 2018. http://www.panstanford.com,
- [2] World population projected to reach 9.7 billion by 2050 | UN DESA | United Nations Department of Economic and Social Affairs. (n.d.). http://www.un.org/en/development/desa/news/population/2015-report.html. Accessed 9 Apr, 2017.
- [3] B. Hussain, A. Ebong, and I. Ferguson, "Zinc Oxide and Silicon Based Heterojunction Solar Cell Model," 42nd Photovoltaic Specialist Conference, 2015. doi: 10.1109/PVSC.2015.7356242,
- [4] P. Würfel and U. Würfel, Physics of Solar Cells, Wiley-VCH Verlag GmbH & Co.KGaA, Boschstr. 12, 69469 Weinheim, Germany, 2016.
- [5] S. Anwar, H. Efstathiadis, and S. Qazi, Handbook of Research on Solar Energy Systems and Technologies, IGI Global. USA, 2013.
- [6] A. Reinders, P. Verlinden, W.V. Sark, and A. Freundlich, Photovoltaic Solar Energy From Fundamentals to Applications, John Wiley & Sons, Ltd, United Kingdom, 2017.
- [7] World Energy Outlook, https://www.iea.org/reports/world-energy-outlook-2019.
- [8] A. A. Ojo, W. M. Cranton, and I. M. Dharmadasa, Next generation multilayer graded band gap solar cells, Springer International Publishing, Switzerland, 2019.
- [9] L. Zang, Energy efficiency and renewable energy through nanotechnology, Springer-Verlag London, New York, 2011.
- [10] K. Ellmer, A. Klein, and B. Rech, Transparent Conductive Zinc Oxide Basics and Applications in Thin Film Solar Cells, Springer-Verlag Berlin Heidelberg, Springer, 2008.
- [11] https://www.nrel.gov/pv/cell-efficiency.html
- [12] P. K. Nayak, S. Mahesh, H. J. Snaith, and D. Cahen, "Photovoltaic solar cell technologies: analyzing the state of the art," Nature Reviews Materials, vol 4, pp. 269-285, 2019.
- [13] K. Masuko, M. Shigematsu, T. Hashiguchi, D. Fujishima, M. Kai, N. Yoshimura, T. Yamaguchi, Y. Ichihashi, T. Mishima, N. Matsubara T. Yamanishi, T. Takahama, M. Taguchi, E. Maruyama, and S. Okamoto, "Achievement of more than 25% conversion efficiency with crystalline silicon heterojunction solar cell," IEEE Journal of Photovoltaics, vol. 44, pp. 1433-1435, 2014.
- [14] M. Jlassi, I. Sta, M. Hajji, and H. Ezzaouia, "Effect of nickel doping on physical properties of zinc oxide thin films prepared by the spray pyrolysis method," Applied Surface Science, vol. 301, pp. 216-224, 2014.

- [15] S. Ilican, K. Gorgun, S. Aksoy, Y. Caglar, and M. Caglar, "Fabrication of p-Si/n-ZnO:Al heterojunction diode and determination of electrical parameters," Journal of Molecular Structure, vol. 1156, pp. 657-683, 2018.
- [16] J. H. Kang, K. S. Lee, and E. K. Kim, "Photovoltaic property of n-ZnO/p-Si heterojunctions grown by pulsed laser deposition," Thin Sold Films, vol. 658, pp. 22-26, 2018.
- [17] B. El Filali, J. A. Jaramillo Gomez, T. V. Torchynska, J. L. Casas Espinola, and L. Shcherbyna, "Band-edge emission, defects, morphology and structure of indoped ZnO nanocrystal films," Optical Materials, vol. 89, pp. 322-328, 2019.
- [18] P., D'Amico, A. Calzolari, A. Ruini, and A. Catellani, "New energy with ZnS: novel applications for a standard transparent compound," Scientific Reports, 2017. doi:10.1038/s41598-017-17156-w.
- [19] H. Dhasmana, S. H. Shital, and V. Dutta, "ZnO nanostructure thin films by continuous spray pyrolysis using doped precursor for Si solar cell application," Journal of Materials Science- Materials in Electronics, 2014. ISSN: 0957-4522, 25, 4095-4102.
- [20] O. O. Abegunde, E. T. Akinlabi, O. P. Oladijo, S. Akinlabi, and A. U. Ude, "Overview of thin film deposition techniques," AIMS Materials Science, vol. 6, no.2, pp. 174-199, 2019.
- [21] M. Fortunato, C. R. Chandraiahgari, G.D. Bellis, P. Ballirano, P. Soltani, S. Kaciulis, L. Caneve, F. Sarto, and M. S. Sarto, "Piezielectric thin films of ZnOnanorods/nanowalls grown by chemical bath deposition," IEEE Transactions of Nanotechnology, vol. 17, pp. 311-319, 2018.
- [22] P. Uday Bhaskar, G. Suresh Babu, Y. B. Kishore Kumar, Y. Jayasree, and V. Sundara Raja, "Effect of bath concentration, temperature on the growth and properties of chemical bath deposition ZnS films," Materials Chemistry and Physics, vol. 134, pp. 1106-1112, 2012.
- [23] M. Sinha, R. Mahapatra, B. Mondal, T. Maruyama, and R. Ghosh, "Ultrafast and reversible gas-sensing properties of ZnO nanowire arrays grown by hydrothermal technique," Journal of Physics Chemistry, vol. 120, pp. 3019-3025, 2016.
- [24] R. Pietruszka, B. S. Witkowski, E. Zielony, K. Gwozdz, E. Placzek-Popko, and M. Godlewski, "ZnO/Si heterojunction soalr cell fabricated by atomic layer deposition and hydrothermal methods," Solar Energy, vol. 155, pp. 1282-1288, 2017.
- [25] B. Hussain, A. Aslam, T. M. Khan, M. Creighton, and B. Zohuri, "Electron affinity and bandgap optimization of zinc oxide for improved performance of ZnO/Si heterojunction solar cell using PC1D simulations," Electronics, vol. 8, no. 238, 2019. doi: 10.3390/electronics8020238.
- [26] L. Chabane, N. Zebbar, M. Trari, and M. Kechouane, "Opto-capacitive study of n-ZnO/p-Si heterojunctions elaborated by reactive sputtering method: Solar cell application," Thin Solid Films, vol. 636, pp. 419-424, 2017.

- [27] J. Jo, O. Seo, H. Choi, and B. Lee, "Enhancement-mode ZnO thin-film transistor grown by metalorganic chemical vapor deposition," Applied Physics Express, vol. 1, pp. 041202, 2008.
- [28] M. I. Khan, K. A. Bhatti, R. Qindeel, N. Alonizan, and H. S. Althobaiti, "Characterizations of multilayer ZnO thin films deposition by sol-gel spin coating technique," Results in Physics, vol. 7, pp. 651-655, 2017.
- [29] T. Hildebrandt, M. Kozolinsky, N. Loones, M. Bouttemy, J. Vigneron, A. Etcheberry, D. Lincot, F. Donsanti, and N. Naghavi, "Fast chemical bath deposition process at room temperature of ZnS-based materials for buffer application in high- efficiency Cu(In,Ga)Se2-based solar cells," IEEE Journal of Photovoltaics, vol. 8, no. 6, 2018. doi,10.1109/JPHOTOV.2018.2871601.
- [30] D. Akcan, A. Gungor, and L. Arda, "Structural and optical properties of Na doped ZnO films," Journal of Molecular Structure, vol. 1161, pp. 299-305, 2018.
- [31] N. Kamoun Allouche, T. Ben Nasr, N. Turki Kamoun, and C. Guasch, "Synthesis and properties of chemical bath deposition ZnS multilayer films", Materials Chemistry and Physics, vol. 123, pp. 620-624. 2010.
- [32] S. Kahraman, H. M. Çakmak, S. Çetinkaya, F. Bayansal, H. A. Çetinkara, and H. S. Güder, "Characteristics of ZnO thin films doped by various elements," Journal of Crystal Growth, vol. 363, pp. 86-92, 2013.
- [33] A. A. M. A. Noor, S. Shaari, and S. A. R. Mohammad, "Improving the production of self-assembled ZnS:Mn nanocrystals through the modification of Sol Gel spin coating approaches," Advance Materials Research, vol. 1024, pp. 23-26, 2014.
- [34] K. Qiu, D. Qiu, L. Cai, S. Li, W. Wu, Z. Liang, and H. Shen, "Preparation of ZnS thin films and ZnS/p-Si heterojunction solar cell," Materials Letters, vol. 198, pp. 23-26, 2017.
- [35] S. M. Sze, and M. K. Lee, Semiconductor Devices: Physics and technology, John Wiley and Sons, Inc, 2012.
- [36] P. Y. Yu, and M. Cardona, Fundamentals of semiconductors: Physics and Materials Properties, Springer-Verlag, Berlin Heidelberg, 2010.
- [37] P. Hofmann, Solid State Physics, Wiley-VCH Verlay GmbH & Co., Germany, 2015.
- [38] I. J. Pankove, Optical Processes in Semiconductors, Dover Publications, Inc, 1971.
- [39] S. M. Sze, and K. K. Ng, Physics of Semiconductors Devices, John Wiley and Sons, Inc, 2007.
- [40] D. E. Ortiz-Ramos, L. A. Gonzalez, and R. Ramirez-Bon, "p-Type transparent Cu doped ZnS thin films by the chemical bath deposition method," Materials Letters, vol. 124, pp. 267-270, 2014.
- [41] S. Q. Wang, "A comparative first-principles study of ZnS and ZnO in zinc blende structure," Journal of Crystal Growth, vol. 287, pp. 185-188, 2006.

- [42] U. M. Nayef, "Improve the efficiency of UV-detector by modifying the Si and porous silicon substrate with ZnS thin films," Optik, vol. 130, pp. 441-447, 2017.
- [43] W. Cai-Feng, H. Bo, Y. Hou-Hui, L. and Wei-Bing, "Structure and photoluminescence properties of ZnS film grown on porous Si substrate," Optics Laser Tech., vol. 43, pp. 1453-1457, 2011.
- [44] K. Qiu, Q. Xie, D. Qiu, L. Cai, W. Wu, W. Lin, Z. Yao, B. Ai, Z. Liang, and H. Shen, "Power-loss analysis of a dopant-free ZnS/p-Si heterojunction solar cell with WO3 as hole-selective contact," Solar Energy, vol.165, pp. 35-42, 2018.
- [45] A. Azmand, and H. Kafashan, "Al-doped ZnS thin films: Physical and electrochemical characterizations," Journal of Alloys and Compounds, vol. 779, pp. 301-313, 2019.
- [46] J. McCloy, and R. Tustison, Chemical Vapour Deposited Zinc Sulfide, Society of Photo-Optical Instrumentation Engineers (SPIE), USA, 2013.
- [47] Y. J. Hsiao, T. H. Meen, L. W. Ji, J. K. Tsai, Y. S Wu, and C. J. Huang, "Preparation of ZnS microdisks using chemical bath deposition and ZnS/p-Si heterojunction solar cell," Journal of Physics and Chemistry of Solids, vol. 74, pp. 1403-1407, 2013.
- [48] H. Absike, H. Labrim, B. Hartiti, K. Douhou, and H. Ez-Zahraouy, "Ab initio calculations on electronic, optical and thermoelectric properties of (Si, Pb) (co)-doped ZnS for solar cell device applications," Journal of Physics and Chemistry of Solids, vol. 132, pp. 10-17, 2019.
- [49] X. Yang, B. Chen, J. Chen, Y. Zhang, W. Liu and Y. Sun, "ZnS thin film functionalized as back surface field in Si solar cell," Materials Science in Semiconductor Processing, vol. 74, pp. 309-312, 2018.
- [50] G. Arandhara, J. Bora, and P. K. Saikia, "Effect of pH on the crystallite size, elastic properties and morphology of nanostructured ZnS thin films prepared by chemical bath deposition technique," Materials Chemistry and Physics, vol. 241, pp. 122277, 2020.
- [51] P. O. Offor, S. N. Ude, G. S. Whyte, C. S. Obayi, P. S. Nnamchi, A. D. Omah, F. U. Whyte, S. Madu, U. O. Ogbuefi, C. C. Daniel-Mkpume, B. O. Anyaka, F. Okorie, and I. Ezema, "The influence of substrate temperature on properties of zinc sulfide thin films synthesized by chemical spray pyrolysis," Asian Journal of Basic Science & Research, vol. 2, pp. 1-15, 2020.
- [52] F. Ongul, U. Ulutas, S. Aydin Yuksel, S. S. Yesilkaya, and S. Gunes, "Influences of annealing temperature and thickness on ZnS buffer layers for inverted hybrid solar cells," Synthetic Metals, vol. 220, pp. 1-7, 2016.
- [53] D. Agraval, S. L. Patel, H. S. Chander, M. D. Kannan, and M. S. Dhaka, "Role of properties for buffer layers," Optik, vol. 199, pp. 163307, 2019.
- [54] M. Sathiskumar, M. Saroja, M. and Venkatachalam, "Influence of (Cu, Al) doping concentration on structural, optical and antimicrobial activity of ZnS thin films prepared by sol-gel dip coating techniques," Optik, vol. 182, pp. 774-785, 2019.

- [55] T. Hurma, "Structural and optical properties of nanocrystalline ZnS and ZnS:Al films," Journal of Molecular Structure, vol. 1161, pp. 279-284, 2018.
- [56] S. Joishy, A. Antony, P. Poornesh, R. J. Choudhary, and B. V. Rajendra, "Influence of Cd on structure, surface, morphology, optical and electrical properties of nanocrystalline ZnS films," Sensors and Actuators A: Physical, vol. 303, pp. 111719, 2020.
- [57] R. A. Colina-Ruiz, J. A. Hoy-Benitez, J. S. Lezema-Pachero, J. Mustre de Leon, and F. J. Espinosa-Faller, "Multivalance states and optical band-tail effectin heavily V-doped ZnS thin films," Materials Letters, vol. 257, pp. 126774, 2019.
- [58] S. Ebrahimi, B. Yarmand, and N. Naderi, "Enchanced optoelectronical properties of Mn-doped ZnS films deposited by spay pyrolysis for ultraviolet detection applications," Thin Solid Films, vol. 676, pp. 31-41, 2019.
- [59] A. Goktas, A. Tumbul, Z. Aba, A. Kilic, and F. Aslan, "Enhancing crystalline/optical quality, and photoluminescence properties of the Na and Sn substituted ZnS thin films for optoelectronic and solar cell applications; a comparative study," Optical Materials, vol. 107, pp. 110073, 2020.
- [60] S. S. Yesilkaya, U. Ulutas, M. M. Abd Alqader, "Effect on Na doping on the properties of ZnS thin films and ZnS/Si heterojunction cells," Materials Letters, vol. 288, pp. 129-347, 2021.
- [61] T. Amakali, L. S. Daniel, V. Uahengo, N. Y. Dzade, and N. H. De Leeuw, "Structural and optical oroperties of ZnO thin films prepared by molecular precursor and sol-gel methods," Crystals, vol. 132, pp. 10020132, 2020.
- [62] C. Jagadish, and S. Pearton, Zinc Oxide Bulk, Thin Films and Nanostructures, Elsevier Ltd., UK, 2006.
- [63] C. F. Klingshirn, B. K. Meyer, A. Waag, A. Hoffmann, and J. Geurts, Zinc Oxide: From Fundamental Properties Towards Novel Applications, Springer-Verlag Berline Heidelberg, 2010.
- [64] H. I. Efkere, A. Tataroglu, S. S. Cetin, N. Topaloglu, M. Polat Gonullu, H. Ates, "The effect of thickness on the optical, structural and electrical properties of ZnO thin film deposited on n-type Si," Journal of Molecular Structure, vol. 1165, pp. 367-380, 2018.
- [65] G. Hübschen, I. Altpeter, R. Tschuncky, and H. G. Herrmann, Materials Characterization Using Nondestructive Evaluation (NDE) Methods, Woodhead Publishing Series in Electronic and Optical Materials: no. 88, Elsevier LTD, 2016.
- [66] H. Lüth, Solid Surfaces, Interfaces and Thin Films, Springer- Verlag Berlin Heidelberg, 2010. doi: 10.1007/987-3-642-13592-7.
- [67] H. H. Perkampus, UV-VIS Spectroscopy and its Applications, Springer-Verlag Berline Heidelberg, 1992.
- [68] R. D. Capua, F. Offi, and F. Fontana, "Check the Lambert-Beer-Bougure Law: a simple trick to boost the confidence of students toward both exponential lows and the discrete approach to experimental physics," European Journal of Physics, 2014. doi: 10.1088/0143-0807/35/4/045025.

- [69] A. Nakaruk, and C. C. Sorrell, "Conceptual model for spray pyrolysis mechanism: fabrication and annealing of titania thin films," Journal of Coating Technology and Research, vol. 7, pp. 665-676, 2010. doi 10.1007/s11998-010-9245-6.
- [70] K. O. Ukoba, A. C. Eloka-Eboka, and F. L. Inambao, "Review of nanostructured NiO thin film deposition using the spray pyrolysis technique," Renewable and Sustainable Energy Reviews, vol. 82, pp. 2900-2915, 2018.
- [71] M. Smirnov, C. Baban, and G. I. Rusu, "Structural and optical characteristics of spin-coated ZnO thin films," Applied Surface Science, vol. 256, pp. 2405-2408, 2010.
- [72] C. A. Rodríguez, M. G. Sandoval-Paz, G. Cabello, M. Flores, H. Fernández, and C. Carrasco, "Characterization of ZnS thin films synthesized through a non-toxic precursor chemical bath," Materials Research Bulletin, vol. 60, pp. 313-321, 2014.
- [73] S. Tec-Yam, J. Rojas, V. Rejon, and A. L. Oliva, "High quality antireflective ZnS thin films prepared by chemical bath deopsition," Materials Chemistry and Physics, vol. 136, pp. 386-393, 2012.
- [74] S. C. Pillai and S. Hehir, Sol-Gel Materials for Energy, Environment and Electronic Applications, Springer International Publishing, 2017. doi: 10.1007/978-3-319-50144-4,.
- [75] Z. Q. Ma, W. G. Zhao, and Y. Wang, "Electrical properties of Na/Mg co-doped ZnO thin films," Thin Solid Films, vol. 515, pp. 8611-8614, 2007.
- [76] J. D. Desai, "Nickel oxide thin films by spray pyrolysis," Journal of Materials Science Materials in Electronics, Springer, 2016. doi: 10.1007/s10854-016-5617-8.
- [77] L. Filipovic, S. Selberherr, G. C. Mutinati, E. Brunet, S. Steinhauer, A. Köck, J. Teva, J. Kraft, J. Siegert, and F. Schrank, "Methods of simulating thin film deposition using spray pyrolysis technique," Microelectronic Engineering, vol. 117, pp. 57-66, 2014. doi: org/10.1016/j.mee.2013.12.025.
- [78] Y. S. Sakhare, N. R. Thakare, and A. U. Ubale, "Influence of quantity of spray solution on the physical properties of spray deposited nanocrystalline MgSe thin films," St. Petersburg Polytechnical University Journal: Physical and Mathematics, vol. 2, pp. 17-26, 2016.
- [79] E. Bacaksiz, M. Parlak, M. Tomakin, A. Özçelik, M. Karakiz, M. Altunbaş, "The effects of zinc nitrate, zinc acetate and zinc chloride precursor on investigation of structural and optical properties of ZnO thin films," Journal of Alloys and Compounds, vol. 466, pp. 447-450, 2008.
- [80] A. Mellit and M. Benghanem, A practical guide for advanced methods in solar photovoltaics systems, Springer, 2020.
- [81] V. Nelson, Introduction to Renewable Energy, Taylor & Francis Group, LLC., 2011.
- [82] G. Conibeer and A. Willoughby, Solar Cell Materials Developing Technologies, John Wiley & Sons, Ltd, 2014.

- [83] A. Kitai, Principles of Solar Cells, LEDs and related devices, John Wiley & Sons Ltd, 2019.
- [84] S. S. Li, Semiconductor Physical Electronics, Springer Science & Business Media, LLC, 2006.
- [85] R. Varache, O. N. Aguila, A. Valla, N. Nguyen, and D. Munoz, "Role of the front electron collector in rear emitter silicon heterojunction solar cell," IEEE Journal of Photovoltaics, vol. 5, pp. 711-717, 2015.
- [86] A. S. Teran, C. Chen, E. Lopez, P. G. Linares, I. Artacho, A. Marti, A. Luque, and J. D. Phillips, "Heterojunction band offset limitation on open-circuit voltage in p-ZnTe/n-ZnSe solar cell," IEEE Journal of Photovoltaics, vol. 5, pp. 874-877, 2015.
- [87] H. K. Kaplan, S. K. Akay, and M. Ahmetoglu, "Photoelectrical properties of fabricated ZnS/Si heterojunction device using thermoionic vacuum arc method," Superlattics and Microstructures, vol. 120, pp. 402-409, 2018.
- [88] K. Yang, B. Li, and G. Zeng, "Effects of temperature on properties of ZnS thin films deposited by pulsed laser deposition," Superlattice and Microstructures, vol. 130, pp. 409-415, 2019.
- [89] U. Wurfel, A. Cuevas, and P. Wufel, "Charge Carriers Separation in Solar Cell," IEEE Journal of Photovoltaics, vol. 5, pp. 461-469, 2015.
- [90] T. Soga, Nanostructured Materials for Solar Energy Conversion, Elsevier, 2006.
- [91] A. P. Kirk, Solar Photovoltaic Cells Photons to Electricity, Elsevier, 2015.
- [92] M. A. Green, Solar Cells Operating Principles Technology and System Applications, Prentice Hall Inc., 1982.
- [93] S. R. Kodigala, Thin film solar cells from earth abundant materials, Growth and characterization of Cu₂ZnSn(SSe)₄ thin films and their solar cell, Elsevier Inc., 2014.
- [94] S. J. Fonash, Solar Cell Device Physics, Elsevier, 2010.
- [95] R. H. Bube, Photovoltaic Materials, Imperial College Press, 1998.
- [96] R. Zein, and I. Alghoraibi, "Influence of bath temperature and deposition time on topographical and optical properties of nanoparticles ZnS thin films synthesized by a chemical bath deposition method," Journal of Nanomaterials, 2019. doi: org/10.1155/2019/7541863.
- [97] F. Göde, C. Gümüş, and M. Zor, "Investigation on the physical properties of the polycrystalline ZnS thin films deposited by the chemical bath deposition method," Journal of Crystal Growth, vol. 299, pp. 136-141, 2007.
- [98] T. Ivanova, A. Harizanova, T. Koutzarova, and B. Vwrtruyen, "Study of ZnO sol–gel films: Effect of annealing," Material Letters, vol. 64, pp. 1147-1149, 2010.

- [99] K. Ravichandran, and P. Philominathan, "Fabrication of antimony doped tin oxide (ATO) films by an inexpensive, simplified spray technique using perfume atomizer," Material Letter, vol. 62, pp. 2980-2983, 2008.
- [100] K. Ravichandran, and P. Philominathan, "Comparative study on structural and optical properties of CdS films fabricated by three different low-cost techniques," Applied Surface Science, vol. 255, pp. 5736-5741, 2009.
- [101] K. Ravichandran, G. Muruganantham, and B. Sakthivel, "Highly conducting and crystalline doubly doped tin oxide films fabricated using a low-cost and simplified spray technique," Physica B, vol. 404, pp. 4299-4302, 2009.
- [102] J. B. Mooney and S. B. Radding, "Spray pyrolysis processing," Annual Review of Material Science", vol. 12, pp. 81-101, 1982.
- [103] E. Arca, K. Fleischer, and V. Shvets, "Influence of the precursors and chemical composition of the solution of the properties of the ZnO thin films grown by spray pyrolysis," The Journal of Physical Chemistry, vol. 113, pp. 21074-21081, 2009.
- [104] K. Ravichandran and P. Philominathan, "Investigations on microstructural and optical properties of CdS films fabricated by a low-cost, simplified spray technique using perfume atomizer for solar cell applications," Solar Energy, vol. 82, pp. 1062-1066, 2008.
- [105] H. Markoç, and Ü.Özgür, Zinc oxide Fundamental, Materials and Device Technology, Wiley-VCH Verlag GmbH & Co. KGaA, Weinheim, 2006.
- [106] J. D. Weiss, "A comparison of two van-der-Pauw measurements configurations of resistivity," Materials Science in Semiconductor Processing, vol. 16, pp. 1637-1644, 2013.
- [107] G. Golan, A. Axelevitch, B. Gorenstein, and V. Mane, "Hot-probe method for evaluation of impurities concentration in semiconductors," Microelectronics Journal, vol. 37, pp. 910-915, 2013.
- [108] F. Zakerian, and H. Kafashan, "Investigation the effect of annealing parameters on the physical properties of electrodeposited ZnS thin films," Superlattices and Microstructures, vol. 124, pp. 92-106, 2018.
- [109] M. A. Yildirim, A. Ates, A. Astam, "Annealing and light effect on structural, optical, and electrical properties of CuS, CuZnS and ZnS thin films grown by the SILAR method," Physica E, vol. 41, pp. 1365-1372, 2009.
- [110] S. W. Shin, S.R. Kang, J. H. Yun, A. V. Moholkar, J. Ha-Moon, J. Y. Lee, and J. H. Kim, "Effect of different annealing conditions on the properties of chemically deposited ZnS thin films on ITO coated glass substrates", Solar Energy Materials and Solar Cell," vol. 95, pp. 856-863, 2011.
- [111] Z. Munirah Raza Khan, A. Aziz, M. Shahid Khan and M. U. Khandker, "Influence of zinc concentration on band gap and sub-band gap adsorption on ZnO nanocrystalline thin films sol-gel grown," Materials Science-Poland, vol. 35, pp. 246-253, 2017.

- [112] C. Y. Tsay, K. S. Fan, Y. W. Wang, C. J. Chang, Y. K. Tseng, and C. K. Lin, "Transparent semiconductor zinc oxide thin films deposited on glass substrate by sol-gel process," Ceramics International, vol.36, pp. 1791-1795, 2010.
- [113] Y. Infahsaeng, and S. Ummartyotin, "Investigation on structural properties of Al-substituted ZnS particle prepared from wet chemical synthetic route," Results in Physics, vol. 7, pp. 1245-1251, 2017.
- [114] K. Ben Bacha, N. Bitri, and H. Bouzouita, "Effect of annealing parameters on structural and morphological properties of sprayed ZnS thin films," Optik, vol. 127, pp. 3100-3104, 2016.
- [115] Z. C. Feng, Handbook of Zinc Oxide and Related Materials, Taylor and Francis Group, LLC., 2013.

PUBLICATIONS FROM THE THESIS

Conference Papers

1. H. Abd Alqader, S. S. Yesilkaya, "Effect of thickness on the optical and electrical properties of ZnO thin films," in Processing of the 78th international conference on Society of Engineering and Technology, Computer, Basic and Applied Sciences, ECBA, 2020, pp. 12.

Papers

1. S. S. Yesilkaya, U. Ulutas, M. M. Abd Alqader, "Effect on Na doping on the properties of ZnS thin films and ZnS/Si heterojunction cells," Materials Letters, vol. 288, pp. 129-347, 2021